This is to certify that the
thesis entitled

Numerical Model for Hemodialysis

presented by

Andrew W. Siefert

has been accepted towards fulfillment
of the requirements for the

M.S. degree in Mechanical Engineering

Craig W. Somerton
Major Professor's Signature

August 21, 2009
Date

NUMERICAL MODEL FOR HEMODIALYSIS

By

Andrew W. Siefert

A THESIS

Submitted to
Michigan State University
in partial fulfillment of the requirements
for the degree of

MASTER OF SCIENCE

Mechanical Engineering

2009

ABSTRACT

NUMERICAL MODEL FOR HEMODIALYSIS

By

Andrew W. Siefert

The human kidneys are a unique set of organs that maintain a homeostatic balance of the body's fluids by filtering blood of metabolic waste products and excess water. If the kidneys loose their ability to remove these materials, an individual must either receive a kidney transplant or begin a hemodialysis regimen to sustain the healthy function of the body's kidneys. Hemodialysis is a medical treatment that uses an extracorporeal device to filter the body's blood. The most accurate method for assessing the deliverable dose for hemodialysis has not been established, providing the motivation for this work. A hemodialysis computer model is developed and tested with the ability to estimate treatment time, toxin clearance, diffusive membrane permeability, water permeability, compartmental pressure drop, and the toxin mass fraction in the blood, hollow-fiber membrane, and dialysate volumes. To simulate a treatment, the program requires the patient's weight, blood toxin concentration, and design parameters of existing dialyzers or future designs. Simulation results demonstrate good agreement to published works with respect to the aforementioned parameters, while providing strong physical insight to waste and water removal in hemodialysis. Advantages of this work include ease of use in comparison to one and two-compartment models, ability to change dialyzer parameters to optimize performance, and the ability to design dialyzers tailored to specialized treatments.

TABLE OF CONTENTS

LIST OF TABLES

LIST OF FIGURES

NOMENCLATURE

$\hat{A}_{c,b}$	Cross-sectional flow area available to the blood
$\hat{A}_{c,d}$	Cross-sectional flow area available to dialysate
$\hat{A}_{f,d}$	Flow area available to dialysate
$\hat{A}_{f,pores}$	Total area available for plasma flow through the membrane pores
$\hat{A}_{pore}$	Area of a circular membrane pore
$\hat{A}_{s,d}$	Inner surface area of the dialysate volume bounded by $\hat{r}_c$
$\hat{A}_{s,b}$	Outer surface area perpendicular to the bulk flow direction for blood
$\hat{A}_{s,m}\Big\vert_{\hat{r}+\Delta\hat{r}}$	Membrane surface area at $\hat{r}+\Delta\hat{r}$
$\hat{A}_{s,m}\Big\vert_{\hat{r}}$	Membrane surface area at $\hat{r}$
$\hat{d}_h$	Hydraulic diameter
$\hat{d}_{h,CCA}$	Hydraulic diameter for the Cell Centered Array
$\hat{k}''_b$	Convective mass transfer coefficient for blood per unit area
$\hat{k}''_d$	Dialysate convective coefficient per unit area,
$\hat{l}$	Length of a hollow-fiber membrane
$\hat{L}$	Length of a pore
$\dot{\hat{m}}_b$	Blood mass flow rate

$\hat{\dot{m}}_d$	Dialysate mass flow rate
$m_{i,A}$	Mass fraction of toxin i at interface A
$m_{i,b}$	Bulk mass fraction of solute i in the blood
$m_{i,b}\Big\|_{\hat{z}}$	Mass fraction of solute i in the blood at location $\hat{z}$
$m_{i,b}\Big\|_{\hat{z}+\Delta\hat{z}}$	Mass fraction of solute i at the $\hat{z}+\Delta\hat{z}$ location
$m_{i,B}$	Mass fraction of toxin i at interface B
$m_{i,C}$	Mass fraction of toxin i at interface C
$m_{i,d}$	Bulk mass fraction of solute i in the dialysate
$m_{i,d}\Big\|_{\hat{z}}$	Mass fraction of solute i in the dialysate at location $\hat{z}$
$m_{i,d}\Big\|_{\hat{z}+\Delta\hat{z}}$	Mass fraction of solute i in the dialysate at the $\hat{z}+\Delta\hat{z}$ location,
$m_{i,m}\Big\|_{\hat{r}}$	Mass fraction of solute i in the membrane at location $\hat{r}$
$m_{i,m}\Big\|_{\hat{r}+\Delta\hat{r}}$	Mass fraction of solute i in the membrane at the $\hat{r}+\Delta\hat{r}$ location
$\hat{\dot{m}}_p\Big\|_{all\,\hat{r}}$	Mass flow rate of plasma at all $\hat{r}$ locations in the membrane
$\hat{\dot{m}}''_p\Big\|_{\hat{r}}$	Mass flow rate of plasma per unit area at the $\hat{r}$ location
$\hat{\dot{m}}_p\Big\|_{\hat{r}_A}$	Mass flow rate of plasma at the $\hat{r}=\hat{r}_A$

N_{fibers}	Number of fibers in the dialyzer
$\hat{P}_w$	Wetted perimeter
$\Delta\hat{r}$	Change in radial distance within the membrane
r	Radial distance
$\hat{r}_A$	Inner radius of the hollow-fiber membrane
$\hat{r}_B$	Radius to the outer surface of the membrane skin layer
r_B	Non-dimensional radial distance to interface B
$\hat{r}_C$	Outer radius of the hollow-fiber membrane
r_C	Non-dimensional radial distance to interface C
$\hat{r}_{DC}$	Inner radius of the dialyzer casing
$\hat{t}_m$	Thickness of the hollow-fiber membrane
$\hat{u}_b$	Area averaged velocity of blood
$\hat{u}_{pore}$	Velocity of plasma water through a cylindrical pore in the membrane
$\hat{w}$	Distance between the centers of one hollow-fiber to another
$\Delta\hat{z}$	Change in axial distance
z	Non-dimensional axial distance

Greek Symbols

Φ	Coefficient in the blood mass species equation neglecting axial diffusion
Γ	Coefficient in the dialysate mass species equation neglecting axial diffusion
Λ	Coefficient in the blood mass species equation
Θ	Coefficient for mass species equation in the dialysate
ς	Coefficient for boundary condition B
Ω	Péclet Number
Ψ_m	Coefficient for mass species equation for the membrane
α	Coefficient for boundary condition A
β	Coefficient for boundary condition A
χ	Coefficient for boundary condition C
ε_A	Area based membrane porosity
η	Hollow-fiber packing density of the dialyzer
$\hat{n}''_{i,b}\Big\|_{\hat{z}}$	Diffusive flux per unit area of solute i at location $\hat{z}$
$\hat{n}''_{i,b}\Big\|_{\hat{z}+\Delta\hat{z}}$	Diffusive flux of solute i at the $\hat{z}+\Delta\hat{z}$ location
$\hat{n}''_{i,d}\Big\|_{z}$	Diffusive flux of solute i at location $\hat{z}$,
$\hat{n}''_{i,d}\Big\|_{\hat{z}+\Delta\hat{z}}$	Diffusive flux of solute i in dialysate at the $\hat{z}+\Delta\hat{z}$ location.
$\hat{n}''_{i,m}\Big\|_{\hat{r}}$	Diffusive flux per unit area of solute i in the membrane at location $\hat{r}$

$\hat{\eta}''_{i,m}\Big\|_{\hat{r}+\Delta\hat{r}}$	Diffusive flux per unit area of solute i in the membrane at the
κ	Coefficient for boundary condition C
λ	Coefficient for boundary condition B
$\hat{\rho}_b$	Blood density
$\hat{\rho}_p$	Density of plasma water
τ	Membrane tortuosity
ζ	Coefficient for mass species equation in the dialysate

Additional

$\hat{\wp}_{i,b}$	Diffusion coefficient for solute i in the blood
$\hat{\wp}_{i,m}$	Apparent diffusion coefficient for solute i in the membrane

Chapter 1
Introduction

The human body possesses a unique set of organs that are responsible for providing a homeostatic balance to the body's fluids. Of these, the kidneys regulate the body's water level, electrolyte, mineral, and acid-base balance by filtering the body's blood. When the kidneys are unable to remove these materials, waste products can accumulate to toxic levels within the body. High concentrations of waste and excess water can degrade body tissues, cause illness, increase the likelihood of kidney failure, and eventually affect the function of the cardiovascular system and brain. To assess this growing problem, medical techniques are used to sustain the body's homeostatic balance by utilizing extracorporeal devices to filter the body's blood.

The most popular of these techniques is known as hemodialysis. Today, hemodialysis is the most widely-used and effective means for removing waste products from the blood. In this technique, small amounts of blood are pumped from a patient to a machine called a hemodialyzer. Blood inside the machine is filtered of waste and water utilizing differences in solute concentration and pressure gradient across a porous, semi-permeable membrane. The degree to which the excess waste is removed will depend on the hemodialyzer operating conditions and sieving properties of the porous membrane. After exiting the machine, blood is returned to the patient and allowed to re-circulate within the body. This process will continue until the level of waste products and excess water in the patient's blood reach allowable levels.

A typical hemodialysis regimen will consist of a treatment lasting 2 to 4 hours thrice weekly. To determine the proper hemodialysis dose, doctors and medical technicians use mathematical models to predict the treatment time required to lower the body's toxin concentrations to healthy levels. The models differ by complexity and application requiring substantial knowledge of the hemodialyzer, localized toxin concentrations, pressure gradients, and physiological phenomena within the human body. The required constants and parameters can accumulate large errors if calculated incorrectly, leading to an over or underestimation of treatment dose.

The most accurate method for assessing the delivered dose for hemodialysis has not been established. This provides a need for developing an improved model for prescribing hemodialysis treatment. It should avoid the pitfalls present in current models and employ a simple approach that can be easily employed in clinical settings. Identifying the barriers and roadblocks to a successful model are of great interest. Current mathematical models are reviewed and evaluated within the Literature Review in Section 1.1. Review of current models will lead to the motivation and goals of this work in Section 1.2.

1.1 Literature Review

An accurate estimate for the dose of dialysis is an important issue for the long-term outcomes of patient survival. A typical dialysis treatment will last anywhere up to four hours, thrice weekly until the patient declines further treatment, receives a

kidney transplant, or passes away.[1-9] During a hemodialysis treatment, a wide range of blood toxins and excess water are removed from the body's blood sustaining a homeostatic balance of the body's fluids. In all, 90 toxins have been identified that can accumulate in blood as a result of insufficient kidney function.[10] These toxins can be categorized as low molecular weight compounds, middle molecules, and protein binding. Modeling focuses on using low molecular weight compounds as markers for treatment-the most popular of which is urea.[11] Although the metabolic waste product urea is not classified as a toxic substance, all current indices of dialysis dose are based on urea measurements, and thus set urea removal as the major goal of hemodialysis.[12-21]

In 1951, Wolf and his collaborators were the first to describe the kinetics of hemodialysis and dialyzer clearance for urea.[22] Five years later, Renkin described the relationships between dialysance, membrane area, permeability, and blood flow in the artificial kidney.[23] Later in the 1970's, Sargent and Gotch successfully introduced one-compartment modeling to clinical practice.[24-25] This mathematical model has the form of an ordinary differential equation describing the rate change of a toxin's concentration with time. It shows that the rate of toxin concentration is a decreasing function of time and is proportional to the time variable toxin concentration, dialyzer clearance; and inversely proportional to the toxin distribution volume.

Within one-compartment modeling, all of the body's fluids are considered to be a single volume of distribution hence giving the model its name.[24-25] The primary

assumptions of this model are that urea generation and residual removal by the kidneys are very low in comparison to dialyzer clearance and the change in the patient's fluid volume during treatment has little influence on modeling efficiency.[26] The mathematical equation from the one-compartment model can be used to determine the treatment time necessary to decrease the initial toxin concentration to a target value. One-compartment models have been found to be good for approximating treatment time provided the volume, clearance, and initial concentrations are not encumbered with significant errors.

Two-compartment modeling was introduced in the late 1980s to early 1990s with the premise of being a more accurate alternative to one-compartment models.[29-32] In the two-compartment model; the body's fluids can be divided into two parts: fluid that is directly accessible to the dialyzer and fluid that is not. The fluid that is directly accessible to the dialyzer is called exterior body water, while the fluid that is not is considered to be interior body water. The concept of this model is the volume of exterior fluid and toxin levels are less than that of the interior fluid. Thus, the toxin level in the exterior fluid will decrease at a faster rate. The downside is compartmental mass transfer coefficients and other constants need to be calculated are both complex and widely misunderstood.

Described by Daugirdas, there have been a number of problems with using the one and two-compartment models for modeling hemodialysis. First, there can be a high level of difficulty in estimating dialyzer urea clearance accurately.[33] It has been found

that dialyzer clearance when supplied by the manufacturer overestimates experimentally found toxin clearance resulting in inadequate or overdose in treatments.[33-34] According to Gotch, there has been considerable controversy in dialysis therapy literature concerning the relative merits of single-pool versus double pool urea modeling and the validity of dialysis collection methods to measure kinetic parameters.[19] The controversy has resulted in some uncertainty regarding the use of one and two-pool kinetic models as guidance of dialysis therapy.

1.2 Motivation and Goals

Today, methods exist that can adequately model toxin removal during hemodialysis but are limited in their ease of use and ability to provide an accurate and quantified dose for a variety of blood toxins. Many variations have been proposed to improve on the one and two-compartment models whose methods require additional constants impeding the ease of use. For the administering medical staff, the model should not only be easy to use but limit the use of parameters whose calculation possesses high levels of uncertainty. Goals of the work are to:

1. Develop a hemodialysis computer model with the ability to estimate treatment time, toxin clearance, diffusive permeability, water permeability, and other treatment statistics that may help doctors and medical staff to best choose a course of treatment.

2. The model should use parameters that can be found from hemodialyzer manufacturer data or those than can be easily calculated using only widely accepted methods to limit error and dose uncertainty.

3. Compare and contrast the sieving properties of membranes to develop a framework for designing an optimized dialyzer tailored to a specific treatment.

4. Validate claims in previous works for dialyzer operating conditions by testing parameters within the created model.

5. Develop ideas for future works that could lead to modeling improvement.

Chapter 2
Background

The hemodialysis treatment of today is a cornucopia of study areas that includes but is not limited to blood physiology, rheology, nephrology, mass transfer, fluid dynamics, and membrane technology. This work will focus on modeling a hemodialysis treatment using principles spanning each of the aforementioned areas. Blood physiology and rheology are used to determine the physical and flow properties of blood explored in Section 2.1. In Section 2.2, nephrology is introduced as the study of kidney function, kidney failure, and statistics for kidney disease in the United States. Section 2.3 describes the functions and processes of hemodialysis that are a combination of fluid dynamics and mass transfer. The focus of Section 2.4 is to describe the functional filter of hemodialysis and the membrane technology that allows the blood to be cleansed. In the final section, a term used to describe the capacity of a dialyzer for toxin removal is introduced along with membrane permeability.

2.1 Determining the Physical and Flow Properties of Blood

Blood provides life to human body. The purpose of blood is to transport oxygen and other nutrients to the body's tissues and organs while at the same time removing excess water and metabolic waste products. Blood itself can be described as a suspension of particles in an aqueous solution of formed elements.[36] This heterogeneous solution is principally made up of plasma, erythrocytes (red blood

cells), leukocytes (white blood cells), and thrombocytes (platelets). The composition of blood can be divided into percents of total blood volume as presented in Figure 2.1.

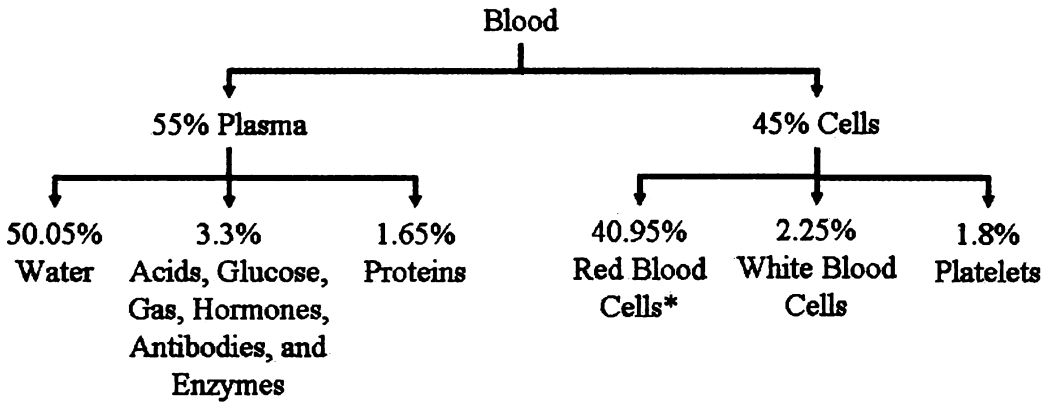

Figure 2.1 Blood's constituents presented as a percent of the total blood volume, asterisk on the Red Blood Cells percent is an average for human males whose value is dependent on the level of hematocrit in the blood

The aqueous solution known as plasma occupies approximately 55% of the total blood volume. Plasma consists of 91% water by weight, 3% proteins, and the remainder is made up of acids, glucose, gas, hormones, antibodies, and enzymes.[36] The remaining 45% of the total blood volume is occupied by red blood cells, white blood cells, and platelets. White blood cells play a major role in fighting disease but are very small in number averaging 9000 cells/mL of blood and contributing only 2.25% to the total volume. Although platelets are extremely large in number (3×10^6 cells/mL), they are very small in size contributing only 1.8% to the total volume of blood.[36] Since both white blood cells and platelets constitute only 4% of the total volume of blood, red blood cells are the primary contributors to the physical and flow properties of blood.

One important physical property of blood is whole blood density. Whole blood density is a function of the volume concentration of red blood cells known as hematocrit.[36] In males, hematocrit varies from 40 to 54% while in females it ranges from 37 to 47%.[2] Although the density of blood changes with hematocrit, previous works assume whole blood density to be constant at 1040 kg/m^3.[37-41] The total volume of blood within a human can then be estimated on the basis of previous research acknowledging blood to constitute approximately 7.5% of a human's body weight.[38-42] Using this standard, a 70 kg woman will have roughly 5 L of blood within her body providing a very useful estimation for total patient blood volume.

In the flow properties of blood, whole blood viscosity is not constant. Viscosity can be mathematically defined as the ratio of shear stress to shear rate of a fluid. For a Newtonian fluid the relationship between shear stress and shear rate is entirely linear; and, therefore, viscosity is constant. For blood, the viscosity of blood is large at low shear rates due to blood's viscoelastic behavior that is attributed to the reversible aggregation, deformation, and orientation of red blood cells in shear flow.[43] Thus, whole blood is commonly classified as a Casson fluid.[44-45]

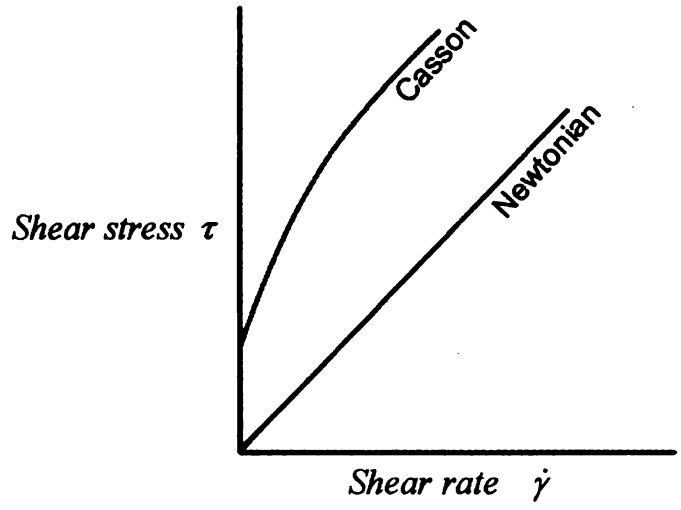

Figure 2.2 The relationship of shear stress and shear rate of fluids

A Casson fluid demonstrates that blood will not begin to flow until a known shear stress has been reached. At a shear rate of 50 sec^{-1} or greater, aggregates of red blood cells are gradually broken up under the influence of lager velocity gradients. These aggregates, known as rouleaux, are stacks of red blood cells whose aggregation is based on the large surface areas of red blood cells adhering to one another under low shear rates. In the presence of velocity gradients exceeding 100 sec^{-1}, an asymptotic value of blood viscosity is reached and blood may be considered a fluid with constant viscosity and therefore behave as a Newtonian fluid.[38] For shear rates exceeding 100 sec^{-1}, blood viscosity has been experimentally estimated at 3 centipoise.[46] Care is taken later in the Results and Discussion to verify that all blood flow within the modeling exhibits a shear rate greater than 100 sec^{-1} in order to validate modeling blood as a Newtonian fluid.

2.2 The Kidneys and Renal Failure

As blood circulates through the body, toxins and excess water can accumulate within the blood from the ongoing metabolic processes of the body. The level of excess waste must remain at a healthy level to maintain a homeostatic balance of the body's fluids. To maintain this balance, the renal system is responsible for removing toxins and water from the body's blood and excreting the waste from the body. The renal system consists of the kidneys, ureters, and bladder. The role of the kidneys is to regulate fluid volume, maintain an electrolyte balance, regulate the pH of blood, and remove metabolic waste products and excess ions from the blood.[47]

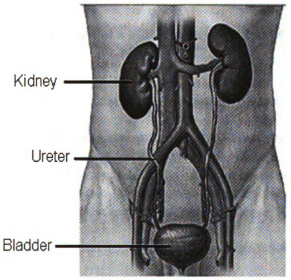

Figure 2.3 The renal system consists of the kidneys, ureters, and bladder [28]

During healthy function, blood enters the kidneys and is quickly dispersed among tiny tubules leading to the functional filters of the kidneys known as nephrons. The neprhon consists of a series of tubules that filter excess water and toxins using a

pressure and concentration gradient across an arterial wall. After excess toxins and water have been removed, cleansed blood circulates back to the heart while waste products funnel through the ureters to the bladder.

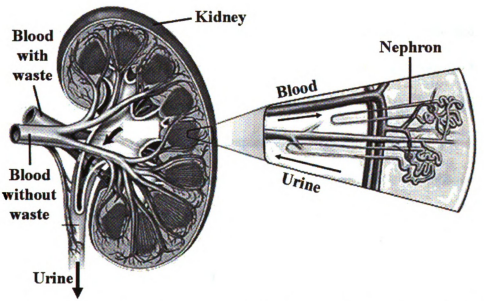

Figure 2.4 Cross-sectional view of a kidney with directions of blood and urine flow highlighted[48]

Over time, the kidneys can suffer a loss of nephron function and become unable to remove metabolic waste products and excess water. The loss of nephron function is known as kidney disease and renal failure. Chronic Kidney Disease (CKD) is an advanced condition where the kidneys lose approximately 90% of nephron function. From 1999 to 2004, an estimated 13% of adults ages 20 or older (26 million adults) have physiological evidence of CKD determined from data collected through the National Health and Nutrition Examination Survey.[49]

Since 1998, The treatment of kidney disease in the United States has increased at an alarming rate. Types of treatment include dialysis, kidney transplantation, or refusal

of treatment. Worldwide, over 1.5 million people are currently kept alive through dialysis or transplantation. This number is forecasted to double within the next 10 years.[50] From 1998 to 2006, the number of dialysis patients has increased 54% from 229,918 to 354,754.[51] During the same period, kidney transplants grew 46% but only reached 15,800 in 2006; far less than the number of individuals on the transplant waiting list. Figure 2.5 reports the trends in dialysis patients from 1998 to 2006 as reported by the United States Renal Data System (USRDS).[51] On the left ordinate the number of patients receiving kidney transplants, number of patients on the national kidney transplant waiting list, and patient mortality is shown. On the right ordinate, the total number of dialysis patients from 1998 to 2007.

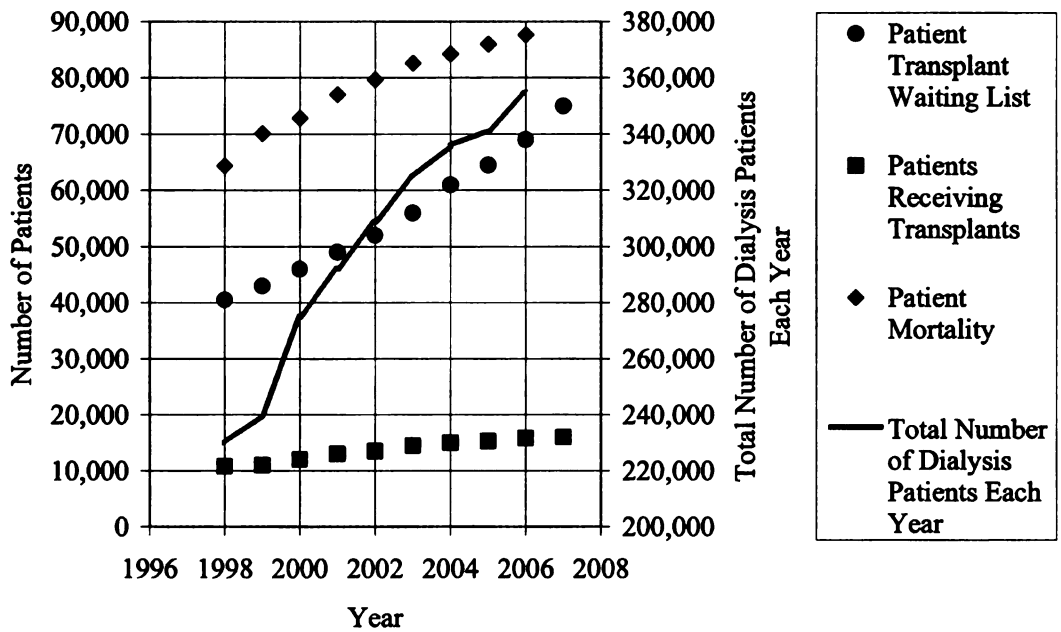

Figure 2.5 Total number of dialysis patients in the United States including those who are currently on a transplant waiting list, have passed, and have received a kidney transplant as reported by the United State Renal Data System[51]

Along with the rising number of dialysis patients, the cost of treatment has increased. The increase in CKD over the past decade has prompted the USRDS to issue for the first time a separate report documenting the magnitude of the disease which accounts for more than 24% of Medicare costs.[52] The USRDS is funded by the National Institute of Diabetes and Digestive and Kidney Diseases, part of the National Institutes of Health. Today, the most cost effective and health improving treatment to sustaining kidney function is hemodialysis.

2.3 Hemodialysis

Hemodialysis is the most widely used method in the United States for treating advanced to permanent kidney failure accounting for 92% of all dialysis treatments.[53] Since its conception is the 1960s, hemodialysis has evolved and become a practical treatment of renal insufficiency largely due to advances in technology and understanding of the physical processes involved. A drawing of a typical hemodialysis machine is presented in Figure 2.6. This machine houses a wide range of technology whose functions are designed to control the flow of two fluids through its comprising devices.

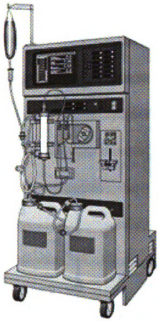

Figure 2.6 Typical hemodialysis machine used to treat renal insufficiency[54]

A hemodialysis houses and supplements two fluid loops. The patient and the hemodialysis machine form a closed loop-where blood flows from the patient into the machine then back into the patient. The second loop consists of a cleansing fluid known as dialysate. Dialysate is water containing a dilute mixture of electrolytes and minerals whose function is to carry toxins that have been removed from the blood out of the hemodialysis machine. Within the open dialysate loop, dialysate flows from dialysate concentrate containers in then out of the machine where the spend solution is disposed of as waste. A schematic of the blood and dialysate loops within the machine are drawn in Figure 2.7.

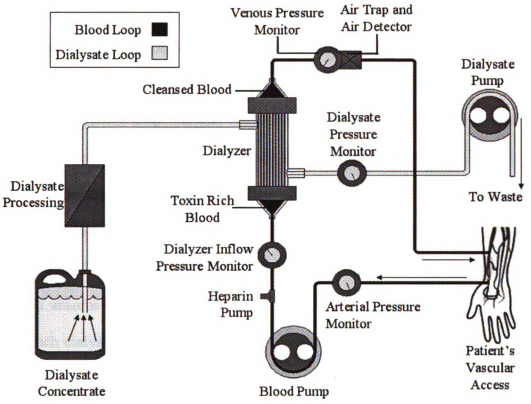

Figure 2.7 Diagram of the basic components of a hemodialysis machine

Blood inside the patient will flow to the hemodialysis machine via a vascular access normally located in the patient's forearm. Once inside the machine, blood passes an arterial pressure monitor before receiving a positive pressure boost to the heparin pump. Heparin is a widely used anticoagulant that is pumped into the blood preventing blood clotting within the machine. Passing the dialyzer inflow pressure monitor, toxin rich blood at high positive pressure enters the dialyzer. Inside the dialyzer, blood is cleansed of toxins and excess water similar to that of the native kidney (A more in-depth look at how the dialyzer cleanses blood is presented in the Section 2.4). Exiting the dialyzer, cleansed blood flows to a venous pressure monitor,

air trap, air detector, then finally back to the patient's venous vascular access completing the closed, blood-side loop.

In the open dialysate loop, dialysate concentrate flows from its container to a staged processing section via a negative pressure gradient supplied by a pump. Within the staged processing, the dialysate is heated to 37°C, mixed with minerals and electrolytes, and diluted with pure water to a desired dialysate composition tailored to each individual treatment. From the processing unit, dialysate flows into the dialyzer where it absorbs and carries away toxins that have been removed from the blood. Toxin rich dialysate exits the dialyzer and through a negative pressure pump before being disposed of as waste. During treatment, both the blood and dialysate loops continue until the toxin concentration and water levels within the blood reach their target treatment values.

2.4 The Dialyzer

The dialyzer is the artificial kidney of the hemodialysis machine. It possesses a nearly cylindrical case that contains a blood and dialysate compartment. The blood and dialysate compartments are separated by a circular array of hollow-fiber membranes numbering in the thousands. Each fiber is held in place at the ends of the dialyzer by a potting material that provides spacing between each fiber. Blood flows on the inside of the hollow-fibers while dialysate flows on the outside. A vertical, cross-sectional view of the dialyzer is presented in Figure 2.8.

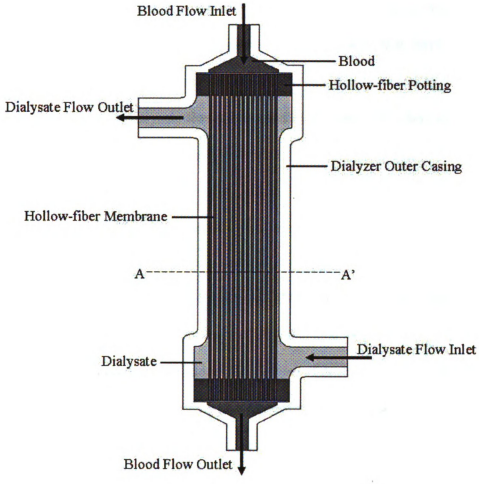

Figure 2.8 Cross-sectional view of a typical hollow-fiber dialyzer

During operation, blood flows through the inlet of the dialyzer where it disperses throughout the hollow-fibers. While flowing through the fibers, toxins and excess water transport from the blood into the porous, semi-permeable membrane walls of the hollow-fibers. Toxin and water transport are driven by a transmembrane pressure and concentration gradient between the blood and dialysate compartments. The cleansed blood exits each fiber to a nozzle where it flows back to the patient's venous vascular access. Alternatively, dialysate flows into the dialyzer from a lateral location. Through the inlet, dialysate submerges the hollow-fiber array and flows over

each hollow-fiber in the direction opposite to blood flow. Dialysate flowing over each fiber will absorb and carry toxins and excess water away that have transported through the hollow-fiber membrane walls from the blood. At the end of the dialysate chamber, the toxin rich dialysate flows through the dialysate exit where it is collected and disposed of as waste.

2.5 Hollow-Fiber Membranes

Most hollow-fibers have a relatively standard inner diameter of approximately 180 to 220 μm, a length of 20-24 cm, and a wall thickness of 20-50 μm.[55] The fibers are analogous to the tubules in the kidney's nephron. They allow toxins and water to filter from the blood while retaining vital proteins and blood cells. The sieving properties of a hollow-fiber will depend on the pore size, porosity, tortuosity, and wall thickness. A simplified drawing of a small section of a hollow-fiber membrane is presented in Figure 2.9. The pictured cross-section possesses straight, cylindrical pores that are large enough to allow smaller solutes to pass but also small enough to retain larger solutes to the blood-side of the fiber. In a real membrane, the membrane pores are non-circular and follow tortuous paths through the membrane walls. Modeling pore geometry is presented later in Section 3.1.

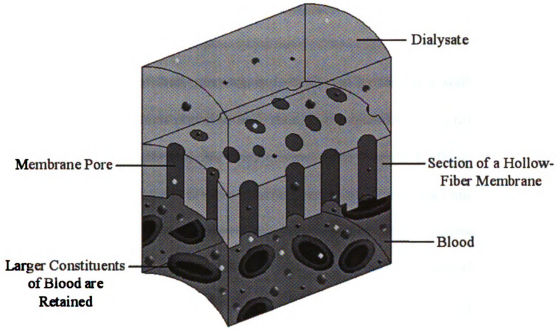

Figure 2.9 Section of a hollow-fiber membrane modeled to have straight, cylindrical pores

Dialysis membranes are historically classified by material and can be divided into three distinct groups that include unmodified cellulose, modified cellulose, and synthetic membranes. Each group exhibits different filtering characteristics and different degrees of alternative complement pathway activation. Alternative complement pathway activation describes a biochemical cascade that ends with the destruction of the body's pathogens. However during dialysis, blood interaction with the membrane can inadvertently activate these pathways causing infections and treatment complications.[56] This activation is caused by the plasma enzymes interacting with membrane hydroxyl groups. The abundance of hydroxyl groups is particularly pronounced for unmodified Cellulose membranes.[57]

2.5.1 Unmodified Cellulose Membranes

The long popularity of these membranes is explained by their low wall thickness in the 5-15 μm range; high porosity; and, thus, high suitability for a diffusion-based process.[55] These membranes are homogeneous with respect to their composition implying uniform resistance to mass transfer over the membrane wall thickness.[57] The main organic component comprising the structure of unmodified cellulose membranes is cellobiose-a saccharide found in a number of naturally occurring substances.[58] The most important characteristic of cellobiose is its high density of hydroxyl groups leading to pronounced alternative complement activation. In addition, these membranes have a small mean pore size and high degree of hydrophilicity making them unsuitable for filtering middle to larger size toxins and prolonged use. The combination of pronounced complement pathway activation, small mean pore size, and hydrophilicity has contributed to the steady decline of unmodified cellulose membrane use in hemodialysis treatments.

2.5.2 Modified Cellulose Membranes

Emerging in the 1980s, these membranes had less pronounced complement activation and generally a larger mean pore size.[59] The larger mean pore size allows these membranes to have greater water permeability and better middle molecule clearances. Modified cellulose membranes are manufactured by substituting 75% of their hydroxyl groups for acetate groups leading to less pronounced complement

activation.[55] Like unmodified cellulose membranes, they have a low wall thickness (6-15 μm) and homogeneous structures.[57] Modified cellulose membranes are still widely used today in a range of dialysis treatments.

2.5.3 Synthetic Membranes

Synthetic membranes were first created and developed in response to concerns related to the narrow scope of solute removal and pronounced complement activation by cellulose type membranes. The structure of most synthetic membranes can be classified as being asymmetric. That is pore size increases in the direction of mass transport. These membranes can be described as having a very dense skin layer with a thickness of approximately 1 μm and a porous support layer that varies between 20 to 55 μm.[55] According to Ronco, Ballestri, and Cappelli; the inner skin layer of the membrane is the real sieving barrier for solutes while the rest of the membrane structure offers mechanical resistance and structural support.[60] This claim is tested later in the Results and Discussion in Chapter 5. Geometric modeling of these layers is discussed in Section 3.2.

2.6 Describing Toxin Removal and Membrane Permeability

Three new parameters are introduced in order to quantify the rate at which toxins are removed during hemodialysis. These are toxin clearance, water permeability, and diffusive permeability. Describing a dialyzer's capacity to remove toxins from blood

is widely described as toxin clearance. Clearance in hemodialysis describes the volume of blood that has been cleared of a toxin per unit time. Clearance, $\hat{K}d$, can be mathematically shown as Equation (2.1) where $\hat{Q}_b$ is the blood flow rate into the dialyzer, $m_{i,b}\big|_{exit}$ is the mass fraction of a toxin in blood at the dialyzer blood exit, and $m_{i,b}\big|_{inlet}$ is the mass fraction of a toxin i in the blood at the dialyzer blood inlet.

$$\hat{K}d = \hat{Q}_b \frac{m_{i,b}\big|_{inlet} - m_{i,b}\big|_{exit}}{m_{i,b}\big|_{inlet}} \tag{2.1}$$

As previously noted, toxin clearance describes the dialyzer's ability to remove toxins. This ability is strongly dependent on the sieving properties of the hollow-fiber membranes. In the basic sense, hollow fibers serve a dual purpose. One is to act as a physical barrier between the blood and the dialysate compartments, and two, to allow small toxins to pass through the membrane while retaining the larger more vital blood constituents. The rate at which this toxins and water move through a membrane is commonly referred in membrane literature as permeability.[61] In hemodialysis; two parameters are used to describe the sieving properties that include water and diffusive permeability.

Manufacturers measure dialyzer water permeability using dead-end filtration. Reverse osmosis water is fed into the blood-side compartment and the transmembrane pressure between the blood side and permeate side is measured. Collecting the permeated water and recording the duration of time, the volumetric flow rate of water

passing through the membrane can be calculated. Water permeability, $\hat{L}_p$, can be calculated using

$$\hat{L}_p = \frac{\hat{Q}_f}{\hat{A}_s \Delta\hat{P}} \tag{2.2}$$

where $\hat{Q}_f$ is the volumetric flow rate through the membrane, $\hat{A}_s$ is the inner fiber surface area and $\Delta\hat{P}$ is the transmembrane pressure. The diffusivity of solutes in blood, blood plasma, and dialysate can be estimated from the Stokes-Einstein equation consistent with previous works in hemodialysis.[45,62-65] The relation assumes a solute to be spherical in shape with a radius, $\hat{a}$.[45] The radius is estimated based on the molecular weight and density of the solute. The diffusion of solutes within this model becomes especially important when determining the transport characteristics of toxins through the pores of the hollow-fiber membrane.

Diffusive permeability is used to describe the rate at which solute transport occurs across a membrane. Within this model, the membrane pores are assumed to by cylindrical and of radius $\hat{r}$. When a spherical toxin flows through the pore, in many cases the solute's radius will be comparable to the size to the pore; resulting in a reduced rate of solute diffusion across the membrane. This reduced rate is named apparent diffusivity. The reduced rate of diffusion is a result of the solute experiencing hydrodynamic drag caused by the flow of plasma water over the surface of the solute. As the solute radius increases, drag will increase and vise-versa. To

describe the apparent diffusivity $\hat{\wp}_m$ for a spherical solute in a cylindrical pore, the Renkin Equation can be used shown as Equation (2.3).[66]

$$\hat{\wp}_m = \hat{\wp}_p\left[1-2.1\left(\frac{\hat{a}}{\hat{r}}\right)+2.09\left(\frac{\hat{a}}{\hat{r}}\right)^3-0.95\left(\frac{\hat{a}}{\hat{r}}\right)^5\right] \tag{2.3}$$

where $\hat{\wp}_p$ is the diffusivity of the solute in plasma and $\hat{a}/\hat{r}$ is the ratio of the solute radius to the pore radius. Once the apparent diffusive permeability has been determined, the diffusive permeability of the membrane can be found using Equation (2.4) where ε_A is the area based porosity of the membrane, τ is the membrane tortuosity, and $\hat{t}_m$ is the membrane thickness.

$$\hat{P}_m = \frac{\varepsilon_A \hat{\wp}_m}{\hat{t}_m \tau} \tag{2.4}$$

Chapter 3

Model Geometry and Derivation of the Mass Species Conservation Equations

Before developing the mathematical descriptions for toxin transport in the blood, membrane, and dialysate compartments; the geometry of the model is described. The geometry is developed by beginning with the geometry of the dialyzer and ending with the geometry of a single hollow-fiber. During operation, dialysate flows through the void spaces created by the hollow-fiber array requiring the development of the hydraulic definition in Section 3.1. In Section 3.2, the geometry of a homogeneous and asymmetric membrane is presented. Following the descriptions for geometry, the mass species equation for toxin transport in the blood is developed in Section 3.3. A similar derivation for toxin transport in dialysate is developed in Section 3.5. The boundary conditions at the membrane interfaces for both a homogeneous and asymmetric case are derived in Section 3.6. For readers already familiar with mass species derivation, a summary of the derived equations and boundary conditions is presented in Section 3.7.

3.1 Development of Hydraulic Definition

The enclosed volume of a dialyzer consists of a large array of circular fibers submerged in a bath of flowing dialysate. In the case of the dialyzer, dialysate flows around each fiber through the void space created by the spacing between the fibers that can be modeled as noncircular conduit flow. For the model, all mass transfer will

be handled on a per hollow-fiber basis requiring the need to calculate the flow area of dialysate around each fiber. The equivalent circular flow area for each fiber can be calculated by developing a definition for the hydraulic diameter.

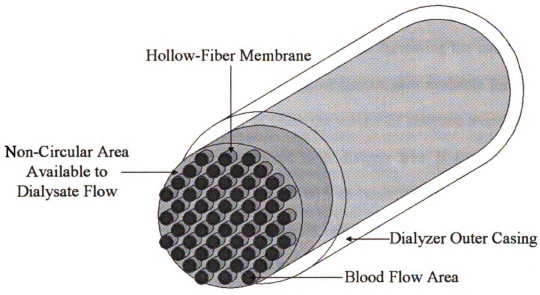

Figure 3.1 Inner components of the dialyzer are extruded to show their geometry and flow areas

The hydraulic diameter for the flow of dialysate around each hollow-fiber is dependent on the hollow-fiber-dialyzer packing density. The packing density is defined as the ratio of the total hollow-fiber volume to the volume within the inner dialyzer casing. Here it will be assumed that all fibers are straight; thus, the packing density is calculated based on dialyzer cross-sectional area. Mathematically, the area based packing density,η, is calculated by

$$\eta = \frac{N_{fibers}\hat{r}_c^2}{\hat{r}_{DC}^2} \tag{3.1}$$

where

N_{fibers} : number of hollow-fibers in the dialyzer

$\hat{r}_C$: outer radius of the hollow-fiber

$\hat{r}_{DC}$: inner radius of the dialyzer casing.

The packing density is important from two perspectives. Increasing the number of hollow-fibers in the dialyzer will increase the fiber surface area available for mass transport. Secondly, for a high number of fibers the volume of dialysate around each fiber decreases for a constant cross-sectional inner dialyzer area. If a hollow-fiber possesses a surface area that is not in contact with dialysate, the capacity for mass transfer will decrease. Further detail on optimal range of fiber packing density is discussed in the Results and Discussion in Section 5.2.1. The hydraulic diameter of flow through a non-circular conduit is mathematically calculated by

$$\hat{d}_h = \frac{4\hat{A}_{f,d}}{\hat{P}_w} \tag{3.2}$$

where

$\hat{A}_f$: flow area available to dialysate

$\hat{P}_w$: wetted perimeter.

To calculate $\hat{A}_{f,d}$ and $\hat{P}_w$, the area based packing density for dialyzer must be determined. The highest packing density for straight fibers within the dialyzer is the Cell Centered Array (CCA). In the CCA, a hollow-fiber is centered on each corner of a square with one additional fiber placed at the center. Four of these arrays are shown in Figure 3.2.

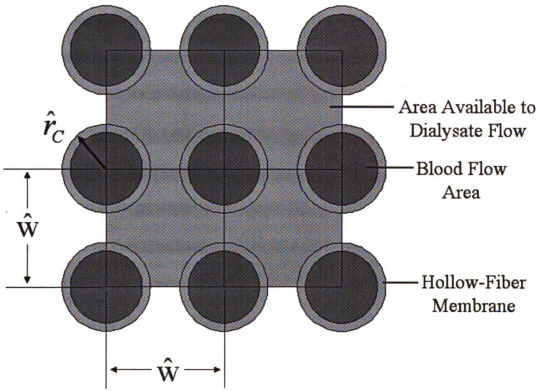

Figure 3.2 Cell-centered array

In Figure 3.2, each square array has a side of length $\hat{w}$ spanning from the center of one fiber to another. Length $\hat{w}$ can be calculated based on the dialyzer area based packing density shown to equal

$$\hat{w} = \sqrt{\frac{2\pi\hat{r}_c^2}{\eta}} \tag{3.3}$$

Using Equation (3.2), the hydraulic diameter for a hollow-fiber within the CCA can be mathematically show as

$$\hat{d}_{h,CCA} = \frac{\hat{w}^2 - 2\pi\hat{r}_c^2}{\hat{r}_c(\pi - 2) + \hat{w}} \tag{3.4}$$

3.2 Development of Radial Geometry

In the radial direction, two geometric cases are explored-Case 1 for a homogeneous membrane and Case 2 for an asymmetric membrane. For a homogeneous membrane, three regions are defined that include a blood, membrane, and dialysate region. These regions meet at two interfaces denoted as interface A and interface C. Interface A is located where the outer perimeter of the blood at $\hat{r} = \hat{r}_A$ meets the inner perimeter of the membrane. Interface C is located where the outer perimeter of the membrane at $\hat{r} = \hat{r}_C$ meets the inner perimeter of the dialysate area. Figure 3.3 displays a drawing of this geometry with all regions, interfaces and radii displayed.

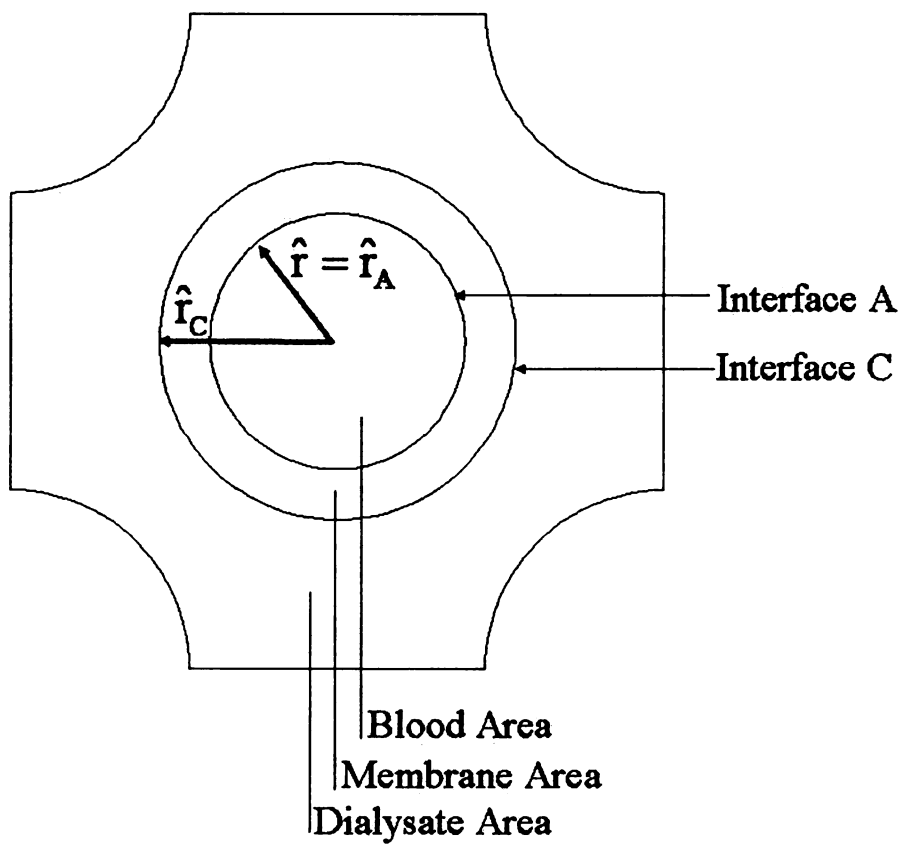

Figure 3.3 Radial nomenclature for a homogeneous membrane geometry

Case 2 is for the asymmetric membrane geometry. In Section 2.5, asymmetric membranes were discussed explaining their unique geometry. These membranes are often described as having a skin layer and a porous support. Within this model, each layer will be assumed to be homogeneous and have the ability to possess different pore sizes, area based porosities, and thicknesses. For this geometry, the membrane will be divided into two regions denoted as the membrane skin and porous support. The skin area is defined radially for $\hat{r}_A \le \hat{r} \le \hat{r}_B$ and the membrane porous support area by $\hat{r}_B \le \hat{r} \le \hat{r}_C$. Figure 3.4 displays the radial and interfacial nomenclature for the asymmetric membrane's radial geometry.

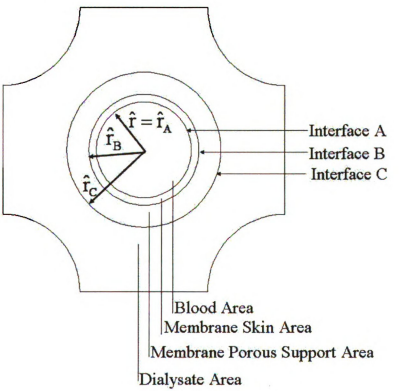

Figure 3.4 Radial nomenclature for an asymmetric membrane geometry

Now that both radial geometries have been defined, each of the dimensional, radial quantities will be non-dimensionalized. For quantities of length, the fiber length $\hat{l}$ will be used for scaling. For radial quantities, the hollow-fiber inner radius $\hat{r}_A$ will be used to non-dimensionalize each radial distance. The new, non-dimensional terms can be shown by

$$z = \frac{\hat{z}}{\hat{l}} \quad \text{and} \quad 1 = \frac{\hat{r}_A}{\hat{r}_A} \qquad r_B = \frac{\hat{r}_B}{\hat{r}_A} \qquad r_C = \frac{\hat{r}_C}{\hat{r}_A}$$

Using the new non-dimensional radial terms, the geometric drawings of Figures 3.3 and 3.4 are shown in Figure 3.6.

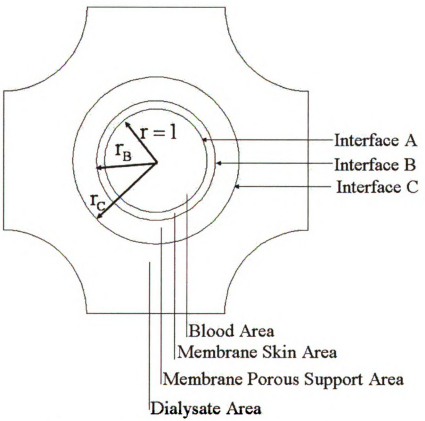

Figure 3.5. Non-dimensional radial geometry

The final parameter to be discussed is the hollow-fiber membrane pore geometry. From Section 2.5, both homogeneous and asymmetric membranes are known to have pores of both varied size and porosity. A number of authors have modeled the membrane's pores using a cylindrical pore model with good accuracy when comparing analytical prediction of membrane properties to experimental results.[68-69] This model assumes pores within the membrane walls are cylindrical, straight pores equally distributed throughout the membrane.

To account for non-straight membrane pores, a secondary model can be used, known as the tortuous pore model. This model assumes that all pores in the membrane remain circular and equally distributed; but possess tortuous paths through the membrane's walls. Since the pores are of a curved shape within the membrane, the pore length can be larger than the membrane's thickness. Tortuosity can therefore be mathematically shown to equal

$$\tau = \hat{L} / \hat{t}_m$$

where

$\hat{L}$: length of the pore

$\hat{t}_m$: membrane thickness.

3.3 Mass Species Derivation for Blood

Blood flow and toxin transport in a hollow-fiber can be mathematically described by deriving the conservation of mass species for a differential element. The blood volume's differential element is drawn in Figure 3.6. This element has a radius equal to the inner radius of the hollow-fiber, $\hat{r} = \hat{r}_A$, and a length $\Delta\hat{z}$ containing one inflow and two outflows. The inflow is a combination of advection and diffusion while the outflows are comprised of advection and diffusion in the axial direction, and convection through the element's outer surface perpendicular to the bulk flow direction. The resulting mass species conservation can be described in words by the mass flux into the volume equal to the mass flux out.

$$\text{Advection}|_{IN} + \text{Diffusion}|_{IN} = \text{Advection}|_{OUT} + \text{Diffusion}|_{OUT} + \text{Convection}|_{OUT}$$

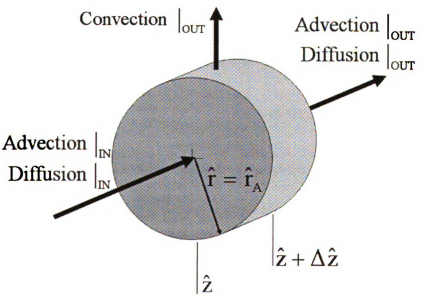

Figure 3.6. Blood differential element

Each term in the conservation equation can be represented by its respective mathematical expression with units of mass per time presented as

$$\hat{\dot{m}}_b \, m_{i,b}\Big|_{\hat{z}} + \hat{A}_{c,b} \, \hat{\dot{\eta}}''_{i,b}\Big|_{\hat{z}} = \hat{\dot{m}}_b \, m_{i,b}\Big|_{\hat{z}+\Delta\hat{z}} + \hat{A}_{c,b} \, \hat{\dot{\eta}}''_{i,b}\Big|_{\hat{z}+\Delta\hat{z}} + \ldots + \ldots + \hat{\dot{k}}''_b \hat{A}_{s,b}\left(m_{i,b} - m_{i,A}\right) \tag{3.5}$$

where

$\hat{\dot{m}}_b$	blood mass flow rate
$m_{i,b}\Big\|_{\hat{z}}$	mass fraction of solute i in the blood b at location $\hat{z}$
$\hat{A}_{c,b}$	cross-sectional flow area available to the blood
$\hat{\dot{\eta}}''_{i,b}\Big\|_{\hat{z}}$	diffusive flux per unit area of solute i at location $\hat{z}$
$m_{i,b}\Big\|_{\hat{z}+\Delta\hat{z}}$	mass fraction of solute i at the $\hat{z}+\Delta\hat{z}$ location
$\hat{\dot{\eta}}''_{i,b}\Big\|_{\hat{z}+\Delta\hat{z}}$	diffusive flux of solute i at the $\hat{z}+\Delta\hat{z}$ location
$\hat{\dot{k}}''_b$	convective mass transfer coefficient for blood
$\hat{A}_{s,b}$	outer surface area perpendicular to the bulk flow direction
$m_{i,b}$	mass fraction of toxin i in the blood
$m_{i,A}$	mass fraction of toxin i at interface A.

Please note all terms possessing circumflex accents are dimensional terms. The bulk mass flow rate is expanded and shown to equal

$$\hat{\dot{m}}_b = \hat{\rho}_b \hat{u}_b \hat{A}_{c,b} \tag{3.6}$$

where

$\hat{\rho}_b$: density of blood

$\hat{u}_b$: area-averaged velocity of blood.

The mass flow rate is then substituted into the mass balance written as

$$\begin{aligned} \hat{\rho}_b \hat{u}_b \hat{A}_c m_{i,b}\Big|_{\hat{z}} + \hat{A}_{c,b} \hat{\dot{\eta}}''_{i,b}\Big|_{\hat{z}} &= \hat{\rho}_b \hat{u}_b \hat{A}_{c,b} m_{i,b}\Big|_{\hat{z}+\Delta\hat{z}} + \ldots \\ \ldots + \hat{A}_{c,b} \hat{\dot{\eta}}''_{i,b}\Big|_{\hat{z}+\Delta\hat{z}} &+ \hat{\dot{k}}''_b \hat{A}_{s,b}\left(m_{i,b} - m_{i,A}\right) \end{aligned} \tag{3.7}$$

Equation (3.7) is rearranged to group like terms and divided by the volume of the differential element resulting in

$$\begin{aligned} \left(\frac{\hat{\dot{\eta}}''_{i,b}\Big|_{\hat{z}+\Delta\hat{z}} - \hat{\dot{\eta}}''_{i,b}\Big|_{\hat{z}}}{\Delta\hat{z}}\right) + \hat{\rho}_b \hat{u}_b \left(\frac{m_{i,b}\Big|_{\hat{z}+\Delta\hat{z}} - m_{i,b}\Big|_{\hat{z}}}{\Delta\hat{z}}\right) + \ldots \\ \ldots + \frac{2\hat{\dot{k}}''_b}{\hat{r}_A}\left(m_{i,b} - m_{i,A}\right) = 0 \end{aligned} \tag{3.8}$$

Using Fick's Law of Diffusion, the diffusive flux term in Equation (3.8) can be substituted by the expression shown below

$$\hat{\dot{\eta}}''_{i,b}\Big|_{\hat{n}} = -\hat{\rho}_b \hat{\wp}_{i,b} \frac{dm_{i,b}}{d\hat{z}}\Big|_{\hat{n}} \tag{3.9}$$

where

$\hat{n}$: location

$\hat{\wp}_{i,b}$: diffusion coefficient for solute i in the blood.

After substitution, the resulting expression is written as

$$-\hat{\rho}_b\hat{\wp}_{i,b}\left(\frac{\left.\frac{dm_{i,b}}{d\hat{z}}\right|_{\hat{z}+\Delta\hat{z}} - \left.\frac{dm_{i,b}}{d\hat{z}}\right|_{\hat{z}}}{\Delta\hat{z}}\right)+\hat{\rho}_b\hat{u}_b\left(\frac{\left.m_{i,b}\right|_{\hat{z}+\Delta\hat{z}} - \left.m_{i,b}\right|_{\hat{z}}}{\Delta\hat{z}}\right)+\ldots \qquad (3.10)$$

$$\ldots+\frac{2\hat{k}''_b}{\hat{r}_A}\left(m_{i,b}-m_{i,A}\right)=0$$

Taking the limit of $\Delta\hat{z}$ going to zero and applying the definition of the derivative shown as

$$f'(x)=\lim_{h\to 0}\frac{f(h)-f(a)}{h} \qquad (3.11)$$

Equation (3.10) arrives at a second-order, homogeneous differential equation describing the rate at which the mass fraction of solute i in the blood decreases as a function of length $\hat{z}$.

$$\frac{d^2m_{i,b}}{d\hat{z}^2}-\left(\frac{\hat{u}_b}{\hat{\wp}_{i,b}}\right)\frac{dm_{i,b}}{d\hat{z}}-\left(\frac{2\hat{k}''_b}{\hat{\rho}_b\hat{\wp}_{i,b}\hat{r}_A}\right)\left(m_{i,b}-m_{i,A}\right)=0 \qquad (3.12)$$

Equation (3.12) can become non-dimensional by using the scaled expression z developed in Section 3.1 shown as $z = \hat{z}/\hat{l}$. Using the scaled expression, Equation (3.12) is transformed to the dimensionless Equation (3.13).

$$\frac{d^2 m_{i,b}}{dz^2} - \left(\frac{\hat{u}_b \hat{l}}{\hat{\wp}_{i,b}}\right)\frac{dm_{i,b}}{dz} + \left(\frac{2\hat{k}''_b \hat{l}^2}{\hat{\rho}_b \hat{\wp}_{i,b} \hat{r}_A}\right)\left(m_{i,A} - m_{i,b}\right) = 0 \qquad (3.13)$$

After further simplification, the equation becomes

$$\frac{d^2 m_{i,b}}{dz^2} - \Omega\frac{dm_{i,b}}{dz} + \Lambda\left(m_{i,A} - m_{i,b}\right) = 0 \qquad (3.14)$$

where two dimensionless parameters are identified

$$\Omega = \frac{\hat{u}_b \hat{l}}{\hat{\wp}_{i,b}} \quad \text{and} \quad \Lambda = \frac{2\hat{k}''_b \hat{l}^2}{\hat{\rho}_b \hat{\wp}_{i,b} \hat{r}_A}$$

For cases when the axial flow rate is large and the diffusive coefficient is small, diffusion in the axial direction can be neglected. This is most clearly demonstrated by calculating the mass transfer Péclet number (Ω) for blood flow through a hollow-fiber. Consider a dialyzer with 11,000 hollow-fibers with an inner diameter of 100 μm, length of 23 cm, and a blood flow rate into the dialyzer of 250 mL/min. The diffusivity of urea in blood using the Stokes-Einstein relation is found to be 2.91×10^{-6} cm/s. The resulting Péclet number is equal to 1.05×10^{8}. For such a large ratio of axial advection to diffusion, it is reasonable to assume axial diffusion contributes very little to toxin transport within the hollow-fiber. Additionally, the term Λ is the product of

the Sherwood number and fiber length divided by the inner radius of the hollow-fiber. Therefore in the absence of axial diffusion, Equation (3.14) reduces to

$$\frac{dm_{i,b}}{dz} + \Phi\left(m_{i,b} - m_{i,A}\right) = 0 \tag{3.15}$$

where

$$\Phi = \frac{2\hat{k}_b \hat{l}}{\hat{u}_b \hat{\rho}_b \hat{r}_A}$$

which is the Sherwood number divided by the mass transfer Péclet number.

3.4 Mass Species Derivation for a Hollow-fiber Membrane

Solute flow through the hollow-fiber membrane is accomplished through a combination of advection and diffusion. An axial slice of the hollow-fiber is drawn in Figure 3.7 with the directions of mass transfer shown. As discussed in Section 3.2, the hollow-fiber membrane layers are assumed to be homogeneous and contain an array of tortuous, cylindrical pores. Within this geometric model, all mass transfer through the membrane will be restricted to the radial direction through the cylindrical pores. Assuming the potential for mass transfer in a radial direction is equal to all radial directions at a given $\hat{z}$ location, mass transfer in the angular direction is neglected.

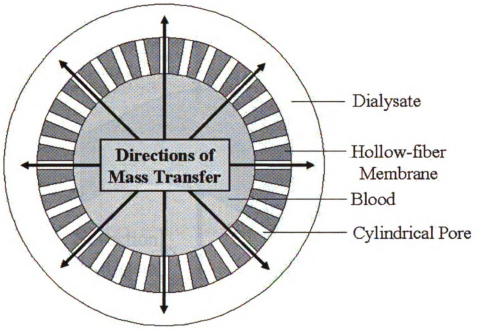

Figure 3.7. Direction of mass transfer through a porous, hollow-fiber membrane is restricted to the radial direction

Mass transfer through the membrane's pores will be a combination of diffusion and advection. These modes are shown for a radial slice of the hollow-fiber membrane in Figure 3.8. Note this figure does not picture any of the membrane pores. The mass species conservation for a hollow-ring element of the membrane can in words be written as

$$\text{Advection}\big|_{\text{IN}} + \text{Diffusion}\big|_{\text{IN}} = \text{Advection}\big|_{\text{OUT}} + \text{Diffusion}\big|_{\text{OUT}}$$

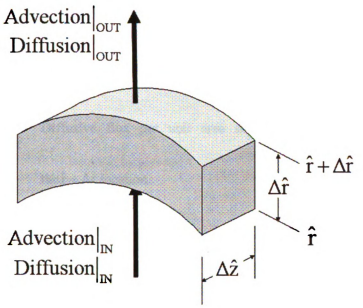

Figure 3.8. Differential element for the membrane

Each term in the conservation can be substituted by its respective mathematical expression with units of mass per time presented as

$$\hat{m}_p\Big|_{\hat{r}}\, m_{i,m}\Big|_{\hat{r}} + \hat{A}_{s,m}\Big|_{\hat{r}}\, \hat{\eta}''_{i,m}\Big|_{\hat{r}} = \hat{m}_p\Big|_{\hat{r}+\Delta\hat{r}}\, m_{i,m}\Big|_{\hat{r}+\Delta\hat{r}} + \ldots + \hat{A}_{s,m}\Big|_{\hat{r}+\Delta\hat{r}}\, \hat{\eta}''_{i,m}\Big|_{\hat{r}+\Delta\hat{r}} \qquad (3.16)$$

Where

$\hat{m}_p\Big|_{\hat{r}}$ Mass flow rate of plasma at the $\hat{r}$ location

$m_{i,m}\Big|_{\hat{r}}$ Mass fraction of solute i in the membrane at location $\hat{r}$

$\hat{A}_{s,m}\Big|_{\hat{r}}$ Membrane surface area at $\hat{r}$

$\hat{\eta}''_{i,m}\Big|_{\hat{r}}$ Diffusive flux per unit area of solute i in the membrane at location $\hat{r}$

$\hat{A}_{s,m}\Big|_{\hat{r}+\Delta\hat{r}}$ Membrane surface area at $\hat{r}+\Delta\hat{r}$

$m_{i,m}\Big|_{\hat{r}+\Delta\hat{r}}$ Mass fraction of solute i in the membrane at the $\hat{r}+\Delta\hat{r}$ location

$\hat{\eta}''_{i,m}\Big|_{\hat{r}+\Delta\hat{r}}$ Diffusive flux per unit area of solute i in the membrane at the $\hat{r}+\Delta\hat{r}$ location.

For all mass to be conserved, the mass flow rate at $\hat{r}$ must be equal to the mass flow rate at $\hat{r}+\Delta\hat{r}$. Therefore, the mass flow rate at any point in the membrane must be equal to the mass flow rate at the inner membrane surface shown as

$$\dot{\hat{m}}_p\Big|_{all\,\hat{r}} = \dot{\hat{m}}_p\Big|_{\hat{r}_A} \tag{3.17}$$

The mass flow rate at the inner surface of the hollow-fiber can be expanded and shown to equal

$$\dot{\hat{m}}_p\Big|_{\hat{r}_A} = \hat{\rho}_p \hat{u}_{pore} \hat{A}_{f,pores} \tag{3.18}$$

where

$\hat{\rho}_p$: density of blood plasma

$\hat{u}_{pore}$: velocity of plasma through a cylindrical pore in the membrane wall

$\hat{A}_{f,pores}$: total area available for plasma flow through inner surface of the hollow-fiber membrane.

The total flow area is defined as the total number of pores per hollow-fiber N_{pores} multiplied by the area of a single pore $\hat{A}_{pore}$.

$$\hat{A}_{f,pores} = N_{pores}\hat{A}_{pore} \tag{3.19}$$

Substitution of the definitions into Equation (3.16) results in

$$\begin{aligned}&\hat{\rho}_p \hat{u}_{pore} N_{pores} \hat{A}_{pore} m_{i,m}\Big|_{\hat{r}} + \hat{A}_{s,m}\Big|_{\hat{r}} \hat{\eta}''_{i,m}\Big|_{\hat{r}} = \ldots \\ &\ldots = \hat{\rho}_p \hat{u}_{pore} N_{pores} \hat{A}_{pore} m_{i,m}\Big|_{\hat{r}+\Delta\hat{r}} + \hat{A}_{s,m}\Big|_{\hat{r}+\Delta\hat{r}} \hat{\eta}''_{i,m}\Big|_{\hat{r}+\Delta\hat{r}}\end{aligned} \tag{3.20}$$

Dividing by the inner surface area of the membrane slice $\hat{A}_{s,m}\Big|_{\hat{r}}$, equation (3.16) reduces to

$$\begin{aligned}&\frac{\hat{\rho}_p \hat{u}_{pore} N_{pores} \hat{A}_{pore}}{\hat{A}_{s,m}\Big|_{\hat{r}}} m_{i,m}\Big|_{\hat{r}} + \hat{\eta}''_{i,m}\Big|_{\hat{r}} = \ldots \\ &\ldots = \frac{\hat{\rho}_p \hat{u}_{pore} N_{pores} \hat{A}_{pore}}{\hat{A}_{s,m}\Big|_{\hat{r}}} m_{i,m}\Big|_{\hat{r}+\Delta\hat{r}} + \frac{\hat{A}_{s,m}\Big|_{\hat{r}+\Delta\hat{r}}}{\hat{A}_{s,m}\Big|_{\hat{r}}} \hat{\eta}''_{i,m}\Big|_{\hat{r}+\Delta\hat{r}}\end{aligned} \tag{3.21}$$

After inspection, a ratio of the total pore area to the inner surface area of the hollow-fiber membrane appears on both sides of the equation. This ratio will be defined as the area based porosity of the hollow-fiber ε_A.

$$\begin{aligned}\hat{\rho}_p \hat{u}_{pore} \varepsilon_{area} m_{i,m}\Big|_{\hat{r}} + \hat{\eta}''_{i,m}\Big|_{\hat{r}} &= \hat{\rho}_p \hat{u}_{pore} \varepsilon_{area} m_{i,m}\Big|_{\hat{r}+\Delta\hat{r}} + \ldots \\ &\ldots + \frac{\hat{A}_{s,m}\Big|_{\hat{r}+\Delta\hat{r}}}{\hat{A}_{s,m}\Big|_{\hat{r}}} \hat{\eta}''_{i,m}\Big|_{\hat{r}+\Delta\hat{r}}\end{aligned} \tag{3.22}$$

where,

$$\varepsilon_A = \frac{N_{pores}\hat{A}_{pore}}{\hat{A}_{s,m}\Big|_{\hat{r}}} \tag{3.23}$$

The diffusive flux term in Equation (3.22) can be substituted using Fick's Law for diffusion where $\hat{n}$ is the location of the diffusive term and $\hat{\wp}_{i,m}$ is the apparent diffusion coefficient of solute i in the membrane.

$$\hat{\eta}''_{i,m}\Big|_{\hat{n}} = -\hat{\rho}_p \hat{\wp}_{i,m} \frac{dm_i}{d\hat{r}}\Big|_{\hat{n}} \tag{3.24}$$

$$\begin{aligned}\hat{\rho}_p \hat{u}_{pore} \varepsilon_A m_{i,m}\Big|_{\hat{r}} - \hat{\rho}_p \hat{\wp}_{i,m} \frac{dm_i}{d\hat{r}}\Big|_{\hat{r}} = \hat{\rho}_p \hat{u}_{pore} \varepsilon_A m_{i,m}\Big|_{\hat{r}+\Delta\hat{r}} - \ldots \\ \ldots - \left(1 - \frac{\Delta r}{r}\right)\hat{\rho}_p \hat{\wp}_{i,m} \frac{dm_i}{d\hat{r}}\Big|_{\hat{r}+\Delta\hat{r}}\end{aligned} \tag{3.25}$$

The density of plasma, $\hat{\rho}_p$ with and change in radius, $\Delta\hat{r}$, are divided through Equation (3.25). Doing so, three fundamental definitions are formed in the equation.

$$\begin{aligned}\wp_{i,m}\left[\left(\frac{\frac{dm_i}{d\hat{r}}\Big|_{\hat{r}} - \frac{dm_i}{d\hat{r}}\Big|_{\hat{r}+\Delta\hat{r}}}{\Delta\hat{r}}\right) - \frac{1}{\hat{r}}\frac{dm_i}{d\hat{r}}\Big|_{\hat{r}+\Delta\hat{r}}\right] + \ldots \\ \ldots + \hat{u}_{pore}\varepsilon_A\left(\frac{m_{i,m}\Big|_{\hat{r}+\Delta\hat{r}} - m_{i,m}\Big|_{\hat{r}}}{\Delta\hat{r}}\right) = 0\end{aligned} \tag{3.26}$$

Taking the limit of $\Delta\hat{z}$ going to zero, applying the definition of the derivative, and dividing by the diffusivity of solute i in the hollow-fiber membrane, Equation (3.26) becomes

$$\frac{d^2 m_i}{d\hat{r}^2} + \frac{1}{\hat{r}}\frac{dm_i}{d\hat{r}} = \left(\frac{\hat{u}_{pore}\varepsilon_A}{\hat{\wp}_{i,m}}\right)\frac{dm_i}{d\hat{r}} \tag{3.27}$$

Equation (3.27) can be non-dimensionalized by introducing the scaled radial expression r where $\hat{r}_A$ is the inner radius of the hollow-fiber membrane.

$$r = \hat{r} / \hat{r}_A$$

After substitution, Equation (3.27) becomes a second-order, variable coefficient, homogeneous differential equation describing the rate at which the mass fraction of solute i decreases as a function of scaled radial distance.

$$\frac{d^2 m_{i,m}}{dr^2} + \frac{1}{r}\frac{dm_{i,m}}{dr} = \Psi_m \frac{dm_{i,m}}{dr} \tag{3.28}$$

where

$$\Psi_m = \frac{\hat{u}_{pore}\varepsilon_A \hat{r}_A}{\hat{\wp}_{i,m}}$$

3.5 Mass Species Derivation for Dialysate

Dialysate flow and toxin transport on the outer surface of each hollow-fiber can be described mathematically in a fashion very similar to the blood flow species conservation development by describing the conservation of mass for a differential volume. A sketch of the differential volume is shown in Figure 3.9. The dialysate element contains two inflows and one outflow. The inflow is comprised of a combination of advection, diffusion, and convection; while the outflow consists of advection and diffusion. The resulting conservation of mass described in words can be written as

$$\text{Advection}|_{IN} + \text{Diffusion}|_{IN} + \text{Convection}|_{IN} = \text{Advection}|_{OUT} + \text{Diffusion}|_{OUT}$$

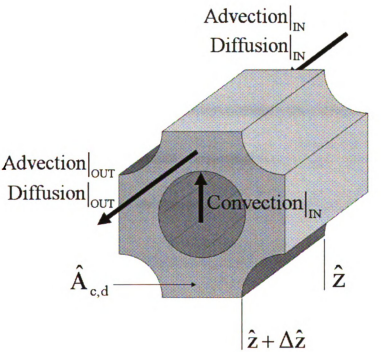

Figure 3.9. Dialysate volume with directions of mass transfer indicated

Each term in the conservation equation can be represented by its respective mathematical expression with units of mass per time presented as

$$\hat{\dot{m}}_d \, m_{i,d}\Big|_{\hat{z}} + \hat{A}_{c,d} \, \hat{\dot{\eta}}''_{i,d}\Big|_{\hat{z}} + \hat{A}_{s,d} \, \hat{\dot{k}}''_d \left(m_{i,C} - m_{i,d} \right) = \ldots$$
$$\ldots = \hat{\dot{m}}_d \, m_{i,d}\Big|_{\hat{z}+\Delta\hat{z}} + \hat{A}_{c,d} \, \hat{\dot{\eta}}''_{i,d}\Big|_{\hat{z}+\Delta\hat{z}} \tag{3.29}$$

where,

$\hat{\dot{m}}_d$ bulk dialysate mass flow rate

$m_{i,d}\Big|_{\hat{z}}$ mass fraction of solute i in the dialysate at location $\hat{z}$

$\hat{A}_{c,d}$ cross-sectional flow area available to dialysate

$\hat{\dot{\eta}}''_{i,d}\Big|_{z}$ diffusive flux of solute i at location $\hat{z}$,

$\hat{A}_{s,d}$ inner surface area of the dialysate volume bounded by $\hat{r}_C$,

$\hat{\dot{k}}''_d$ dialysate convective coefficient per unit area,

$m_{i,C}$ mass fraction of solute i at r_C,

$m_{i,d}$ bulk mass fraction of solute i in the dialysate,

$m_{i,d}\Big|_{\hat{z}+\Delta\hat{z}}$ mass fraction of solute i in the dialysate at the $\hat{z}+\Delta\hat{z}$ location

$\hat{\dot{\eta}}''_{i,d}\Big|_{\hat{z}+\Delta\hat{z}}$ diffusive flux of solute i in dialysate at the $\hat{z}+\Delta\hat{z}$ location.

Since all mass is conserved, the mass flow rate into the volume will be equal to the mass flow rate out of the volume. This term can be expanded and shown to equate to

$$\hat{\dot{m}}_d = \hat{\rho}_d \hat{u}_d \hat{A}_{c,d} \tag{3.30}$$

where

$\hat{\rho}_d$: density of the dialysate

$\hat{u}_d$: area-averaged velocity of dialysate.

Equation (3.29) is expanded as follows

$$\begin{aligned} \hat{\rho}_d \hat{u}_d \hat{A}_{c,d} m_{i,d}\Big|_{\hat{z}} + \hat{A}_{c,d} \hat{\dot{\eta}}''_{i,d}\Big|_{\hat{z}} + \hat{\dot{k}}''_d \hat{A}_{s,d}\left(m_{i,C} - m_{i,d}\right) = \ldots \\ \ldots = \hat{\rho}_d \hat{u}_d \hat{A}_{c,d} m_{i,d}\Big|_{\hat{z}+\Delta\hat{z}} + \hat{A}_{c,d} \hat{\dot{\eta}}''_{i,d}\Big|_{\hat{z}+\Delta\hat{z}} \end{aligned} \tag{3.31}$$

After dividing Equation (3.31) by the cross-sectional area and the differential length $\Delta\hat{z}$, the mass balance can be shown to equal

$$\begin{aligned} \left(\frac{\hat{\dot{\eta}}''_{i,d}\Big|_{\hat{z}+\Delta\hat{z}} - \hat{\dot{\eta}}''_{i,d}\Big|_{\hat{z}}}{\Delta\hat{z}}\right) + \hat{\rho}_d \hat{u}_d \left(\frac{m_{i,d}\Big|_{\hat{z}+\Delta\hat{z}} - m_{i,d}\Big|_{\hat{z}}}{\Delta\hat{z}}\right) + \ldots \\ \ldots + \frac{\hat{\dot{k}}''_d \hat{A}_{s,d}}{\Delta\hat{z}\,\hat{A}_{c,d}}\left(m_{i,d} - m_{i,C}\right) = 0 \end{aligned} \tag{3.32}$$

The diffusive flux term is replaced by Equation (3.32) where $\hat{n}$ is the applied location and $\hat{\wp}_{i,d}$ is the diffusion coefficient of solute i in the dialysate.

$$\hat{\dot{\eta}}''_{i,d}\Big|_{\hat{n}} = -\hat{\rho}_d \hat{\wp}_{i,d} \frac{dm_{i,d}}{d\hat{z}}\Big|_{\hat{n}} \tag{3.33}$$

After substitution, the resulting expression is as follows.

$$-\hat{\rho}_d\hat{\wp}_{i,d}\left(\frac{\left.\frac{dm_{i,d}}{d\hat{z}}\right|_{\hat{z}+\Delta\hat{z}}-\left.\frac{dm_{i,d}}{d\hat{z}}\right|_{\hat{z}}}{\Delta\hat{z}}\right)+\hat{\rho}_d\hat{u}_d\left(\frac{m_{i,d}\big|_{\hat{z}+\Delta\hat{z}}-m_{i,d}\big|_{\hat{z}}}{\Delta\hat{z}}\right)+\ldots$$
$$\ldots+\frac{\hat{k}''_d\hat{A}_{s,d}}{\Delta\hat{z}\hat{A}_{c,d}}\left(m_{i,d}-m_{i,C}\right)=0 \qquad (3.34)$$

By applying the definition of a derivative, Equation (3.34) arrives at a second-order, homogeneous differential equation describing the rate at which the mass fraction of solute i in the dialysate increases as a function of length $\hat{z}$, Equation (3.35).

$$\frac{d^2m_{i,d}}{d\hat{z}^2}-\left(\frac{\hat{u}_d}{\hat{\wp}_{i,d}}\right)\frac{dm_{i,d}}{d\hat{z}}-\left(\frac{\hat{k}''_d\hat{A}_{s,d}}{\hat{\rho}_d\hat{\wp}_{i,d}\Delta\hat{z}\hat{A}_{c,d}}\right)\left(m_{i,d}-m_{i,C}\right)=0 \qquad (3.35)$$

Using the same scaled expression z defined during the blood mass balance, Equation (3.35) transforms into the dimensionless expression of

$$\frac{d^2m_{i,d}}{dz^2}-\left(\frac{\hat{u}_d\hat{l}}{\hat{\wp}_{i,d}}\right)\frac{dm_{i,d}}{dz}+\left(\frac{\hat{k}''_d\hat{A}_{s,d}\hat{l}^2}{\hat{\rho}_d\hat{\wp}_{i,d}\Delta\hat{z}\hat{A}_{c,d}}\right)\left(m_{i,C}-m_{i,d}\right)=0 \qquad (3.36)$$

Equation (3.36) can be further simplified to

$$\frac{d^2m_{i,d}}{dz^2}-\Theta\frac{dm_{i,d}}{dz}+\zeta\left(m_{i,C}-m_{i,d}\right)=0 \qquad (3.37)$$

where

$$\Theta = \left(\frac{\hat{u}_d \hat{l}}{\hat{\wp}_{i,d}} \right) \quad \text{and} \quad \zeta = \left(\frac{\hat{k}''_d \hat{A}_{s,d} \hat{l}^2}{\hat{\rho}_d \hat{\wp}_{i,d} \Delta\hat{z} \hat{A}_{c,d}} \right)$$

For cases when the axial flow rate is large and the diffusive coefficient is small, diffusion in the axial direction can be neglected. As demonstrated in Section 3.3, the Péclet Number for blood flow in the hollow-fibers is very large. Likewise, the Péclet Number for the flow of dialysate around a hollow fiber is 3.36×10^6. Therefore, in the absence of axial diffusion, Equation (3.37) reduces to

$$\frac{dm_{i,d}}{dz} + \Gamma\left(m_{i,d} - m_{i,C} \right) = 0 \tag{3.38}$$

where,

$$\Gamma = \frac{\hat{k}''_d \hat{A}_{s,d} \hat{l}}{\hat{\rho}_d \hat{u}_d \Delta\hat{z} \hat{A}_{c,d}}$$

3.6 Boundary Conditions

The boundary conditions for a homogeneous and asymmetric membrane are now developed. The boundary conditions for a homogeneous membrane are found to be a special case of the conditions found in the asymmetric membrane. For an asymmetric membrane, a boundary condition exists at all three interfaces A, B, and C as seen in Figure 3.5. For a homogeneous membrane, a boundary condition exists only at

interfaces A and C. The boundary conditions are developed based on the mass balance at each interface written in words to the right of Figure 3.10.

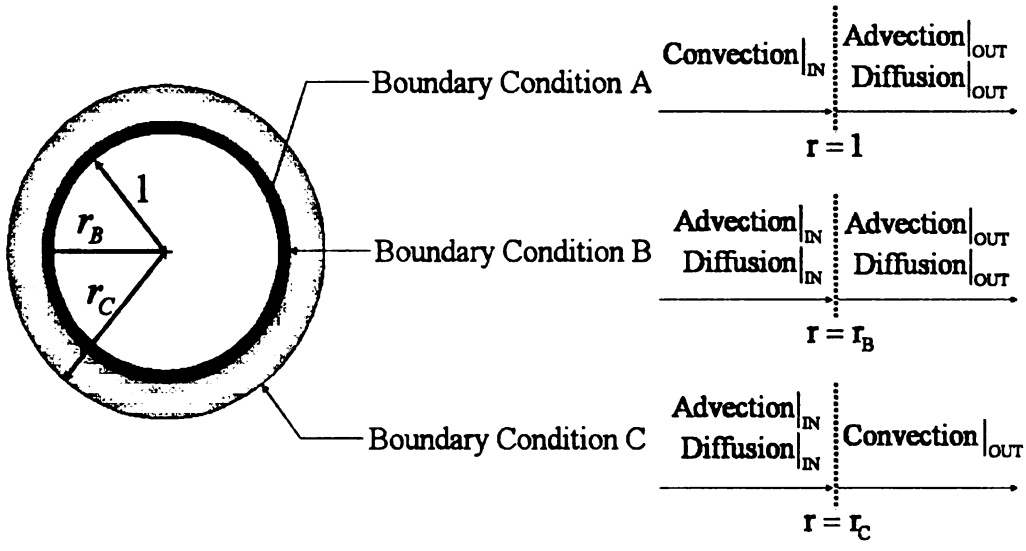

Figure 3.10. Boundary conditions for an asymmetric membrane at r=1,r=r_B, and r=r_C

At r=1, the non-homogeneous boundary condition is the convection from the blood-side equal to the advection and diffusion in the membrane skin. This balance is mathematically shown by

$$\hat{k}''_b \hat{A}_{s,m}\Big|_{r=1}\left(m_{i,b} - m_{i,1}\right) = \hat{\dot{m}} m_{i,1} + \hat{A}_{s,m}\Big|_{r=1} \hat{\eta}''_{i,m}\Big|_{r=1} \tag{3.39}$$

Substituting for the diffusive flux, mass flow rate, dividing by the inner membrane surface area, scaling the dimensional radius, and grouping the mass fractions; the boundary condition shortens to

$$m_{i,b} = \left(1 + \frac{\hat{\rho}_p \hat{u}_{pore,ms} \varepsilon_{area,ms}}{\hat{k}''_b}\right) m_{i,1} - \left(\frac{\hat{\rho}_p \hat{\varphi}_{i.ms}}{\hat{k}''_b \hat{r}_A}\right) \frac{dm_i}{dr}\Big|_{r=1} \tag{3.40}$$

Two new non-dimensional terms are defined as

$$\alpha = \left(1 + \frac{\hat{\rho}_p \hat{u}_{pore,ms} \varepsilon_{area,ms}}{\hat{k}''_b} \right) \quad \text{and} \quad \beta = \left(\frac{\hat{\rho}_p \hat{\varphi}_{i.ms}}{\hat{k}''_b \hat{r}_A} \right)$$

Simplifying the boundary condition at r=1 to

$$m_{i,b} = \alpha\, m_{i,1} - \beta \left. \frac{dm_i}{dr} \right|_{r=1} \tag{3.41}$$

At $r=r_B$, the non-homogeneous boundary condition is the advection and diffusion from the membrane skin layer equal to the advection and diffusion in the membrane porous support. This balance is mathematically shown by

$$\begin{aligned} \hat{\dot{m}}_{p,ms} m_{i,ms}\Big|_{r=r_B} + \hat{A}_{s,B} \hat{\dot{\eta}}''_{i,ms}\Big|_{r=r_B} &= \hat{\dot{m}}_{p,ps} m_{i,ps}\Big|_{r=r_B} + \ldots \\ &\ldots + \hat{A}_{s,B} \hat{\dot{\eta}}''_{i,ps}\Big|_{r=r_B} \end{aligned} \tag{3.42}$$

A matching condition for the mass fraction in the membrane skin and porous support at $r=r_B$ can be used shown by

$$m_{i,ms}\Big|_{r=r_B} = m_{i,ps}\Big|_{r=r_B} = m_{i,B} \tag{3.43}$$

Substituting for the diffusive fluxes, mass flow rates, dividing by surface area at $r=r_B$, scaling the dimensional radius, and grouping the like terms; the boundary condition shortens to

$$m_{i,B}\left(\hat{u}_{pore,ms}\varepsilon_{area,ms}-\hat{u}_{pore,ps}\varepsilon_{area,ps}\right)+\ldots$$
$$\ldots+\left.\frac{dm_{i,ps}}{dr}\right|_{r=r_B}\left(\frac{\hat{\wp}_{i,ps}}{\hat{r}_A}\right)=\left.\frac{dm_{i,ms}}{dr}\right|_{r=r_B}\left(\frac{\hat{\wp}_{i,ms}}{\hat{r}_A}\right) \tag{3.44}$$

Additional non-dimensional terms are defined as

$$\varsigma=\hat{r}_A\frac{\hat{u}_{pore,ms}\varepsilon_{area,ms}-\hat{u}_{pore,ps}\varepsilon_{area,ps}}{\hat{\wp}_{i,ms}}\qquad\lambda=\frac{\hat{\wp}_{i,ps}}{\hat{\wp}_{i,ms}}$$

Simplifying the boundary condition at $r=r_B$ to

$$\varsigma m_{i,B}+\lambda\left.\frac{dm_{i,ps}}{dr}\right|_{r=r_B}=\left.\frac{dm_{i,ms}}{dr}\right|_{r=r_B} \tag{3.45}$$

At $r=r_C$, the non-homogeneous boundary condition is the advection and diffusion from the membrane porous support equal to the convection into the dialysate. This balance is mathematically shown by

$$\hat{\dot{m}}m_{i,C}+\hat{A}_{s,m}\Big|_{r_C}\hat{\eta}''_{i,m}\Big|_{r_C}=\hat{k}''_d\hat{A}_{s,m}\Big|_{r_C}\left(m_{i,C}-m_{i,d}\right) \tag{3.46}$$

After substitution of the diffusive flux, mass flow rate, dividing by the surface area, scaling the radial component, and grouping the like terms the boundary condition arrives to

$$m_{i,d}=m_{i,C}\left(1-\frac{\hat{\rho}_p\hat{u}_{pore,ps}\varepsilon_{area,ps}}{\hat{k}''_d}\right)+\left(\frac{\hat{\rho}_p\hat{\wp}_{i.ps}}{\hat{k}''_d\hat{r}_A}\right)\left.\frac{dm_i}{dr}\right|_{r_C} \tag{3.47}$$

with non-dimensional terms defined as

$$\chi = \left(1 - \frac{\hat{\rho}_p \hat{u}_{pore.ps} \varepsilon_{area,ps}}{\hat{k}''_d} \right) \quad \text{and} \quad \kappa = \left(\frac{\hat{\rho}_p \hat{\wp}_{i.ps}}{\hat{k}''_d \hat{r}_A} \right)$$

Equation 3.47 reduces to

$$m_{i,d} = \chi m_{i,C} + \kappa \left. \frac{dm_i}{dr} \right|_{r_C} \tag{3.48}$$

3.7 Summary of Mass Species Conservation Equations and Boundary Conditions

The mass species conservation equations derived for the blood, membrane, and dialysate volumes are presented in several summary tables. Table 3.1 presents two equations for the mass species conservation equations for the blood volume. The first equation is a second-order, homogeneous differential equation describes the mass species decrease in blood as function of axial distance with diffusion and convection. The second equation is a first order, homogeneous differential equation describing the mass species decrease as a function of axial distance neglecting diffusion in the axial direction.

Table 3.1 Summary of the blood mass species conservation equations

Equation Description	Mathematical Formulation	Non-dimensional Constants
Mass species decrease as a function of axial distance with diffusion and convection	$\frac{d^2 m_{i,b}}{dz^2} - \Omega \frac{dm_{i,b}}{dz} + \Lambda\left(m_{i,A} - m_{i,b}\right) = 0$	$\Omega = \frac{\hat{u}_b \hat{l}}{\hat{\wp}_{i,b}}$ $\Lambda = \frac{2\hat{k}''_b \hat{l}^2}{\hat{\rho}_b \hat{\wp}_{i,b} \hat{r}_A}$
Mass species decrease as a function of axial distance neglecting diffusion	$\frac{dm_{i,b}}{dz} + \Phi\left(m_{i,b} - m_{i,A}\right) = 0$	$\Phi = \frac{2\hat{k}''_b \hat{l}}{\hat{u}_b \hat{\rho}_b \hat{r}_A}$
Initial Condition	$m_{i,b}\Big\|_{z=0}$ =Patient's Initial Toxin Mass Fraction	n/a

Table 3.2 presents the mass species conservation equation for a membrane. The equation in the table is second-order, variable coefficient, homogeneous differential equation describing the rate at which the mass fraction of solute i decreases as a function of scaled radial distance.

Table 3.2 Summary of the membrane mass species conservation equation

Equation Description	Mathematical Formulation	Non-dimensional Constant
Mass species decrease as a function of radial distance with diffusion and convection	$\frac{d^2 m_{i,m}}{dr^2} + \frac{1}{r}\frac{dm_{i,m}}{dr} = \Psi_m \frac{dm_{i,m}}{dr}$	$\Psi_m = \frac{\hat{u}_{pore,m} \varepsilon_{area,m} \hat{r}_A}{\hat{\wp}_{i,m}}$

Table 3.3 presents two equations for the mass species conservation equations for the dialysate volume. The first equation is a second-order, homogeneous differential equation describing the mass species increase in dialysate as function of axial distance with diffusion and convection. The second equation is a first order, homogeneous differential equation describing the mass species increase as a function of axial distance neglecting diffusion in the axial direction.

Table 3.3 Summary of the dialysate mass species conservation equations

Equation Description	Mathematical Formulation	Non-dimensional Constants
Mass species increase as a function of axial distance with diffusion and convection	$\frac{d^2 m_{i,d}}{dz^2} - \Theta \frac{dm_{i,d}}{dz} + \zeta\left(m_{i,C} - m_{i,d}\right) = 0$	$\Theta = \left(\frac{\hat{u}_d \hat{l}}{\hat{\varphi}_{i,d}}\right)$ $\zeta = \left(\frac{\hat{k}''_d \hat{A}_{s,d} \hat{l}^2}{\hat{\rho}_d \hat{\varphi}_{i,d} \Delta\hat{z} \hat{A}_{c,d}}\right)$
Mass species decrease as a function of axial distance neglecting diffusion	$\frac{dm_{i,d}}{dz} + \Gamma\left(m_{i,d} - m_{i,C}\right) = 0$	$\Gamma = \frac{\hat{k}''_d \hat{A}_{s,d} \hat{l}}{\hat{\rho}_d \hat{u}_d \Delta\hat{z} \hat{A}_{c,d}}$
Initial Condition	$m_{i,d}\big\|_{z=1} = 0$ or User Defined Value	n/a

The membrane interface boundary conditions are summarized in Table 3.4. These boundary conditions represent the interfaces contained in an asymmetric membrane including interface A at $r=r_A$, interface B at $r=r_B$, and interface C at $r=r_C$.

Figure 3.4 Summary of the membrane boundary conditions

Boundary Condition at Interface	Mathematical Formulation	Non-dimensional Constants
A	$m_{i,b} = \alpha\, m_{i,1} - \beta \left.\frac{dm_i}{dr}\right\|_{r=1}$	$\alpha = \left(1 + \frac{\hat{\rho}_p \hat{u}_{pore,ms}\, \varepsilon_{area,ms}}{\hat{k}''_b}\right)$ $\beta = \left(\frac{\hat{\rho}_p \hat{\varphi}_{i.ms}}{\hat{k}''_b \hat{r}_A}\right)$
B	$\varsigma m_{i,B} + \lambda \left.\frac{dm_{i,ps}}{dr}\right\|_{r=r_B} = \ldots$ $\ldots = \left.\frac{dm_{i,ms}}{dr}\right\|_{r=r_B}$	$\varsigma = \hat{r}_A \frac{\hat{u}_{pore,ms}\, \varepsilon_{area,ms}}{\hat{\varphi}_{i,ms}} - \ldots$ $\ldots - \frac{\hat{u}_{pore,ps}\, \varepsilon_{area,ps}}{\hat{\varphi}_{i,ms}}$ $\lambda = \frac{\hat{\varphi}_{i,ps}}{\hat{\varphi}_{i,ms}}$
C	$m_{i,d} = \chi\, m_{i,C} + \kappa \left.\frac{dm_i}{dr}\right\|_{r_C}$	$\chi = \left(1 - \frac{\hat{\rho}_p \hat{u}_{pore.ps}\, \varepsilon_{area,ps}}{\hat{k}''_d}\right)$ $\kappa = \left(\frac{\hat{\rho}_p \hat{\varphi}_{i.ps}}{\hat{k}''_d \hat{r}_A}\right)$

Chapter 4
Method of Solution

The key piece of information needed to reach the modeling goals set in Section 1.2 is the blood toxin mass fraction at the dialyzer's blood exit. This information is reached by coupling an analytical solution for mass transport in the membrane to numerical solutions of the blood and dialysate equations. This coupling allows the mass fraction of a toxin at the blood and dialysate exits to be found at distinct time intervals leading to the prediction for total treatment time and the toxin clearance. A numerical approach was chosen over an analytical solution to simplify the computer simulation developed later.

4.1 Numerical Solution for the Blood Mass Species Equation

The purpose of this analysis is to transform the partial-differential Equation (3.14) into a linear, algebraic equation by partitioning the blood volume into discretized elements. The control volume is depicted in Figure 4.1. Since the potential for mass transfer in the radial direction is assumed to be constant regardless of angular orientation, only a one-dimensional, discretized field is shown. The field is partitioned into a number of mesh nodes at both the control volume centerline and outer surface. Nodes at the centerline represent the average toxin mass fraction in each control volume while the nodes at the outer surface represent the mass fraction at the inner surface of the hollow-fiber membrane. An equation is now developed and applied at each mesh node within the grid for a given spacing and frequency to

determine how the mass fraction of solute i decreases with axial distance in the blood volume.

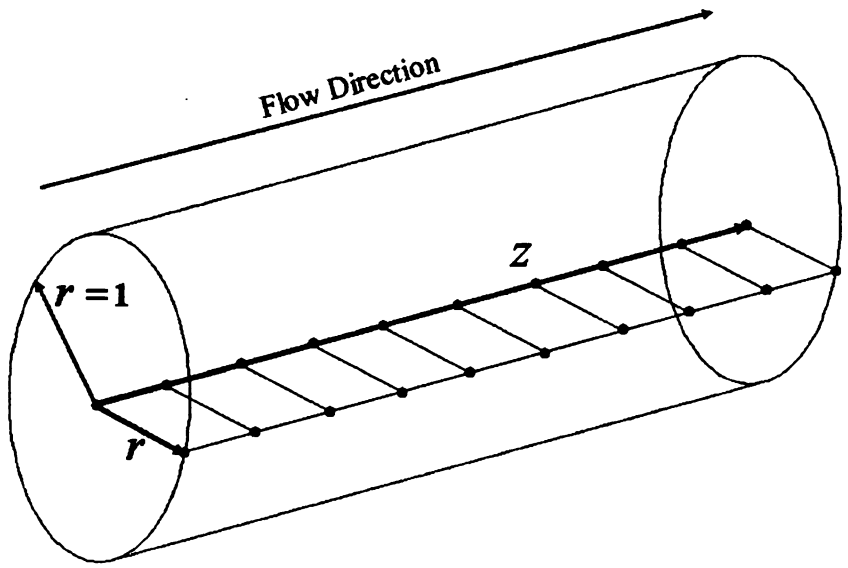

Figure 4.1. The radial and axial directions are discretized to form a grid containing intersecting points

The grid is spaced in intervals of Δz. The value of Δz depends on the desired number of mesh nodes for analysis. As will be tested in the Results and Discussion, for a greater number of mesh nodes, the more accurate the solution should be. The one-dimensional, mesh node grid is drawn in Figure 4.2.

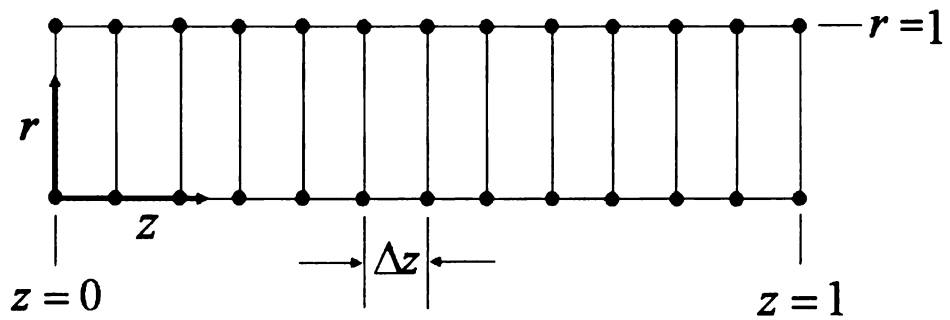

Figure 4.2. A two-dimensional mesh for the blood volume

The numerical analysis will utilize a first-order, central-differencing approach in the z-direction for diffusion and a first-order, forward-differencing approach in the z-direction for advection. Each of these expressions are shown as

$$\frac{\partial^2 m_{i,b}}{\partial z^2} = \frac{m_{i,b}^{j-1} - 2m_{i,b}^{j} + m_{i,b}^{j+1}}{(\Delta z)^2} \qquad \frac{\partial m_{i,b}}{\partial z} = \frac{m_{i,b}^{j+1} - m_{i,b}^{j}}{\Delta z}$$

Referring to Figure 4.3, the j superscript on each $m_{i,b}$ indicates their position relative to a reference node $m_{i,b}^{j}$. Where j is in the axial-direction and the subscript i,b indicates solute i in the blood b.

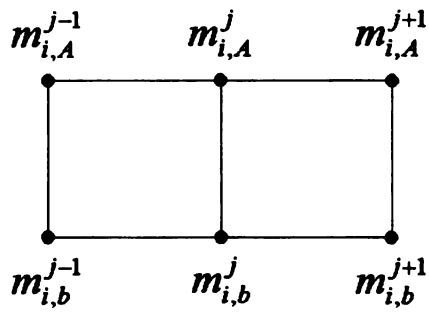

Figure 4.3. Diagram of the indicial notation for each of the grid nodes where *j* is the axial position and *A* is the radial position at $r=r_A$

Substituting the central and forward-differencing expressions into the conservation of mass species equation for the blood (Equation (3.14)) constructs the linear, algebraic equation of

$$\frac{m_{i,b}^{j-1} - 2m_{i,b}^{j} + m_{i,b}^{j+1}}{(\Delta z)^2} - \Omega \frac{m_{i,b}^{j+1} - m_{i,b}^{j}}{\Delta z} + \Lambda\left(m_{i,A}^{j} - m_{i,b}^{j}\right) = 0 \qquad (4.1)$$

Rearranging terms, the explicit form of Equation (4.1) is written as

$$m_{i,b}^{j+1} = \frac{m_{i,b}^{j-1}\left(\frac{1}{(\Delta z)^2}\right) + m_{i,b}^{j}\left(\Lambda + \frac{2}{(\Delta z)^2} - \frac{\Omega}{\Delta z}\right) - m_{i,A}^{j}(\Lambda)}{\left(\frac{1}{(\Delta z)^2} - \frac{\Omega}{\Delta z}\right)} \qquad (4.2)$$

In the absence of axial diffusion, Equation (4.1) is written as

$$m_{i,b}^{j+1} = \Delta z \Phi\left(m_{i,A}^{j} - m_{i,b}^{j}\right) + m_{i,b}^{j} \qquad (4.3)$$

Equations (4.2) and (4.3) are valid for all of the axial nodes in the blood volume. For the node at j=0, an initial condition is required. At the beginning of the hemodialysis treatment, $m_{i,b}^{1}$ will be equal to the initial mass fraction of the toxin at the start of treatment. As the treatment progresses, this value will change as a function of time. After all of the body's blood has been passed through the dialyzer and whose toxin mass fraction is decreased to a new value. The new value is used as the initial mass fraction for the second pass of the body's blood volume through the dialyzer. A summary of the equations and initial conditions derived in this section are shown in Table 4.1.

Table 4.1 Summary of the numerical solution for the blood volume

Equation Description	Mathematical Formulation
Mass species decrease as a function of axial distance j with diffusion and convection (Explicit Form)	$m_{i,b}^{j+1} = \dfrac{m_{i,b}^{j-1}\left(\dfrac{1}{(\Delta z)^2}\right) + m_{i,b}^{j}\left(\Lambda + \dfrac{2}{(\Delta z)^2} - \dfrac{\Omega}{\Delta z}\right) - m_{i,A}^{j}(\Lambda)}{\left(\dfrac{1}{(\Delta z)^2} - \dfrac{\Omega}{\Delta z}\right)}$
Initial condition for mass species decrease with diffusion and convection for j=0	$m_{i,b}^{1} = m_{i,b}^{-1}$ = initial body blood volume mass fraction before treatment or the mass fraction in blood at the end of one full pass of the body's blood through the dialyzer
Mass species decrease as a function of axial distance j neglecting diffusion	$m_{i,b}^{j+1} = \Delta z \Phi\left(m_{i,A}^{j} - m_{i,b}^{j}\right) + m_{i,b}^{j}$
Initial Condition at j=0	$m_{i,b}^{1}$ = initial body blood volume mass fraction before treatment or $m_{i,b}^{1}$ = mass fraction at the end of one full pass of the body's blood through the dialyzer

4.2 Numerical Solution for the Dialysate Mass Species Equation

A numerical solution to the partial-differential Equation (3.37) describing the mass transport of the toxin in dialysate as it passes over a hollow fiber is determined. The control volume is depicted in Figure 4.4. The field is partitioned into differential elements in the axial direction with a discretized length of Δz. An equation is now developed and applied at each node within the grid for a given spacing and frequency to determine the how the mass fraction of solute i increases with axial distance in the dialysate volume.

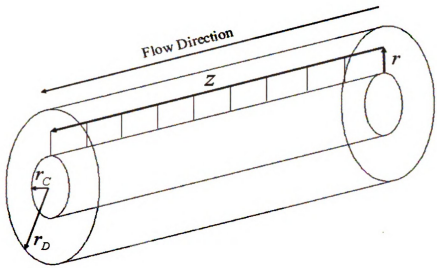

Figure 4.4. The radial and axial directions are discretized to form a grid containing intersecting points

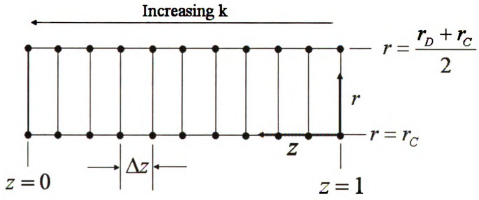

Figure 4.5. The radial and axial directions are discretized to form a grid containing intersecting points

The numerical analysis will utilize a first-order, central-differencing approach in the z-direction for diffusion and a first-order, forward-differencing method in the z-direction for advection. Each of these expressions are shown as

$$\frac{\partial^2 m_{i,d}}{\partial z^2} = \frac{m_{i,d}^{k-1} - 2m_{i,d}^{k} + m_{i,d}^{k+1}}{(\Delta z)^2} \qquad \frac{\partial m_{i,d}}{\partial z} = \frac{m_{i,d}^{k+1} - m_{i,d}^{k}}{\Delta z}$$

Referring to Figure 4.6, the k superscript on each $m_{i,d}$ indicates their position relative to a reference node $m^{k}_{i,d}$. Where k is in the axial-direction and the subscript i,d indicates solute *i* in the dialysate d. Note that the k-direction is opposite to the j-direction used in the numerical solution to the blood flow.

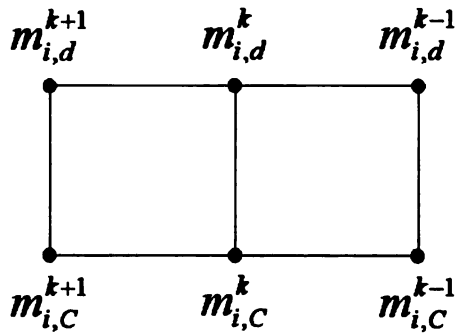

Figure 4.6. Diagram of the indicial notation for each of the grid nodes where *k* is the axial position and *C* is the radial position at $r=r_C$

Substituting the central and forward-differencing expressions into Equation (3.37) constructs the linear algebraic equation of

$$\frac{m^{k-1}_{i,d} - 2m^{k}_{i,d} + m^{k+1}_{i,d}}{(\Delta z)^2} - \Theta\frac{m^{k+1}_{i,d} - m^{k}_{i,d}}{\Delta z} + \zeta\left(m^{k}_{i,C} - m^{k}_{i,d}\right) = 0 \qquad (4.4)$$

Rearranging terms, the explicit form of Equation (4.4) is written as

$$m^{k+1}_{i,d} = \frac{m^{k-1}_{i,d}\left(\frac{1}{(\Delta z)^2}\right) + m^{k}_{i,d}\left(\zeta + \frac{2}{\Delta z} - \frac{\Theta}{\Delta z}\right) - m^{k}_{i,C}(\zeta)}{\left(\frac{1}{(\Delta z)^2} - \frac{\Theta}{\Delta z}\right)} \qquad (4.5)$$

In the absence of diffusion, Equation (4.4) is simplified to

$$m_{i,d}^{k+1} = \Delta z \Gamma \left(m_{i,C}^{k} - m_{i,d}^{k} \right) + m_{i,d}^{k} \tag{4.6}$$

Equations (4.5) and (4.6) are valid for all of the axial nodes in the dialysate volume for increasing k. For the node of k=0, one initial condition is required. At this node, the dialysate toxin mass fraction will always be set to a constant value determined at the start of treatment. This value is normally very small and/or equal to zero. A summary of the equations and initial conditions derived in this section are shown in Table 4.2.

Table 4.2. Summary of the numerical solution for the dialysate volume

Equation Description	Explicit Mathematical Formulation
Mass species increase as a function of axial distance k with diffusion and convection	$m_{i,d}^{k+1} = \dfrac{m_{i,d}^{k-1}\left(\dfrac{1}{(\Delta z)^2}\right) + m_{i,d}^{k}\left(\zeta + \dfrac{2}{\Delta z} - \dfrac{\Theta}{\Delta z}\right) - m_{i,C}^{k}(\zeta)}{\left(\dfrac{1}{(\Delta z)^2} - \dfrac{\Theta}{\Delta z}\right)}$
Initial condition for mass species increase with diffusion and convection for k=0	$m_{i,d}^{1} = m_{i,d}^{-1} =$ constant initial value set at the start of treatment by dialysate processing
Mass species increase as a function of axial distance k neglecting diffusion	$m_{i,d}^{k+1} = \Delta z \Gamma \left(m_{i,C}^{k} - m_{i,d}^{k} \right) + m_{i,d}^{k}$
Initial Condition a k=0	$m_{i,d}^{1}$ = constant initial value set at the start of treatment by dialysate processing

4.3 General Solution for the Hollow-Fiber Membrane Mass Species Equation

To couple the numerical solutions from the blood and dialysate regions, an analytical solution to the membrane's second-order, homogenous, differential equation is found. The differential equation modeling radial change in the mass fraction of solute i of the membrane, m, was found earlier to be

$$\frac{d^2 m_{i,m}}{dr^2} + \left(\frac{1}{r} - \Psi_m\right)\frac{dm_{i,m}}{dr} = 0$$

By defining f as the derivative of the mass fraction with respect to the radial direction, the second-order, homogeneous equation can be transformed to the first-order, homogeneous differential Equation (4.7).

$$f = \frac{dm_{i,m}}{dr}$$

After substitution,

$$\frac{df}{dr} + \left(\frac{1}{r} - \Psi_m\right)f = 0 \tag{4.7}$$

Equation (4.7) can be rearranged to group like terms and integrated with respect to df and dr arriving at

$$\ln(f) + C_1 = \Psi_m r - \ln(r) + C_2 \tag{4.8}$$

Solving for f,

$$f = C_3 \frac{e^{\Psi_m r}}{r} \tag{4.9}$$

where

$$C_3 = e^{\left(C_2 - C_1\right)} \tag{4.10}$$

After substituting the original expression for f into Equation (4.8), both sides are integrated with respect to r.

$$\frac{dm_{i,m}}{dr} = C_3 \frac{e^{\Psi_m r}}{r} \tag{4.11}$$

The general solution to the second-order, homogeneous differential equation for the membrane is found to be

$$m_{i,m}(r) = C_3 \int_1^r \frac{e^{\Psi_m r}}{r} dr + C_4 \tag{4.12}$$

The r terms in the integral can be substituted by the letter u to limit confusion of the integrated terms and integrated boundaries shown as

$$m_{i,m}(r) = C_3 \int_1^r 2 \frac{e^{\Psi_m u}}{u} du + C_4 \tag{4.13}$$

4.4 Analytical Solution for a Homogeneous Membrane

For a homogeneous membrane, only boundary conditions A and C are required to solve the general solution to the radial mass fraction distribution in the membrane. To solve the general solution, the mass fractions and mass fraction partial derivatives in

each boundary condition are solved in terms of the constants $C_{3,hm}$ and $C_{4,hm}$ from the general solution. The two transformed boundary conditions form a system of equations that is used to solve for $C_{3,hm}$ and $C_{4,hm}$, yielding an analytical solution.

$$m_{i,hm}(r) = C_{3,hm}\int_1^r \frac{e^{\Psi_{hm} u}}{u}du + C_{4,hm} \tag{4.14}$$

From Section 3.5, boundary condition A is shown as

$$m_{i,b} = \alpha m_{i,1} - \beta \left.\frac{dm_i}{dr}\right|_{r=1}$$

The homogeneous membrane's general solution is evaluated for the mass fraction and partial mass fraction at r=1.

$$m_{i,hm}(r=1) = m_{i,1} = C_{3,hm}\int_1^1 \frac{e^{\Psi_{m,s} u}}{u}du + C_{4,hm} = C_{4,hm}$$

$$\left.\frac{dm_{i,hm}}{dr}\right|_{r=1} = C_{3,hm}\frac{d}{dr}\int_1^1 \frac{e^{\Psi_{hm} u}}{u}du = 0$$

Substitution of these expressions into Boundary Condition A yields the first of two equations to the system used to solve for the constants of the general solution.

$$m_{i,b} = \alpha C_{4,hm} \tag{4.15}$$

Also from section 3.5, boundary condition C is shown to equal

$$m_{i,d} = \chi m_{i,C} + \kappa \left.\frac{dm_i}{dr}\right|_{r_C}$$

As done at r=1, the homogeneous membrane's general solution is evaluated for the mass fraction and partial mass fraction at $r = r_C$.

$$m_{i,hm}(r = r_C) = m_{i,C} = C_{3,hm}\int_1^{r_C}\frac{e^{\Psi_{hm}u}}{u}du + C_{4,hm}$$

$$\left.\frac{dm_{i,m}}{dr}\right|_{r=r_C} = C_{3,hm}\frac{d}{dr}\int_1^{r_C}\frac{e^{\Psi_{hm}u}}{u}du = C_{3,hm}\left(\frac{1}{r_C}e^{\Psi_{hm}r_C} - e^{\Psi_{hm}}\right)$$

Substitution of these expressions into boundary condition C yields

$$m_{i,d} = C_{3,hm}\left\{\chi\int_1^{r_C}\frac{e^{\Psi_{hm}u}}{u}du + \kappa\left(\frac{e^{\Psi_{hm}r_C}}{r_C} - e^{\Psi_{hm}}\right)\right\} + C_{4,hm}\chi \qquad (4.16)$$

Equations (4.15) and (4.16) form a system of equations that are solved for constants $C_{3,hm}$ and $C_{4,hm}$ to the homogeneous membrane's general solution. Without demonstration, the solution to the homogeneous membrane general solution is revealed as

$$m_{i,hm}(r) = \left(\frac{\chi m_{i,b} - \alpha m_{i,d}}{\alpha\left\{\kappa\left(e^{\Psi m} - \frac{e^{\Psi_{hm}r_C}}{r_C}\right) - \chi\int_1^{r_C}\frac{e^{\Psi_{hm}u}}{u}du\right\}}\right)\cdot\ldots \qquad (4.17)$$

$$\ldots\cdot\int_1^r\frac{e^{\Psi_{hm}u}}{u}du + \left(\frac{m_{i,b}}{\alpha}\right)$$

4.5 Analytical Solution for an Asymmetric Membrane

For an asymmetric membrane, boundary conditions A, B, and C are required to solve the general solution to the radial mass fraction distribution in both the membrane skin and porous support. To solve the general solutions of both the skin and support layers, the mass fractions and mass fraction partial derivatives at each boundary must be expressed in terms of the constants from their respective general solutions. A system of equations is then formed to solve these constants leading to an analytical solution for both layers of an asymmetric membrane.

4.5.1 Analytical Solution to the Membrane Skin Layer

The membrane skin is bounded in the radial direction from r=1 to $r = r_B$. The general solution to the mass fraction as a function of radial distance in the membrane skin, ms, is shown as

$$m_{i,ms}(r) = C_{3,ms}\int_1^r \frac{e^{\Psi_{ms} u}}{u} du + C_{4,ms} \tag{4.18}$$

From Section 4.4, the result from the substitution of the mass fraction and partial mass fractions at r=1 into boundary condition A can be used for the membrane skin.

$$m_{i,b} = \alpha C_{4,ms} \tag{4.19}$$

The boundary condition at interface B for the membrane skin requires the general solution to both the membrane skin and porous support to be used. The mass fraction and partial mass fraction at $r = r_B$ is solved in terms of the membrane skin's general solution constants $C_{3,ms}$ and $C_{4,ms}$.

$$m_{i,ms}\left(r = r_B\right) = m_{i,B} = C_{3,ms}\int_1^{r_B}\frac{e^{\Psi_{ms}u}}{u}du + C_{4,ms}$$

$$\left.\frac{dm_{i,ms}}{dr}\right|_{r=r_B} = C_{3,ms}\frac{d}{dr}\int_1^{r_B}\frac{e^{\Psi_{ms}u}}{u}du = C_{3,ms}\left(\frac{1}{r_B}e^{\Psi_{ms}r_B} - e^{\Psi_{ms}}\right)$$

$$\left.\frac{dm_{i,ps}}{dr}\right|_{r=r_B} = C_{3,ps}\frac{d}{dr}\int_{r_B}^{r_B}\frac{e^{\Psi_{ms}u}}{u}du = 0$$

Substitution of these expressions into boundary condition B for the membrane skin yields

$$C_{3,ms}\left\{(\varsigma)\int_1^{r_B}\frac{e^{\Psi_{ms}u}}{u}du + e^{\Psi_{ms}} - \frac{e^{\Psi_{ms}r_B}}{r_B}\right\} + C_{4,ms}(\varsigma) = 0 \qquad (4.20)$$

Equations (4.19) and (4.20) form a system of equations that can be solved for the membrane skin's general solution constants. The solution to the membrane skin's general solution can be written as

$$m_{i,ms}(r) = \frac{m_{i,b}}{\alpha}\left\{1 - \left(\frac{\varsigma}{\varsigma\int_1^{r_B}\frac{e^{\Psi_{ms}u}}{u}du + e^{\Psi_{ms}} - \frac{e^{\Psi_{ms}r_B}}{r_B}}\right)\int_1^{r}\frac{e^{\Psi_{ms}u}}{u}du\right\} \qquad (4.21)$$

4.5.2 Analytical Solution to the Membrane Porous Support Layer

The membrane's porous support is bounded in the radial direction from $r_B \le r \le r_C$. boundary conditions B and C will be used to solve for constants $C_{3,ps}$ and $C_{4,ps}$ shown in the general solution to a membrane porous support layer as

$$m_{i,ps}(r) = C_{3,ps}\int_{r_B}^{r} \frac{e^{\Psi_{ps}u}}{u}du + C_{4,ps} \tag{4.22}$$

The mass fraction and partial mass fraction at $r = r_B$ are solved similarly to the membrane skin in terms of the membrane's porous support general solution constants $C_{3,ps}$ and $C_{4,ps}$.

$$m_{i,ps}\left(r = r_B\right) = m_{i,B} = C_{3,ps}\int_{r_B}^{r_B} \frac{e^{\Psi_{ms}u}}{u}du + C_{4,ps} = C_{4,ps}$$

$$\left.\frac{dm_{i,ps}}{dr}\right|_{r=r_B} = C_{3,ps}\frac{d}{dr}\int_{r_B}^{r_B} \frac{e^{\Psi_{ms}u}}{u}du = 0$$

$$\left.\frac{dm_{i,ms}}{dr}\right|_{r=r_B} = C_{3,ms}\frac{d}{dr}\int_{1}^{r_B} \frac{e^{\Psi_{ms}u}}{u}du = C_{3,ms}\left(\frac{1}{r_B}e^{\Psi_{ms}r_B} - e^{\Psi_{ms}}\right)$$

Substitution of these expressions into boundary condition B for the membrane porous support yields

$$C_{3,ms}\left(e^{\Psi_{ms}} - \frac{1}{r_B}e^{\Psi_{ms} r_B}\right) + \varsigma C_{4,ps} = 0 \qquad (4.23)$$

The mass fraction and partial mass fraction at $r = r_C$ are similarly solved in terms of the membrane's porous support general solution.

$$m_{i,ps}(r = r_C) = m_{i,C} = C_{3,ps}\int_{r_B}^{r_C}\frac{e^{\Psi_{ps} u}}{u}du + C_{4,ps}$$

$$\left.\frac{dm_{i,m}}{dr}\right|_{r = r_C} = C_{3,ps}\frac{d}{dr}\int_{r_B}^{r_C}\frac{e^{\Psi_{ps} u}}{u}du = C_{3,ps}\left(\frac{1}{r_C}e^{\Psi_{ps} r_C} - \frac{1}{r_B}e^{\Psi_{ps} r_B}\right)$$

After substitution of the mass fraction and partial mass fraction into boundary condition C, the bulk toxin mass fraction in dialysate is expressed by

$$m_{i,d} = C_{3,ps}\left\{\chi\int_{r_B}^{r_C}\frac{e^{\Psi_{ps} u}}{u}du + \kappa\left(\frac{1}{r_C}e^{\Psi_{ps} r_C} - \frac{1}{r_B}e^{\Psi_{ps} r_B}\right)\right\} + C_{4,ps}\chi \qquad (4.24)$$

If the constants to the general solution of the membrane skin have been solved, $C_{4,ps}$ can be easily determined. Substituting its value into Equation (4.24), $C_{3,ps}$ is found. Another way to solving each of the constants to the general solution of the skin and porous support layers is by constructing a system of 4 equations that include Equations (4.19), (4.20), (4.23), and (4.24). The solution to the porous support layer can thus be shown as

$$\dot{m}_{i,ps}(r) = \left(\frac{\dot{m}_{i,d} - C_{3,ms}\chi\left(\frac{e^{\Psi_{ms}}}{\varsigma} - \frac{e^{\Psi_{ms} r_B}}{\varsigma r_B} \right)}{\left\{ \chi \int_{r_B}^{r_C} \frac{e^{\Psi_{ps} u}}{u} du + \kappa\left(\frac{1}{r_C} e^{\Psi_{ps} r_C} - \frac{1}{r_B} e^{\Psi_{ps} r_B} \right) \right\}} \cdot \ldots \right.$$

$$\left. \ldots \cdot \int_{r_B}^{r} \frac{e^{\Psi_{ps} u}}{u} du + C_{3,ms}\left(\frac{e^{\Psi_{ms}}}{\varsigma} - \frac{e^{\Psi_{ms} r_B}}{\varsigma r_B} \right) \right) \tag{4.25}$$

4.6 Computational Modeling for a Hemodialysis Treatment

The computer software used to execute the hemodialysis model is MATLAB 2008b. MATLAB provides a programming language that enables a user to write a series of MATLAB statements into a file and then execute them in a single command. This program is widely available and can be easily translated to other programming languages for future development. The hemodialysis program begins by requiring a user to input a number of treatment parameters. The program then executes outputting an array of treatment and dialyzer operation statistics to the user. Treatment statistics include treatment time, toxin clearance, diffusive permeability, water permeability, and toxin concentration after treatment. Operational statistics include dialysate consumption, blood-fiber shear rate, fiber pressure drop, and the number of iterations to convergence for the numerical solutions. File run time varies from under one

minute to 30 minutes depending on the number of mesh nodes evaluated in the numerical solution.

4.6.1 Input Parameters Required for the Computer Simulation

The developed hemodialysis model requires a number of inputs for the program to run. At the start of the program, the file will ask the user to specify a range of values specific to the patient and the designed dialyzer. For an asymmetric membrane, 23 user values are required; whereas for a homogeneous membrane only 19 are required. If a user's entry for a value is outside allowable bounds, warnings appear in the program window and the user is politely asked to re-enter a value for the parameter. In the model's current version, the user defined inputs can be categorized into four groups that include Patient and Toxin Parameters, Dialyzer Operating and Geometric Parameters, Accuracy, Weighting, and Convergence; followed by Hollow-fiber Membrane Parameters.

Patient and Toxin Parameters include the patient weight, toxin to be modeled, and the initial blood toxin concentration. The patient's weight is used to calculate the total blood volume of the patient developed in Section 2.1. With the total blood volume known, the initial mass fraction of the toxin in blood is found using the initial blood toxin concentration.

Dialyzer Operating and Geometric Parameters includes the inner diameter of the dialyzer casing, blood flow rate into the dialyzer, dialysate flow rate into the dialyzer, and the transmembrane pressure between the blood and dialysate compartments. The inner diameter of the dialyzer casing is used to calculate the hydraulic diameter for dialysate flow through a non-circular void derived in Section 3.1. The hydraulic diameter is principally used to calculate the dialysate side convective mass transfer coefficient using the Sherwood correlation. The blood flow rate into the dialyzer is used to calculate treatment time, toxin clearance, shear rate of blood in a hollow-fiber, and to determine the blood side convective mass transfer coefficient. The transmembrane pressure value drives the water permeability of the membrane as discussed in the Results and Discussion.

Accuracy, Weighting, and Convergence includes the mesh node grid spacing in the numerical solutions, blood and dialysate mass fraction convergence criteria, and the blood and dialysate mass fraction weighting. The time required for the program to run varies from 1 to 30 minutes based on tested parameters. Program running time increases with an increased number of grid spacing in the blood and dialysate numerical solutions. The blood and dialysate convergence criteria are used to determine when the toxin mass fraction in the blood and dialysate regions have reached a definite value. The blood and dialysate weighting is used to help the solution reach a converged value.

The fourth and final group describes parameters needed to define the physical characteristics of the hollow-fiber membrane array of both a homogeneous and asymmetric membrane array. These include the number of fibers in the dialyzer, fiber length, inner diameter of the fiber, outer diameter of the fiber, and additional parameters used to help define the sieving characteristics of an asymmetric membrane. These include the membrane skin porosity, pore size, pore tortuosity, and thickness. Likewise, the porous support's porosity, pore size, and pore tortuosity is similarly defined. In the case of a homogeneous membrane, the parameters entered for the porous support are used to define the membrane.

4.6.2 Estimation of Treatment Time

Within this method all of the body's blood is modeled as one lump volume $V_{patient}$. This volume will host an array of toxins that are assumed to be uniformly distributed and have mass fractions in the blood of $m_{i,b}$. The blood volume will pass through a hemodialysis machine where the toxin mass fraction will be decreased. After the all of the body's blood has passed through the dialyzer, the mass fraction of the toxin in blood is checked against a toxin target mass fraction. If the toxin mass fraction is greater than the target value, then the volume is passed through the machine again. If the toxin mass fraction is equal to or less than the target value, the treatment is stopped.

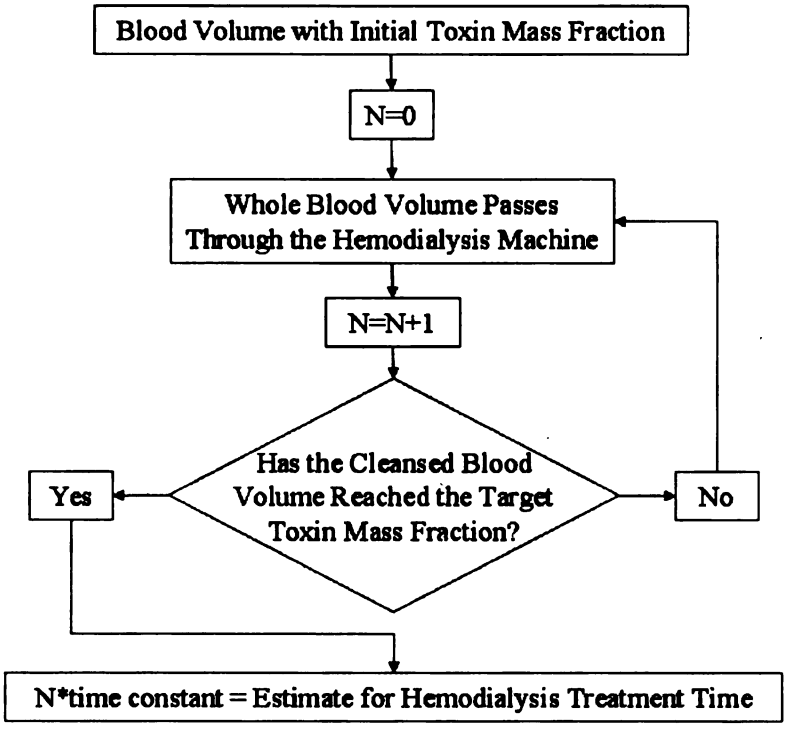

Figure 4.7. General algorithm for determining the hemodialysis treatment time for N passes of the whole blood volume through the hemodialysis machine

The time it takes for a volume of blood to pass through the dialyzer is dependent on the blood flow rate into the dialyzer, number of hollow-fiber membranes, length of the hollow-fibers, and the hollow-fiber inner diameter. The volume flow rate of blood in a hollow-fiber membrane can be modeled using the Hagen-Poiseuille equation shown as

$$\hat{Q}_{\text{fiber}} = \frac{\Delta\hat{P}\pi\hat{r}_A}{8\hat{\mu}_p\hat{l}} \tag{4.26}$$

where $\Delta\hat{P}$ is the pressure drop along the fiber. Since the volume in the fiber is known, the time required for the body's blood volume to pass through the dialyzer can be easily determined.

4.6.3 Solving for the Toxin Mass Fraction in Blood, Dialysate, and Membrane Interfaces

In the estimation of treatment time, blood passing through the dialyzer is checked against a target toxin mass fraction to determine if treatment should be continued or ceased. Within this model an iterative method is used to determine the toxin mass fraction at the dialyzer's blood exit for comparison to a target value. This method assumes that the mass transfer in each hollow-fiber is the same regardless of the fiber's position in the dialyzer. Therefore, only one hollow-fiber submerged in dialysate is modeled whose mass transfer is assumed to be equal to every fiber in the dialyzer.

To begin, the blood, membrane, and dialysate volumes for one hollow-fiber are discretized to a number of intervals specified by the grid spacing desired by the program user. This discretization is shown in Figure 4.9.

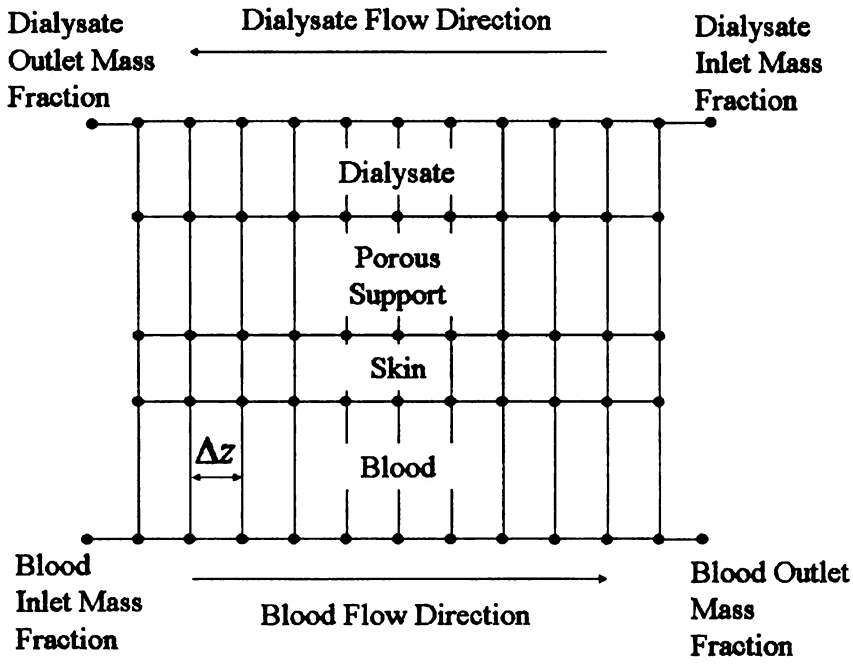

Figure 4.8. Discretization of the blood, membrane skin, porous support, and dialysate volumes

Each of the nodes in Figure 4.9 needs to be solved in order to determine the blood outlet toxin mass fraction. Each node is solved by iteration to a converged toxin mass fraction. During the first iteration, all nodes in the dialysate volume are set to a constant value equal to the initial condition at the dialysate inlet described in Section 4.2. With the mass fraction at the inlet and first node in the blood known from the initial conditions, the mass fraction at the membrane's inner surface (at r=1) and outer surface (at $r=r_C$) are found by solving the membrane's analytical solution. Once the mass fraction at the membrane's inner surface, $m_{i,A,}$ is known, the next downstream node in the blood can be calculated using the numerical solution of the blood mass species equation. This cycle of solving for the mass fraction at the membrane

interfaces and then the downstream blood node is repeated until the blood outlet mass fraction is found.

At this point, the mass fraction for each node in the blood, inner membrane surface, $m_{i,A}$, and outer membrane surface, $m_{i,C}$ is known by assuming each dialysate node is equal to the initial condition of the numerical solution for the dialysate mass species equation. Starting from the dialysate inlet node, the dialysate numerical solution is applied at each node to determine a new dialysate mass fraction based on the initial condition and outer membrane surface mass fraction. Using the new dialysate mass fractions at each dialysate node, the mass fractions in the blood are solved again, only this time the mass fraction at the dialysate nodes are not constant. This process of solving the membrane interface, blood, and dialysate nodes is repeated until the convergence criteria for each node is met. The convergence criterion compares the previous value for the toxin mass fraction to the new, iterated value at a single node. The convergence criterion for a node is the absolute value of the old mass fraction subtracted from the new mass fraction normalized by the old mass fraction.

When the convergence criterion has been met for every node, the mass fraction at the blood exit is checked against the treatment target mass fraction. If the mass fraction at the blood exit is lower than or equal to the target value, the program is stopped and a treatment time is calculated. If the target value has not been reached, the mass fraction at the blood outlet is set as the mass fraction at the blood inlet and the iterative process is begun again.

Chapter 5
Results and Discussion

The ideal dialyzer would possess optimized parameters tailored to removing specific toxins from a patient's blood. In order to design the dialyzer for a desired treatment dose, each parameter within the simulation program is tested for its effect on toxin clearance and treatment time. Before toxin clearance and treatment time can be determined, the convergence criterion for the blood and dialysate numerical solutions is found in Section 5.1. In Section 5.2, the dialyzer's geometric and operating parameters are explored discussing their effect on dialyzer performance. Next, geometric and sieving parameters of homogeneous, hollow-fiber membranes are investigated in Section 5.3. Since the geometric parameters of hollow-fiber length and inner diameter are shared by both homogeneous and asymmetric membranes, only the sieving properties of asymmetric membranes are discussed in Section 5.4.

Four uremic toxins were selected for the tested simulations that include urea, creatine, glucose, and β-2 microglobulin. Urea, creatine, and glucose are all considered to be low molecular weight toxins possessing molecular weights of 60, 131, and 182 g/mol respectively.[10] Beta-2 microglobulin on the other hand is considered a middle molecule with a molecular weight of 11,818 g/mol.[10] This middle molecule was chosen for its widespread use as a uremic marker and the availability of its physical properties. The molecular radius of each of each toxin was estimated by the Stokes-Einstein equation. The radii will help determine the diffusive permeability of the toxin in the membrane.

5.1 Determining the Convergence Criterion for the Numerical Solutions

To determine the toxin mass fraction at the blood and dialysate exits, the numerical solutions to the blood and dialysate volumes require iteration to a converged solution. Iteration describes the number of times all of the blood, dialysate, and membrane mesh nodes are solved for each mesh node to arrive at a converged solution. Convergence is the solution to the finite difference equation that approaches the true solution of the partial differential equation having the same initial condition as the mesh is refined. The convergence criteria at each mesh node can be shown as

$$\frac{m_{i,b}^{j,N} - m_{i,b}^{j,N-1}}{m_{i,b}^{j,N-1}} \leq \varepsilon_b \tag{5.1}$$

In Equation (5.1), $m_{i,b}^{j,N}$ is the value for the toxin mass fraction in the blood at mesh node j and iteration number N; while $m_{i,b}^{j,N-1}$ is the toxin mass fraction at the same mesh node for the previous iteration. Equation (5.1) can be used for the dialysate mesh nodes by substituting k for j and d for b. When the left side of Equation (5.1) reaches a value less than the convergence criterion at each mesh node in the blood and dialysate, a converged solution is reached for the given number of nodes.

Mass fraction weighting in both the blood and dialysate mesh nodes was explored in hopes of decreasing the number of iterations to convergence, while maintaining a stable numerical solution. Between iterations, the blood and dialysate nodal mass

fractions were multiplied by a weighting factor with a value between 0 and 1. It was found that no weighting of the mass fractions between iterations was required since each solution converged the fastest when both weighting values equaled 1 for a convergence criteria equal to 1×10^{-12}.

Results show that the number of iterations to convergence is only a function of dialysate weighting. The number of iterations to convergence can be most closely fitted to a power law function as shown in Figure 5.1. The number of nodes evaluated for this simulation was 700. For the remainder of the simulations, the weighting factors for both the blood and dialysate are set to a value of 1.

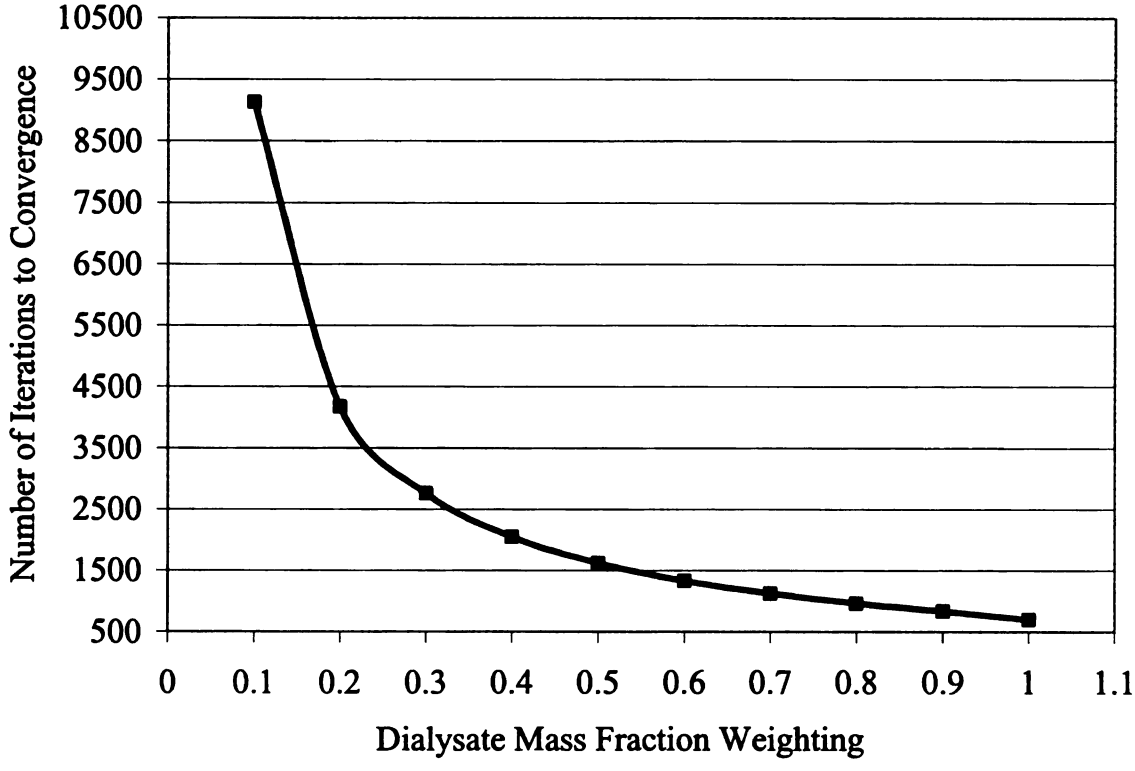

Figure 5.1. The number of iterations to convergence is only a function of dialysate mass fraction weighting and can be best fitted by a power law function

The number of iterations to convergence is also a function of the number of mesh node grid spacing in the blood and dialysate. For a fewer number of grid spacings, fewer number of iterations are required for convergence. In fact, within this model the number of mesh nodes in each volume equals the number of iterations for convergence plus one. For example, if the blood volume is divided into 100 mesh nodes, the solution will require 101 iterations to satisfy convergence.

The urea mass fraction at the blood dialyzer exit was found for increasing number of mesh nodes. As the number of mesh nodes increased, a percent difference was calculated to determine how close the solution was to a converged value. Results are plotted in Figure 5.2. Based on these results, it was decided to use a grid spacing of 700.

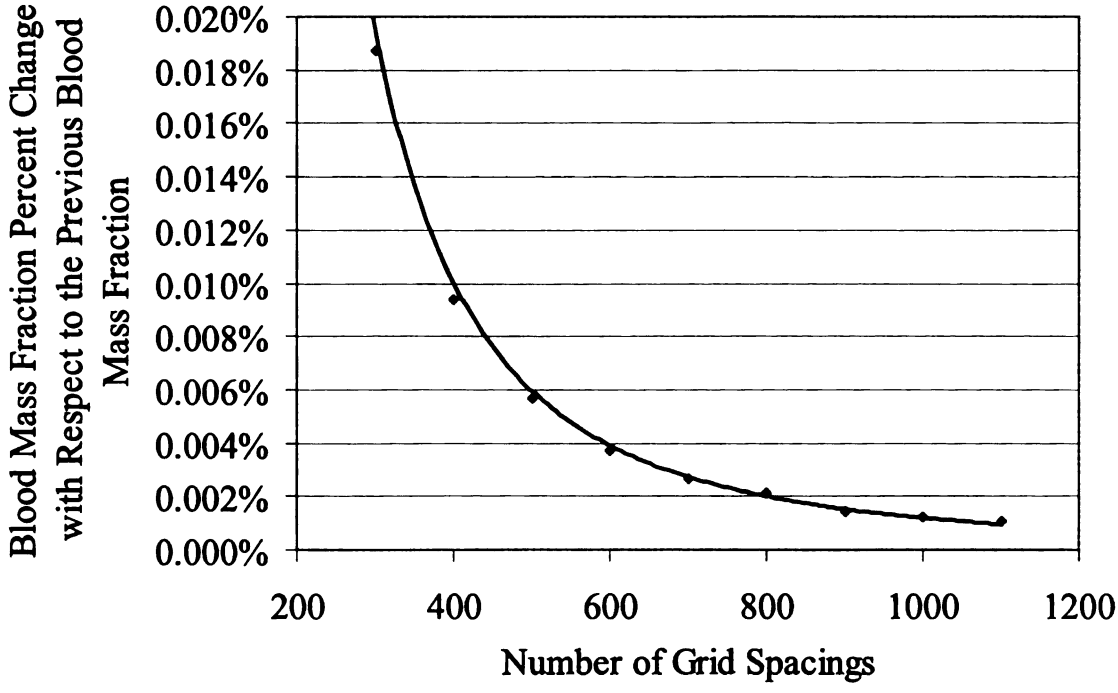

Figure 5.2. Mass fraction at the dialyzer blood exit percent change versus grid spacing

5.2 Dialyzer Parameter Testing

The dialyzer is the artificial kidney of the hemodialysis machine. Its operation and key characteristics were described in Chapter 2. The geometric characteristics and operational parameters of the dialyzer include the inner casing diameter, number of fibers, blood flow rate, dialysate flow rate, and transmembrane pressure. Each of these parameters is displayed in Figure 5.3. The hemodialysis computer model requires all of these parameters to be manually inputted or defined before the program can be executed.

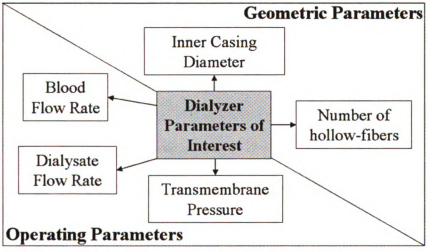

Figure 5.3. Dialyzer parameters to be tested

5.2.1 Inner Casing Diameter, Number of Hollow-fibers, and the Hollow-fiber Packing Density

The two main geometric parameters of a dialyzer are the inner casing diameter and the number of hollow-fibers. Together, they can be used to calculate the hollow-fiber-dialyzer packing density in Equation (3.1). The packing density, as published, should

be maintained between 0.5 and 0.6. This is because the diffusion process can be impaired if there is a mismatch between blood and dialysate flow distribution in the dialyzer (#). For the remainder of this work, the inner diameter of the fiber casing will always be adjusted to provide a fiber packing density of 0.5. As a result, the number of hollow-fibers becomes the most important geometric parameter for the dialyzer.

The number of hollow-fibers is more commonly described by their total inner fiber surface area available to blood flow. With a larger number of fibers, the area available for toxin removal is maximized and treatment time can be decreased provided optimal operating conditions and ideal sieving characteristics of the membrane. Figure 5.4 is a plot of urea clearance and treatment time as a function of the number of hollow fibers and total inner fiber surface area for a homogeneous membrane.

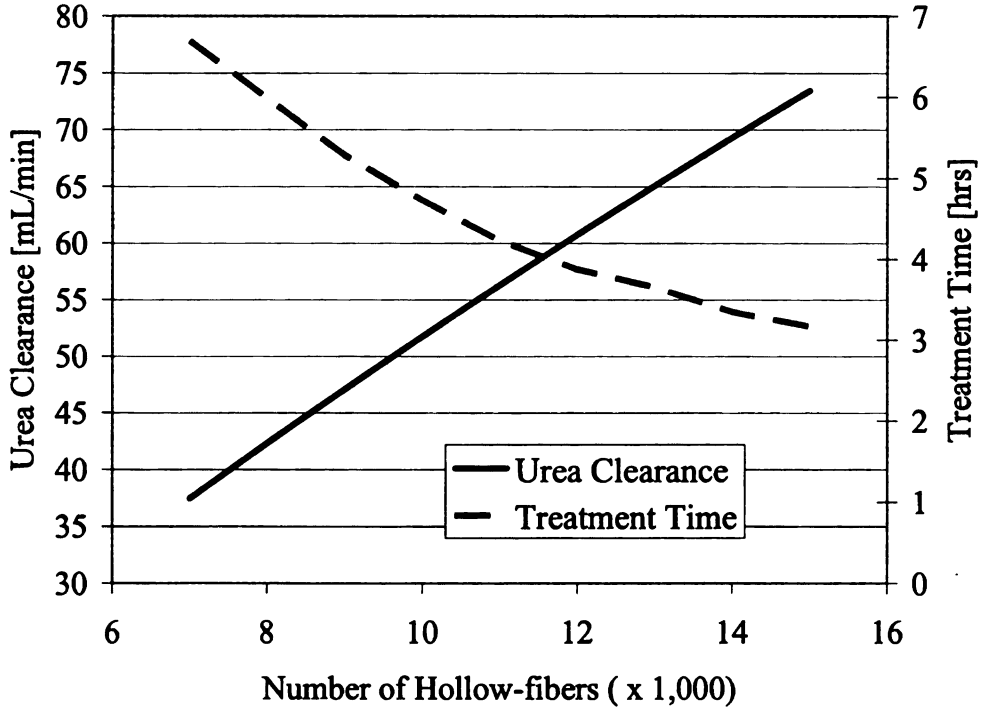

Figure 5.4. Number of hollow-fibers in a dialyzer versus treatment time and urea clearance

As the number of hollow-fibers increase, urea clearance linearly increases from 37 to 76 mL/min. As urea clearance increases, treatment time decreases from 6.7 hours to 3.2 hours. Although increasing the number of hollow-fibers shows positive results, there is one negative aspect in certain treatment cases. One dilemma with using a large number of fibers is the volume of blood removed from the patient during treatment. The volume removed from the patient is identified by dialyzer manufacturers as the priming volume. Most dialyzers displace 60 to 120 mL of blood in the dialyzer (including inlet and dialysate headers) and about 100 to 150 mL in the blood lines leading to and from the dialyzer. In a typical adult, this volumetric range is of little concern; however, the displaced blood volume is much greater concern in smaller adults and pediatric care.[9]

5.2.2 Blood and Dialysate Flow Rates

Two important parameters for optimal removal of toxins during hemodialysis are the blood and dialysate inlet flow rates. The amount of toxin cleared from the blood per unit time was defined earlier as clearance. Clearance is a function of blood flow rate and the mass fraction at the inlet and outlet of the dialyzer. Figure 5.5 displays the clearance of creatine as a function of blood flow rate and the number of hollow-fibers membranes in the dialyzer. For each simulation, the dialysate flow rate is held constant at 500 ml/min. Results show clearance increases for both inlet dialyzer blood flow rate and number of hollow-fibers in the membrane.

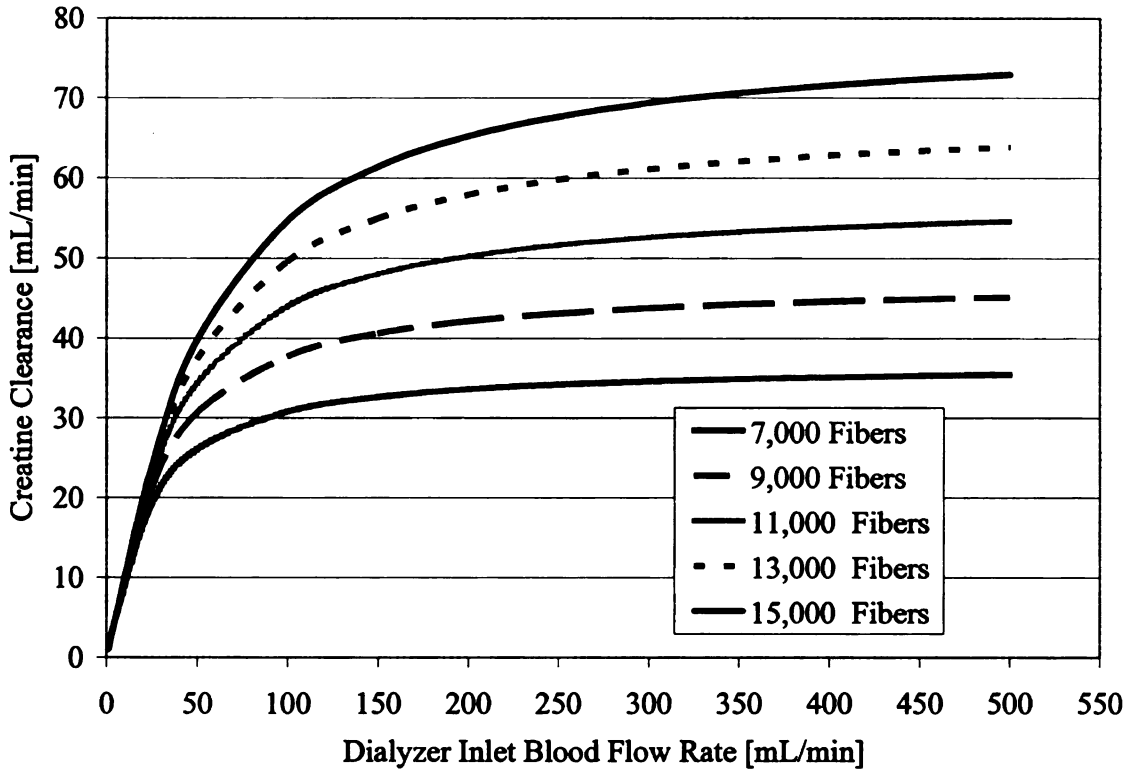

Figure 5.5. Blood flow rate into the dialyzer versus urea clearance for increasing number of hollow-fibers in the dialyzer

Data in Figure 5.5 reveals a transition from a linear to non-linear relationship between clearance and blood flow rate. This transition is a result of the dependence of clearance on blood flow rate and the sieving characteristics of the membrane. At steady state, toxin transport is constant, resulting in clearance being proportional to blood flow rate. Therefore clearance will be linear at lower blood flow rates. At higher blood flow rates, clearance becomes limited by the rate of toxin transport attributed to the sieving characteristics of the membrane. The transition from blood flow limited to membrane limited can be seen in Figure 5.5 by the plot's transition from linear to non-linear in each of the data curves.

Simulated results show dialysate flow rate does not affect toxin clearance for values ranging from 1 to 800 mL/min. The flow of dialysate facilitates a concentration gradient for toxin diffusion by carrying toxins away from the outer surface of the hollow-fiber membranes. Since the toxin mass fraction in the dialysate is always very small compared to the blood mass fraction, the flow rate of dialysate has negligible influence since the net mass fraction gradient barely changes. As the flow rate increases these toxins are transported at a higher rate from the membrane, but the overall gradient remains unchanged.

5.2.3 Transmembrane Pressure

As discussed earlier, fluid flow through a membrane can be described on a per pore basis using the Hagen-Poiseuille equation. The flow rate in a pore is proportional to the transmembrane pressure divided by the pore's resistance to flow. For an increasing transmembrane pressure and constant pore resistance, the flow rate will increase. As the flow rate increases, advection in the membrane will increase leading to greater toxin clearance and lower treatment times. Both of these parameters are tested by increasing the transmembrane pressure shown in Figure 5.6. The data suggests that as the transmembrane pressure is increased, treatment time decreases and urea clearance increases.

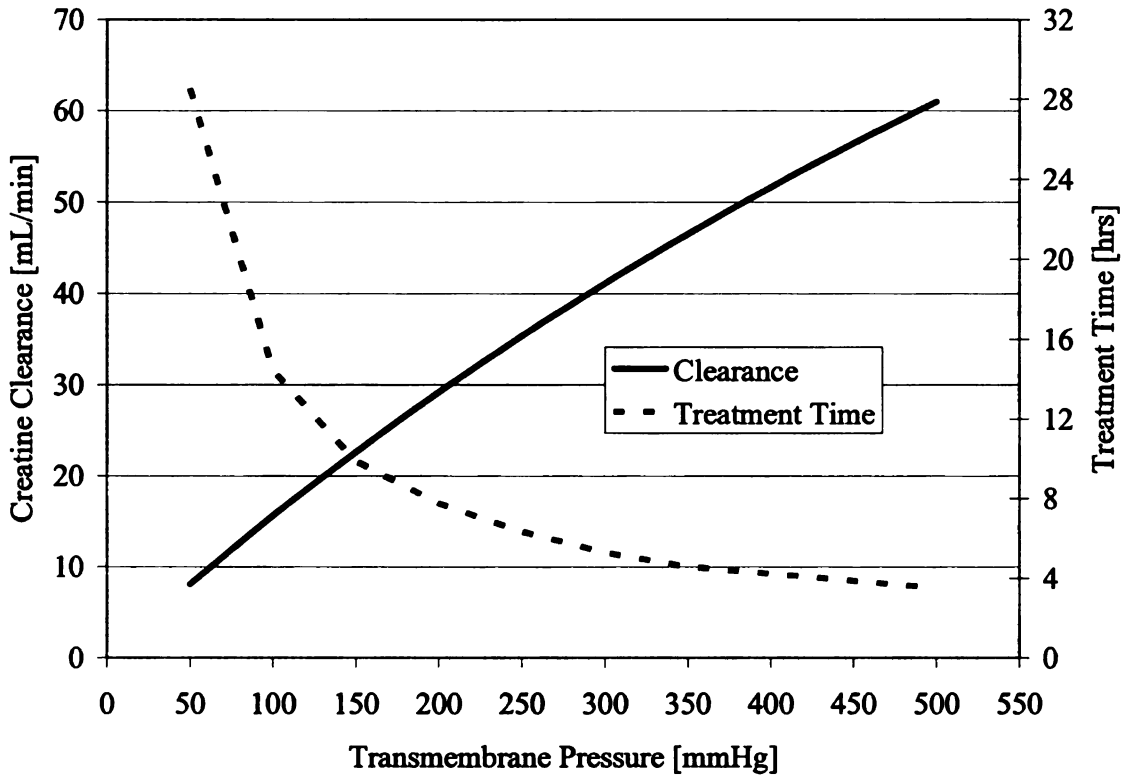

Figure 5.6. Transmembrane pressure versus treatment time and creatine clearance

5.3 Homogeneous Membrane Testing

A membrane whose physical and sieving properties remain constant throughout the membrane volume can be classified as a homogeneous, hollow-fiber membrane. The geometric and sieving properties of the membrane can be defined using six design parameters that include the fiber's inner diameter, outer diameter, length, pore size, porosity, and tortuosity. Each of the parameters is shown in Figure 5.7. The hemodialysis computer model requires each of these parameters to be manually inputted or defined before the program can be executed.

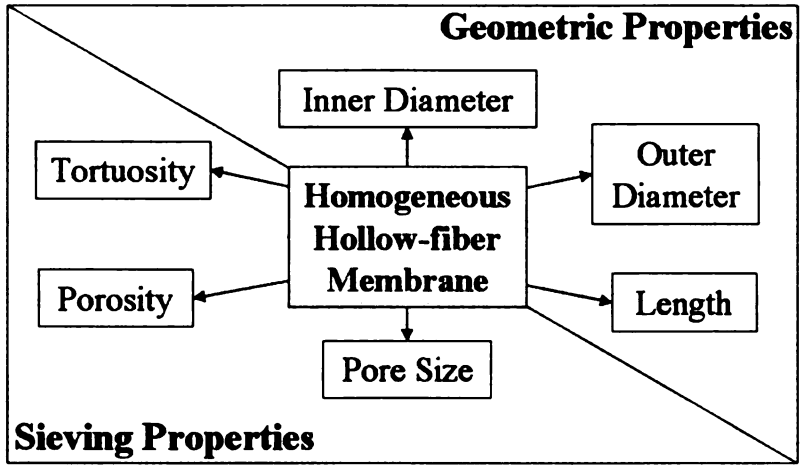

Figure 5.7. Homogeneous Membrane parameters to be tested

The inner hollow-fiber diameter is discussed first in Section 5.3.1 with its impact on toxin clearance, pressure drop due to blood flow, and the shear rate of blood in the fiber. The outer fiber diameter dictates the hollow-fiber membrane's thickness as discussed in Section 5.3.2. This section also highlights the influence of the membrane's thickness on toxin clearance and water permeability. The hollow-fiber length is discussed in Section 5.3.3 where pressure drop and toxin clearance are thoroughly explored. For the homogeneous, hollow-fiber membrane's sieving properties; the pore size, porosity, and tortuosity are examined. All three are investigated in Section 5.3.4 where their intricate role in toxin removal is tested.

5.3.1 Hollow-fiber Inner Diameter

Most hollow-fibers have a relatively standard inner diameter of approximately 180 to 220 μm.[3] This range of values is a compromise between opposing forces. A small

inner diameter increases the fluid shear rate resulting in the attenuation of boundary layer effects generating a fully viscous laminar flow. On the other hand, decreasing the inner diameter will increase the mean velocity of the blood and the pressure drop required to maintain the desired flow rate. This result is most clearly demonstrated after inspection of the Hagen-Poiseuille equation. Pressure drop is inversely proportional to the inner radius of the fiber to the fourth power. Urea clearance and required pressure drop as a function of hollow-fiber inner diameter is shown in Figure 5.8.

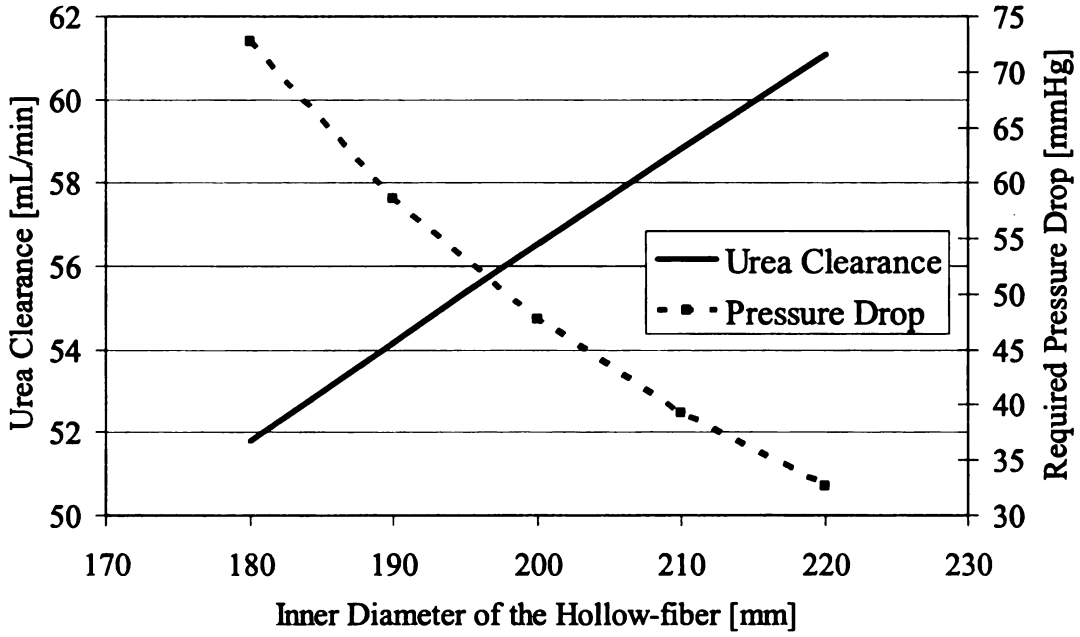

Figure 5.8. Urea clearance and the required pressure drop of each fiber as functions of the inner diameter of the hollow-fiber membrane

For each of the dialyzers simulated in Figure 5.8, constant packing density, blood and dialysate flow rate, membrane length, thickness, and constant sieving properties are maintained. Results show that clearance increases with increasing inner fiber

diameter. As predicted by the Hagen-Poiseuille equation, pressure drop decreases by the power of four for increasing inner fiber diameter as shown by the power law trend line shown by the dotted line in Figure 5.8.

Pressure drop in the blood compartment of the dialyzer is an important design parameter when considering the required pump power for the hemodialysis machine. The more pump power required, the more electricity and thus the more expensive the cost per treatment. For an ideal hemodialysis machine, the pump is designed to maintain a range of blood flow rates for the smallest range of pressure drop. To aid in the pump's selection, a graph can be created that details the required pressure drop to maintain a desired blood flow rate for a given inner hollow-fiber diameter. An example graph created by the developed simulation program is shown in Figure 5.9. The dialyzers simulated in Figure 5.9 possessed 11,000 hollow-fibers, constant packing density, dialysate flow rate, membrane length, thickness, and constant sieving properties.

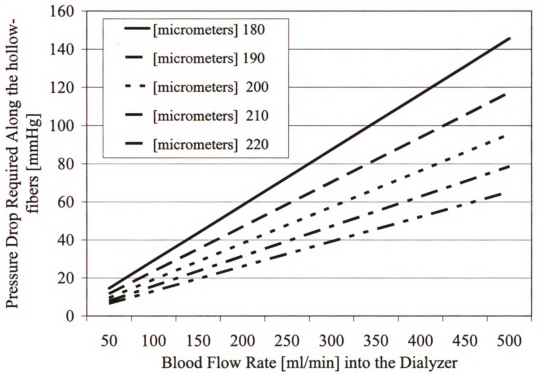

Figure 5.9. Required pressure drop as a function of dialyzer inlet blood flow rate and inner hollow-fiber diameter

As predicted from the Hagen-Poiseuille equation, the pressure drop linearly increased with the blood flow rate. In clinical settings, the blood flow rate is normally set to 250 ml/min giving a range of pressure drops for the simulated dialyzers of 32 to 72 mmHg. In addition to pressure drop, the shear rate inside the dialyzer's hollow-fibers is an important design parameter for modeling the flow properties of blood. Recall for blood to behave as a Newtonian fluid, the fluid shear rate must exceed 100 s^{-1}. The blood shear rate as a function of inner hollow-fiber diameter and blood flow rate is plotted in Figure 5.10.

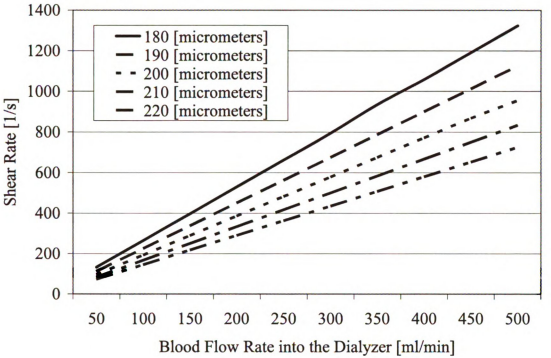

Figure 5.10. The blood shear rate as a function of hollow-fiber inner diameter and blood flow rate into the dialyzer

Shear rate linearly increases with decreasing inner hollow-fiber diameter for increasing blood flow rates. All blood flow rates exceeding 100 ml/min achieved blood shear rates above 100 s^{-1}. In clinical practice, blood flow rates rarely fall below 200 ml/min, thus assuming that blood will behavior as a Newtonian fluid within the hollow-fiber membranes is an approximation within reason. For a blood flow rate of 250 ml/min, the blood shear rate ranges from 362 to 660 s^{-1} for inner hollow-fiber diameters of 180 to 220 μm. It has been published that the threshold for blood shear stress is 1500 dynes/cm^2.[57] This threshold represents the shear stress on blood that coincides with hemolysis. Using this threshold and assuming blood possesses a constant viscosity of 3 cP, a shear rate of 50,000 s^{-1} would need to be reached for blood damage to occur.

The inner diameter of the hollow-fiber will dictate the pressure drop required to maintain a given flow rate while also playing a small role in the dialyzer's ability to remove toxins. Playing a larger role in toxin removal is the fiber wall thickness, dictated by the dimensions of the outer fiber diameter. The wall thickness is important to minimize the transport distance of toxins but also to provide structural support to the fiber. The importance of the outer hollow-fiber diameter is now explored.

5.3.2 Hollow-fiber Outer Diameter

The outer diameter of a hollow-fiber membrane dictates the wall thickness of the fiber. In homogeneous hollow-fiber membranes, the thickness varies from approximately 5 to 50 μm.[58] The thickness of the membrane is important for two reasons. One is to provide structural support to the fiber to withstand the transmembrane pressure between the blood and dialysate compartments. And two, the thickness along with tortuosity prescribes the distance for toxin transport through the membrane wall. This distance is important for estimating fluid flow and toxin transport through the fiber walls. For this study, it will be assumed that for any wall thickness, the membrane's structure will not be compromised for the simulated range of transmembrane pressures.

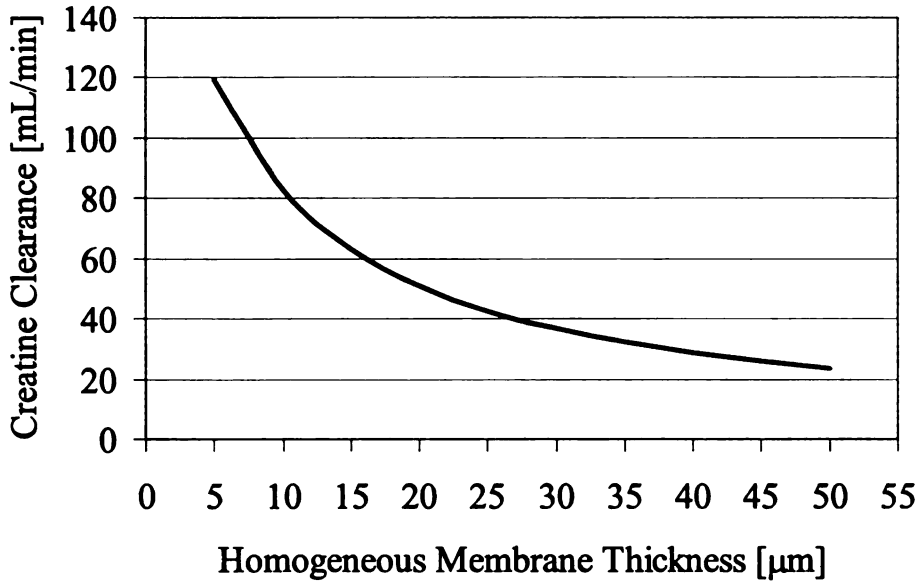

Figure 5.11. Creatine clearance decreases as a function of hollow-fiber membrane thickness

Water permeability at larger fiber thicknesses can be increased by increasing the pore size and porosity while decreasing the membrane tortuosity. The creatine clearance as a function of membrane thickness is shown in Figure 5.11. Since the path length for toxin transport increases with membrane thickness, the urea clearance decreases with thickness. This decay is most closely fitted by a power law not shown in the Figure 5.11. There are more ways to increase toxin clearance beyond decreasing membrane thickness. One way is to maximize the available membrane surface area to toxin transport by increasing the number of fibers in the dialyzer or the hollow-fiber length.

5.3.3 Hollow-fiber Length

The length of the dialyzer's hollow-fibers ranges from 18 to 25 cm in length.[58] Like the inner diameter, the fiber length is a compromise between opposing forces. By

decreasing the fiber's length, the pressure drop required to maintain a given blood flow rate decreases, but the membrane surface area available to the blood and thus mass transport decreases. The opposite is true for extending the hollow-fiber length. If the hollow-fiber is too long, the pressure at the venous end of the fiber could drop below the dialysate pressure leading the backfiltration. Backfiltration is a term used to describe when toxins transport from the dialysate into the blood due to a reversal in the transmembrane pressure at a location in the fiber. Thus, careful consideration is needed to design the fiber's length.

The total membrane surface area will linearly increase with both fiber length and number in the dialyzer. As carried out in section 5.2.1, pressure drop in the hollow-fiber can be estimated using the Hagen-Poiseuille equation. With the inner radius, blood flow rate, and blood viscosity held constant, the pressure drop in the hollow-fiber is directly proportional to the fiber length. The clearance of urea and pressure drop in a hollow-fiber is plotted against the hollow-fiber length and the total dialyzer inner membrane surface area in Figure 5.12.

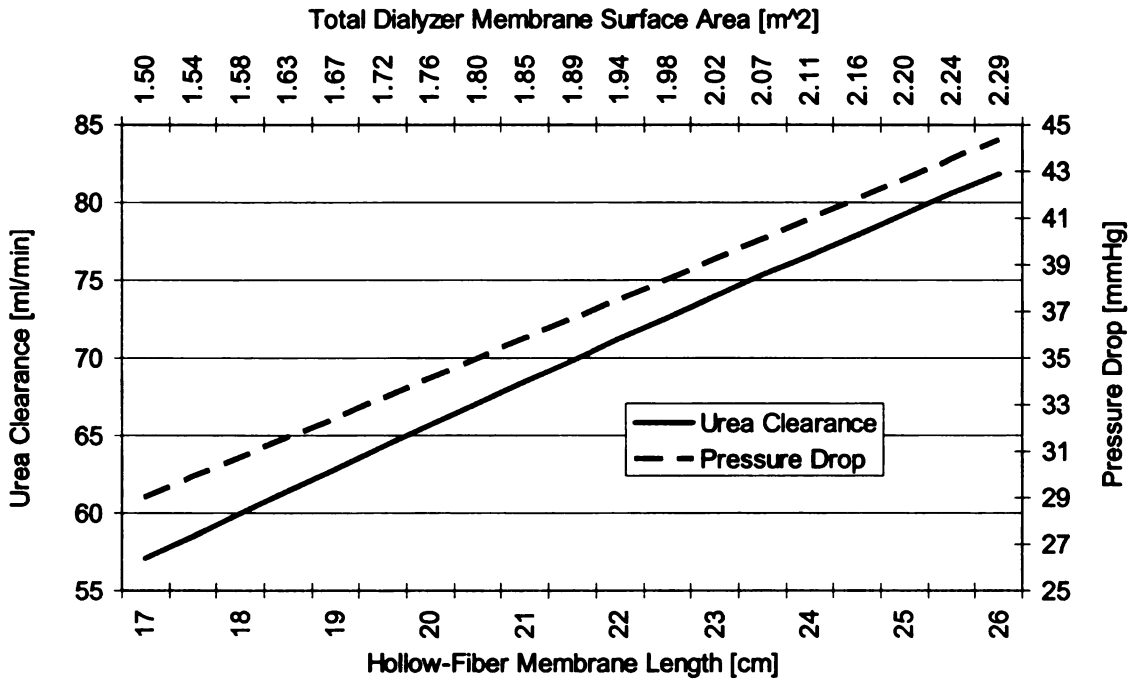

Figure 5.12. Urea clearance and hollow-fiber pressure drop as a function of hollow-fiber length and total dialyzer membrane surface area

From Figure 5.12, an increase in fiber length and surface area results in a linear increase in urea clearance. This is expected since toxin transport in blood is determined by the numerical, linear algebraic solution to the blood mass species equation. The pressure drop is also linear as predicted form the Hagen-Poiseuille equation. For an increase in fiber length from 17 to 26 cm, the pressure drop increases by approximately 15 mmHg. The simulated dialyzer possessed 14,000 fibers and therefore the pressure drop required to sustain a blood flow rate of 250 ml/min is small. For a dialyzer possessing fewer hollow-fibers, the pressure drop for an increase in hollow-fiber length would be much greater.

5.3.4 Pore Size, Porosity, and Tortuosity

The pore size, porosity, and tortuosity are the three most influential parameters for determining the sieving characteristics of a homogeneous, hollow-fiber membrane. The key sieving characteristics defined in Section 2.6 include diffusive permeability and clearance. Ideally, the membrane should have a large number of pores with a relatively narrow distribution of pore size. The number of pores is defined as porosity while the pore size is important for membrane selectivity. Discussed in Section 5.3.2, the thickness of the membrane is important for maximizing clearance when the cylindrical pores follow straight paths through the membrane. In reality, these paths are highly tortuous impacting all both diffusive permeability and clearance.

Diffusive permeability was defined earlier as a term used to describe solute transport across a membrane. The diffusive permeability is proportional to membrane porosity and apparent diffusion coefficient; while it is inversely proportional to the membrane thickness and tortuosity. For a given toxin, as the pore size in the membrane increases, the hindered diffusion coefficient increases thus increasing the diffusive permeability of a toxin. This trend is plotted in Figure 5.13 for urea, creatine, and glucose.

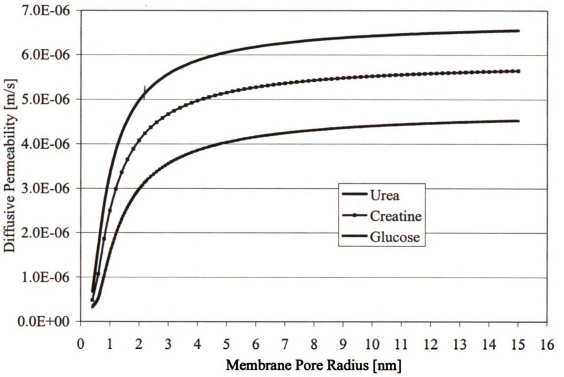

Figure 5.13. Hollow-fiber membrane permeability as a function of pore radius for low molecular weight toxins

The diffusive permeability of the low molecular weight toxins is limited for membrane pore sizes exceeding 3 nm. At this pore size, the average ratio for toxin radius to pore radius is 0.1. At this value, the toxin passing through the pore experiences decreased solute hydrodynamic drag resulting in their diffusive permeability increasing to approximately 80% of their bulk value. To reach 90% of their bulk value, the pore size can be increased to 5.6 nm; however, care must be taken so that the pore size is not so large as to allow blood cells and vital blood proteins such as albumin to filter from the blood.

As membrane pore size increases, larger toxins can be filtered from the blood. One group of toxins that are of wide interest are classified as middle molecules.[10] Beta-2 microglobulin is classified as a middle molecule whose molecular weight is near the average of its molecular siblings. The estimated radius of β-2 is larger than the lower-molecular weight toxins and requires the pore radius to exceed 1.6 nm for it to filter from the blood. The diffusive permeability of β-2 as a function of pore radius is plotted in Figure 5.14. At a pore size of 15 nm, the β-2 diffusive coefficient is 77% of its bulk diffusivity. Shown in Figure 5.15 is the diffusive permeability of the protein albumin.

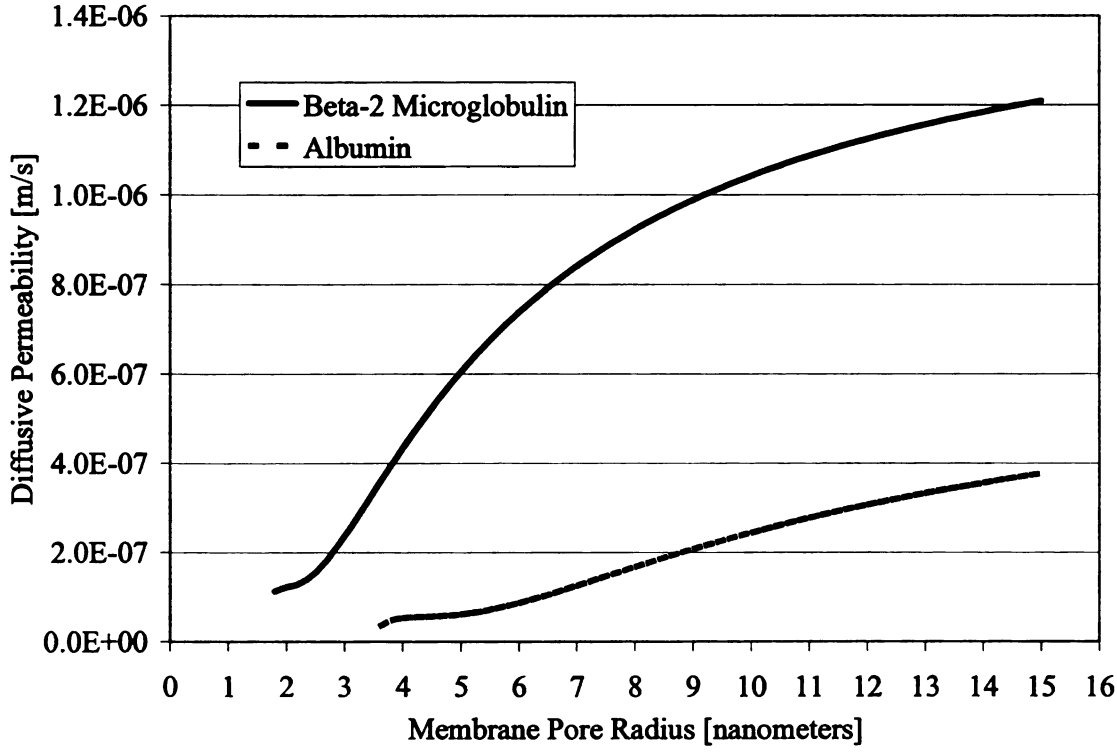

Figure 5.14. Diffusive permeability for β2-Microglobulin and Albumin as a function of membrane pore radius

Under normal circumstances, the removal of albumin protein should be minimized. According to the Stokes-Einstein relation for estimating molecular radius, Albumin will begin to diffuse into the membrane at a pore radius of approximately 3.6 nm. If the pore size of the membrane is set to this value, the diffusive permeability of β-2 is only 22% of its bulk value. The Asahi Kasei Kuraray Medical Company manufactures several dialyzers with experimentally found average pore radii of 4.75 and 5.5 nm.[68] For these radii, the diffusive permeability of albumin is limited to 9% of its bulk value while β-2 reaches 38% of its bulk diffusive permeability. It can therefore be expected that for a hemodialysis treatment requiring extensive removal of β-2 microglobulin, the treatment time will increase for pore radii below 6 nm.

In addition to pore size, diffusive permeability is also affected by membrane porosity and tortuosity. It can be inferred from the equation for diffusive permeability that for increasing porosity, diffusive permeability will increase; and for increasing tortuosity, diffusive permeability will decrease. A plot of diffusive permeability for creatine as a function of pore size and tortuosity is provided in Figure 5.15. A plot relating porosity to diffusive permeability is not provided but shows similar trends.

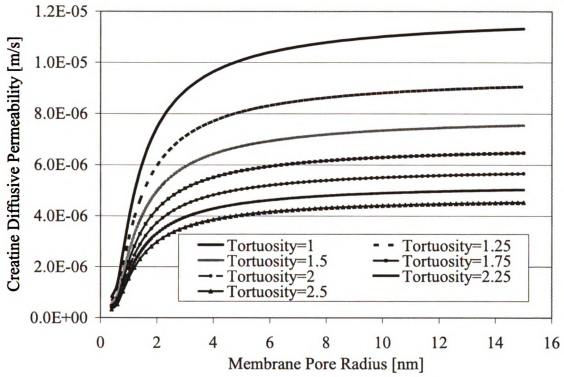

Figure 5.15. Diffusive permeability of creatine as a function of membrane pore radius and tortuosity

A major factor in treatment time is toxin clearance. One way of increasing clearance is by increasing pore size and membrane porosity. Trends for diffusive permeability show that by increasing pore size and porosity, the diffusive permeability increased. As diffusive permeability increases in a membrane, toxins carried by the blood will more readily diffuse into the membrane increasing toxin clearance. In Figure 5.16, the clearance of creatine is plotted as a function of porosity and pore radius.

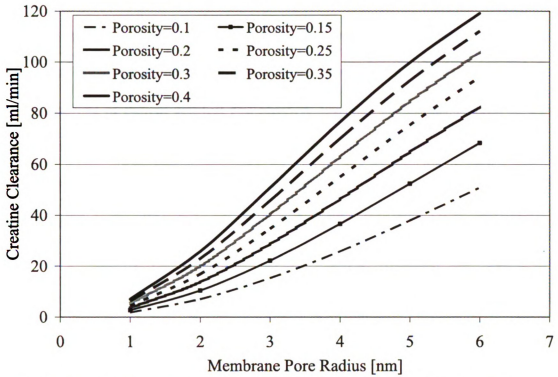

Figure 5.16. Creatine clearance as a function of membrane pore size and porosity

Results from Figure 5.16 illustrate for increasing porosity and pore radius, the clearance of creatine increases as expected. The trend shown for creatine would be similar to results for urea, glucose and β-2 microglobulin. If the pore radius is increased beyond 6 nm, clearance with respect to pore radius linearly increases until creatine's diffusive permeability reaches its bulk value. At this pore size, the creatine's clearance as a function of pore radius decreases in slope and approaches an asymptotic value. Therefore, low molecular weight toxin clearance is membrane limited at a blood flow rate of 250 mL/min. This result is similar to experimental results determined in previous published works.[58]

A direct result of increasing toxin clearance is to decrease the hemodiaylsis treatment time. The higher the rate for toxin removal, the less time it will take to reach the

treatment's target concentration. A unique way of mapping the dependence of treatment time on pore size and porosity is using a two-dimensional map displayed in Figure 5.18 for creatine. In clinical practice, treatment time is limited to 4 hours or less for reasons of patient comfort and physical strain on the patient's body. In the case where a variety of dialzyers are available, the health care provider can choose a dialyzer with the desired sieving characteristics and check the estimated treatment time using a porosity-pore map as shown in Figure 5.17.

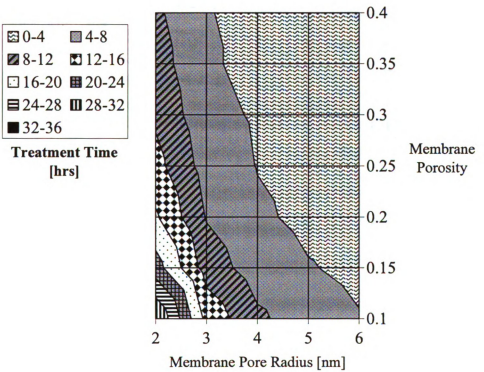

Figure 5.17. Treatment time in hours versus membrane porosity and pore radii

The membrane parameter that inhibits toxin clearance and treatment time is tortuosity. Tortuosity is the results due to the methods used to manufacture the hollow-fiber membrane. Tortuosity is seen to decrease diffusive permeability, as

displayed in Figure 5.18. Water permeability also decreases with tortuosity, since it is inversely proportional to tortuosity. The degree that tortuosity affects the clearance of β-2 microglobulin can be viewed in Figure 5.18. This figure presents the clearance of β-2 for tortuosity equal to 1.25, 1.5, 1.75, 2, 2.25, and 2.5 divided by the clearance of β-2 for tortuosity equal to 1.

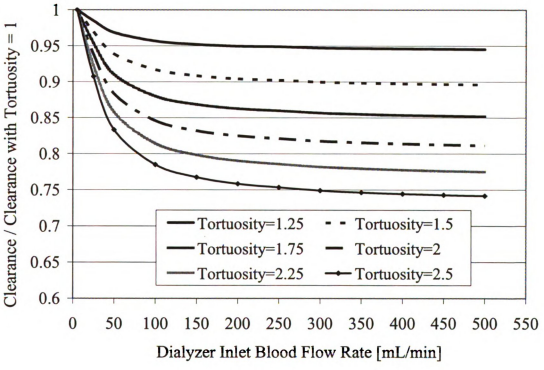

Figure 5.18. Clearance of β2-Microglobulin divided by the clearance of β2-Microglobulin with a tortuosity=1 for increasing dialyzer inlet blood flow rate

Figure 5.18 demonstrates that as membrane tortuosity increases, the clearance of a toxin decreases for increasing blood flow rate. For a membrane possessing a tortuosity of 2.5 and a dialyzer inlet blood flow rate of 300 mL/min, clearance decreases by 25% compared to a membrane with no tortuous pores. From this subsection, it can be seen how strongly diffusive permeability and clearance depend on the sieving properties of the membrane that include pore size, porosity, and

tortuosity. Each of these properties requires careful consideration when designing a membrane to remove select toxins while retaining others.

5.4 Asymmetric Membrane Testing

A membrane with physical and sieving properties increasing in the direction of solute transport can be classified as an asymmetric, hollow-fiber membrane. The sieving characteristics of the membrane can be defined using eight design parameters that include the membrane pore size, porosity, tortuosity, and thickness of both the skin and porous support layers. Each of the parameters is shown in Figure 5.19. The hemodialysis computer simulation requires each of these parameters to be manually inputted or defined before the program can be executed. The geometric parameters explored earlier that include inner fiber diameter and length will not be revisited since their results can be directly applied to the asymmetric case.

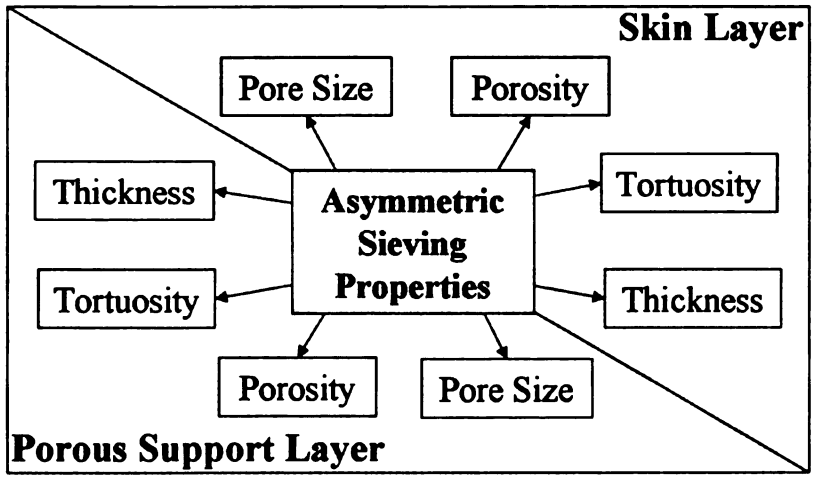

Figure 5.19. The sieving characteristics of an asymmetric membrane can be divided by the layers to which they are applied

The affects of pore size, porosity, tortuosity, and thickness on the membrane skin layer is discussed in Section 5.3.4. This section highlights the results of varying these parameters in determining diffusive permeability, water permeability, and toxin clearance. The same parameters for the porous support are discussed in Section 5.4.1. Comparisons are made between the asymmetric and homogeneous results that lead to the advantages and disadvantages of using each membrane type.

5.4.1 Pore Size, Porosity, Tortuosity, and Thickness of the Membrane Skin Layer

The sieving characteristics of the asymmetric membrane's skin layer are determined by the skin layer's pore size, porosity, tortuosity, and thickness. These parameters are crucial since the skin layer, as will be shown here and within the subsequent section, determines the membrane's ability to remove toxins from the blood. Diffusive permeability was discussed earlier for its dependence on the ratio of toxin to pore radius, tortuosity, porosity, and membrane thickness. To determine the diffusive permeability of a two-layered membrane, a resistance model is applied shown as Equation (5.2) where P_{AS}, P_{SL}, and P_{PS} are the diffusive permeability of the asymmetric membrane, skin layer, and porous support.

$$\frac{1}{P_{AS}} = \frac{1}{P_{SL}} + \frac{1}{P_{PS}} \tag{5.2}$$

For the tested results, the diffusive permeability of the porous support was held constant by defining a pore radius equal to 30 nm, a tortuosity equal to the skin tortuosity, and porosity equal to that of the skin layer. The overall asymmetric

membrane thickness was held constant-as the skin layer thickness was increased, the porous support thickness was decreased. Results of varying skin thickness and skin pore size are plotted in Figure 5.20. This result is presented as a diffusive permeability percent increase from the diffusive permeability of a homogeneous membrane whose pore size, porosity, and tortuosity equal that of the membrane skin. The overall thickness of the asymmetric membrane also equaled the thickness of the homogeneous membrane.

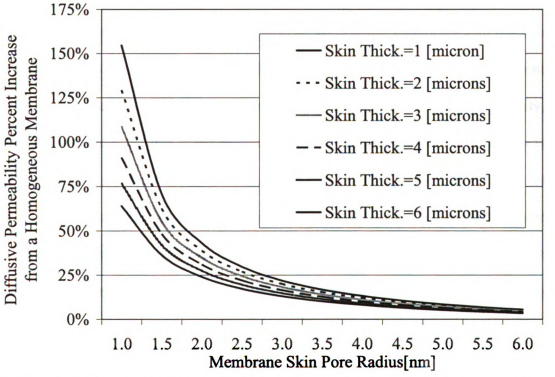

Figure 5.20. Diffusive permeability percent increase from a homogeneous membrane for glucose as a function of membrane skin pore radius and skin thickness

Results show for increasing skin pore radius and thickness, the diffusive permeability percent increase decreases at a rate that can be closely approximated by a power function. At a skin pore radius of 2 nm and thickness equal to 6 μm, diffusive permeability for glucose increases by 24% with respect to a homogeneous membrane.

For a skin pore radius of 5 nm and greater, the percent increase decreases to approximately 5%. Therefore, at larger skin pore sizes the advantage of using an asymmetric membrane decreases with respect to diffusive permeability. It can be concluded that for pore sizes below 2 nm, the advantage of using an asymmetric membrane is greater for diffusive permeability. It can be additionally expected that by increasing porosity, decreasing the overall thickness, and decreasing tortuosity will increase the diffusivity of the asymmetric membrane for constant pore size.

Improving diffusive permeability by adopting an asymmetric membrane also leads to increasing toxin clearance. Figure 5.21 presents the glucose clearance percent increase from the clearance of a homogeneous membrane whose pore size, porosity, and tortuosity are equal that of the membrane skin. The membrane skin thickness was held constant to a value of 1 μm. At a skin pore size of 1 nm, the percent increase for all membrane porosities converges to approximately 25%. As the membrane pore size increases, the percent increase for each membrane diverges from one another decreasing to a range of 10 to 18%. These results reveal asymmetric membranes to hold a distinct advantage to increasing clearance over their homogeneous counterparts possessing equal pore size, porosity, and tortuosity to that of the membrane skin for equal overall membrane thickness.

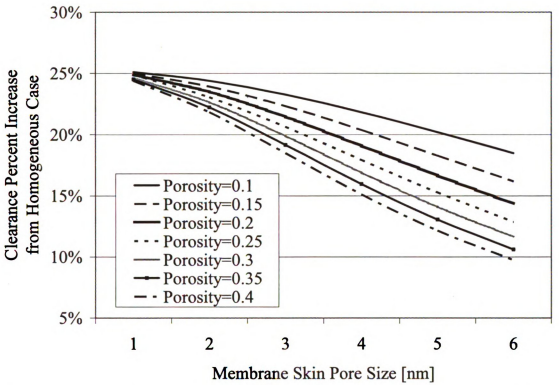

Figure 5.21. Clearance percent increase from homogeneous membrane for glucose as a function of membrane skin pore size and skin porosity

Skin thickness plays a unique role in toxin clearance. By increasing the thickness of the membrane skin and holding the porous support thickness constant, toxin clearance will decrease at a close to linear rate. However, when the membrane skin thickness is increased while holding the overall asymmetric membrane thickness constant (i.e. when skin thickness increases the porous support thickness decreases), toxin clearance remains constant. Both trends are demonstrated by Figure 5.22 for an asymmetric membrane of constant pore size, porosity, and tortuosity.

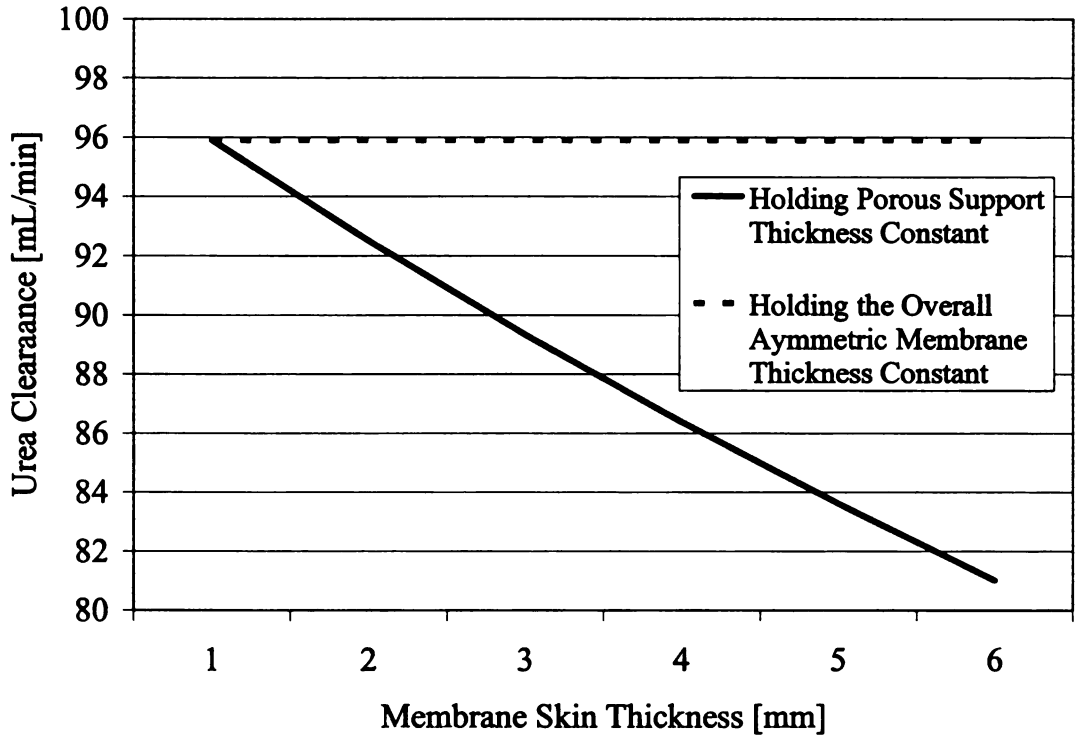

Figure 5.22. Urea clearance as a function of asymmetric membrane skin thickness

Figure 5.22 suggests that the skin thickness does not affect toxin clearance; rather it is the overall thickness of the asymmetric membrane that can increase or decrease clearance at a linear rate. It can therefore be concluded that clearance of an asymmetric membrane with constant pore size, porosity, and tortuosity in the porous support is chiefly determined by the membrane skin radius and porosity. The affects of changing the porous support sieving parameters are discussed in the next section.

5.4.2 Pore Size, Porosity, Tortuosity, and Thickness of the Porous Support Layer

The porous support serves as both a support structure and sieving medium for the asymmetric membrane. The sieving characteristics of the porous support can be

determined from the porous support's pore size, porosity, tortuosity, and thickness. Their impact on the membrane's sieving properties were tested and it was found that only the thickness had an impact on toxin clearance, while all four parameters affected toxin diffusive permeability and water permeability.

As shown in Figure 5.22, the toxin clearance linearly decreases for increasing porous support thickness. With increasing membrane thickness, the path length for a toxin to pass through the membrane increases. This path length increase translates to a greater flow resistance within the membrane decreasing the rate of filtrate flow in the membrane. This decrease in convective transport decreases the rate at which toxins are removed from the blood consequently decreasing toxin clearance.

Increasing pore size and porosity in the porous support will increase both the diffusive and water permeability of the asymmetric membrane. This effect was seen earlier in Section 5.2.4. for a homogeneous membrane. Care must be taken so that the water permeability of the membrane is not too large that an excessive amount of plasma water is removed from the blood. In clinical practice, if too much water is filtered from the blood saline must be added to the patient to supplement the loss.

5.5 Water Permeability for both the Homogeneous and Asymmetric Membranes

Water permeability as previously described in Section 2.6 describes the volumetric flow rate at which plasma water flows through the membrane per unit area and

pressure. With respect to the design parameters of the membrane, water permeability is proportional to the pore radius squared and porosity, while inversely proportional to membrane thickness and tortuosity. For a homogeneous membrane, it can be expected that water permeability will increase linearly for increasing porosity and decrease linearly for increased membrane thickness. The water permeability for a homogeneous membrane is plotted as a function of pore radius and membrane tortuosity in Figure 5.23. As expected, trend line fitting indicated each of these trends to increases by the power of 2 with pore radius.

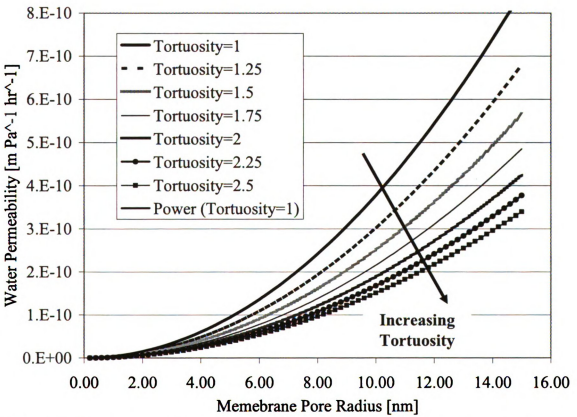

Figure 5.23. Water permeability as a function of increasing pore radius and membrane tortuosity

To determine the water permeability of a two-layered membrane, a resistance model is applied shown as Equation (5.3) where $L_{p,AS}$, $L_{p,SL}$, and $L_{p,PS}$ are the water permeability of the asymmetric membrane, skin layer, and porous support.

$$\frac{1}{L_{p,AS}} = \frac{1}{L_{p,SL}} + \frac{1}{L_{p,PS}} \tag{5.3}$$

The case of water permeability for the homogeneous case has already been explored and is directly applicable to that of the membrane skin layer. Effects of changing the porous support pas investigated was investigated and found to have a large impact on the overall water permeability of the asymmetric membrane. This was found for an asymmetric membrane whose membrane skin layer was increased from 1 to 6 μm. The skin layer maintained a pore radius of 3.5 nm and porosity of 0.3. The total asymmetric membrane thickness was held constant to 20 μm (same as that of the homogeneous case) so as the membrane skin thickness increased, the porous support thickness decreased. The water permeability percent increase from the homogeneous case is presented in Figure 5.24.

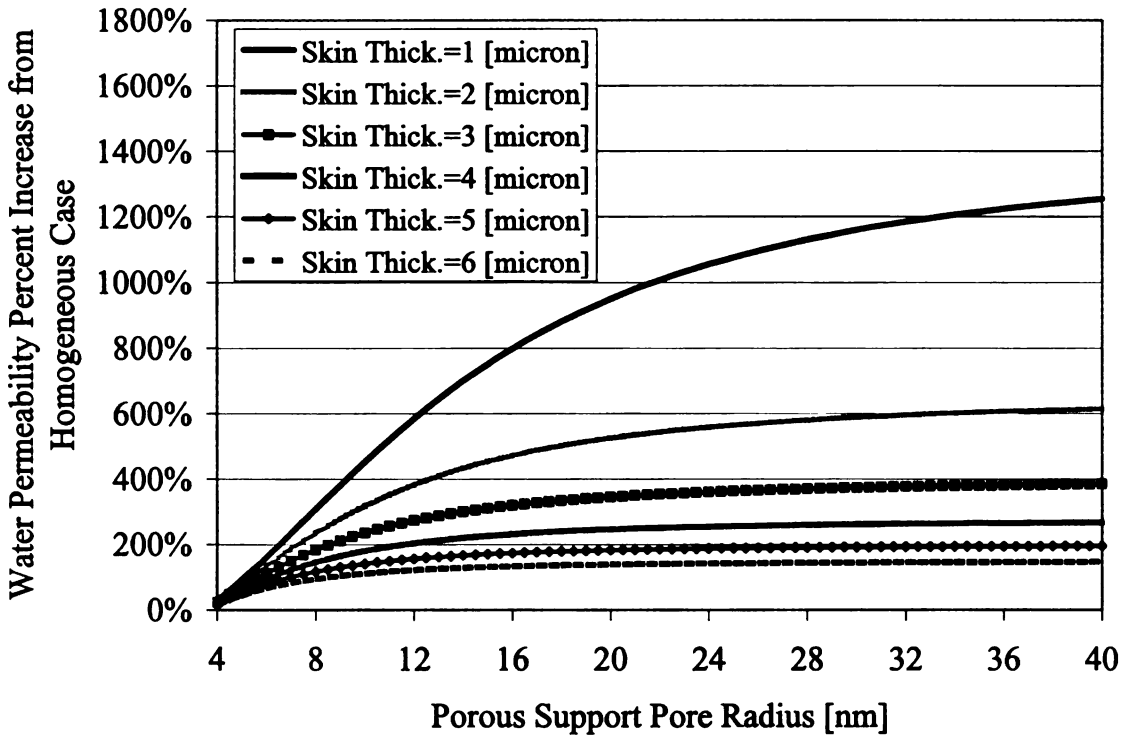

Figure 5.24. Water permeability percent increase from homogeneous case as a function of porous support pore radius and membrane skin layer thickness

The range for which water permeability increases for an asymmetric membrane for a porous support pore radius of 20 nm is 139% to 934% respectively. If a treatment required an excessive amount of water to be removed, then the clinical staff may wish to substitute an asymmetric membrane for a homogeneous membrane of comparable overall thickness. From an opposing viewpoint, excessive amounts of water removed from the patient during treatment can be potentially harmful and require water to be infused to the patient's blood volume.

Chapter 6

Conclusions

1. Model was developed that incorporates the physical and sieving properties of the dialyzer

2. This model calculates diffusive permeability, water permeability, compartmental pressure drops, and the toxin concentration at axial and radial locations in the fiber and dialyzer.

3. Model can allow researchers and dialyzer manufacturers to simulate membrane designs to gain performance estimates without the initial need to manufacture them.

4. Claims made in previous works regarding the limits of clearance, sieving properties of homogeneous membranes, and the sieving properties of asymmetric membranes were tested and results show excellent agreement. Reasons behind these phenomena are explained and developed in the Results and Discussion.

5. Provides many leads to future works.

Chapter 7

Future Recommendations

Upon the completion of this work several subjects presented themselves as opportunities for future study. Due to time constraints, these opportunities were not addressed within the current work. The recommendations are presented in no particular order of importance. These include creating a dialyzer library of parameters, develop a new toxin volume distribution model, comparing results of the current model to one and two-compartment models, use of this simulation program to innovate new dialysis membranes, and finally to use this model as an instructional tool within an undergraduate engineering course.

The first would involve creating a library within the current model of existing dialyzers used on the market today. This library would include the physical and sieving properties of dialyzer and hollow-fiber membranes that could be used to simulate clinical treatments. Using patient parameters, the program's simulation for estimated treatment time, water removed, and in-vivo clearance could be compared and contrasted to experimentally measured values. Upon further testing, the current model can be refined to improve accuracy for prescribing treatment dose.

The second would be to develop a new toxin volume distribution model applied to the current method of solution. Currently, the blood volume is modeled at a given

concentration that when completely passed through the dialyzer decreases to a new toxin concentration. This loop is continued until the blood volume reaches the target concentration. A new model could incorporate blood volume mixing. That is, a given volume of blood is passed through the dialyzer, cleared of toxins; and, at a decreased concentration, is recombined with body's blood volume. This may be one approach at which a model could address the arteriovenous urea gradient that develops during hemodialysis identified by Schneditz in 1992.[69]

The third recommendation would be to compare and contrast the values for treatment time and in-vivo clearance predicted by one and two-compartment modeling to those of the researched work. This would require both clinical data and detailed descriptions of the sieving properties of the dialyzers used. Currently, published works using one and two-compartment models only include dialyzer data such as clearance, fluid flow rates, and toxin concentration levels at given time intervals. Parameters such as porosity, pore size, membrane thickness, transmembrane pressure, tortuosity, and other items are required to determine the clearance in this model are needed for proper comparison.

If this model could be proven clinically, dialyzer manufacturers could use it to design an optimized dialyzer suitable for a smaller range of applications. This could include a dialyzer only suited for removing small molecular weight toxins or a dialyzer whose primary goal is to remove large volumes of body water. Works have suggested membrane adsorption as the predominate method for removing middle-weight toxins

during dialysis but have had limited success in modeling.[70-75] A dialyzer possessing an asymmetric membrane could be simulated whose skin layer consists of large pores and whose porous support that of small pores. The large pores could adsorb a greater level of middle molecules while the smaller pores would be able to filter lower molecular weight compounds provided proper mathematical modeling changes are made.

The final recommendation would be to use the current work as an instructional tool for the process of hemodialysis. A wide variety of topics could be discussed that include fluid dynamics, mass transfer, biomedical engineering, applications to environmental engineering, and membrane technology. Since the program has the flexibility to hold parameters constant while changing others, the program file can be altered so students can only change parameters of interest coming to conclusions similar to that of the

BIBLIOGRAPHY

1. Held, Phillip J, Port, Friedrich K, Wolfe, Robert A, Stannard, David C.,Carrol, Caitlin E., Daugirdas, John T., Bloembergen, Wendy E., Greer, Joel W., Hakim, Raymond M. "The dose of hemodialysis and patient mortality." *Kidney International* Vol. 50 (1996), pp. 550-556.

2. Eknoyan, G. "Effect of Dialysis Dose and Membrane Flux in Maintenance Hemodialysis." *New England Journal of Medicine* Vol. 347 (2002); part 25, pp. 2010-2019.

3. Goldfarb-Rumyantzev, Alexander S. , Cheung, Alfred K. , Leypoldt, John K. "Computer simulation of small-solute and middle-molecule removal during short daily and long thrice-weekly hemodialysis." *American Journal of Kidney Diseases* Vol. 40 (2002), no. 6, pp. 1211-1218.

4. Depner T, Beck G, Daugirdas J, Kusek J, Eknoyan G., "Lessons from the Hemodialysis (HEMO) Study: an improved measure of the actual hemodialysis dose." *American Journal of Kidney Diseases* Jan. 33 (1999), pp.142-149.

5. Gotch F.A., Levin N.W., Port F.K., Wolfe R.A, Uehlinger D.E. "Clinical outcome relative to the dose of dialysis is not what you think : The fallacy of the mean." *American Journal of Kidney Diseases* Vol. 30 (1997), no. 1, pp.1-15.

6.Charra B., Calemard E., Ruffet M., Chazot C., Cherrat J., Vanel T., Laurent G. "Survival as an index of adequacy of dialysis." *Kidney International* Vol. 41 (1992), pp. 1286–1291.

7. Uldall R, Ouwendyk M, Francoeur R, Wallace L, Sit W, Vas S,Pierratos A. "Slow nocturnal home hemodialysis at the WellesleyHospital." *Adv Renal Replace Ther* Vol. 13 (1996), pp. 133–136.

8. Santoro A, Buoncristiani U. "Dialysis schedule in haemodialysis and peritoneal dialysis." *Nephrology Dialysis Transplantation* Vol. 12 (1997), pp.1534–1536.

9. Kenley R. "Tearing down the barriers to daily home hemodialysis and achieving the highest value renal therapy through holisticproduct design." *Advanced Renal Replacement Therapy* Vol. 3 (1996), pp.137–146.

10. Vanholder R, DeSmet R, Glorieux G, Argiles A, Baurmeister U, Brunet P, Clark W, Cohen G, DeDeyn P, Deppisch R, Descamps-Latscha B, Henle T, Jorres A, Lemke H, Massy Z, Passlick-Deetjen J, Rodriguez M, Stegmayr B, Stenvinkel P, Tetta C, Wanner C, Zidek, W, for the European Uremic Toxin Work Group (EUTox).

"Review on uremic toxins:Classification, concentration, and individual variability." *Kidney International* Vol. 63 (2003), pp.1934-1943.

11. Gotch F: "Kinetic modeling in hemodialysis." Clinical Dialysis, Ed. Nissenson AR, Fine RN, Gentile DE, Norwalk Appleton & Lange, 1989, pp 118-146.

12. Sargent, J.A.,Gotch, F.A. "Mathematical modeling of dialysis therapy." *Kidney International* Vol. 18(suppl10) (1980), pp. 2-10.

13. Depner TA. "Hemodialysis urea modeling: the basics." *Seminars in Dialysis* Vol. 4 (1991), pp. 179–184.

14. Depner TA. Prescribing Hemodialysis: A Guide to Urea Modeling. Boston, Kluwer, 1991.

15. Depner, T. A. "Assessing adequacy of hemodialysis: Urea Modeling." *Kidney International* Vol. 45 (1994), pp. 1522-1535.

16. Aebischer P, Schorderet D, Juillerat A, Wauters JP, Fellay G. "Comparison of urea kinetics and direct dialysis quantification in hemodialysis patients." *Trans Am Soc Artif Intern Organs* Vol. 31 (1985), pp.338–341.

17. Barth RH. "Urea modeling and Kt/V: A critical appraisal." *Kidney International* Vol. 43(suppl 41) (1993), pp.S252–S260.

18. Gotch FA, Sargent JA. "A mechanistic analysis of the National Cooperative Dialysis Study (NCDS)." *Kidney International* Vol. 28 (1985), pp. 526–534.

19. Gotch, F. "Kinetic modeling in hemodialysis." Clinical Dialysis 2005, (4th ed), edited by Nissenson A, Fine R, pp 153–202.

20. Bankhead, Molly M., Toto, Robert D., Star, Robert A. "Accuracy of urea removal estimated by kinetic models." *Kidney International* Vol. 48 (1995), pp 785-793.

21. Daugirdas, John T. "Second Generation Logarithmic Estimates of Single-Pool Variable Volume Kt/V: An analysis of Error." *J. Am. Soc. Nephrol* Vol. 4 (1993) pp. 1205-1213.

22. Wolf, A.V., Remp, Donald G.,Kiley, John E., Currie, Gordon D. "Artificial Kidney Function:Kinetics of Hemodialysis." *J Clin Invest* Vol. 30 (1951), pp.1062-1070.

23. Renkin, EW. "The relationship between dialysance, membrane area, permeability, blood flow in the artificial kidney." *ASAIO Trans* Vol. 2 (1956), pp.102-105.

24. Sargent JA, Gotch FA. "Mathematical modeling of dialysis therapy." *Kidney International* Vol. 18(Suppl 10) (1980), pp. 2-10.

25. Sargent JA, Gotch FA. "Dialysis principles and biophysics," in Replacement of Renal Function by Dialysis, edited by Maher JF, New York, Kluwer Academic Publishers, 1989, pp 87-143.

26. Ziolko, M., Pietrzyk, J.A., Grabska-Chrazastowska, J. "Accuracy of hemodialysis modeling." *Kidney International* Vol. 57 (2000), pp. 1152-1163.

29. Keshaviah P, Illstrup K, Shapiro W, Hamson G. "Hemodialysis urea kinetics is not single pool." *Kidney International* Vol. 27 (1985), pp. 165

31. Depner TA. Prescribing Hemodialysis. A Guide To Urea Modeling. Boston, Kluwer Academic Publishers, 1991

32. Star RA, Hogarth L, Garcia E, Hootkins R, Thompson JR, Toto RD. "Two pool urea mass transfer coefficient by urea kinetic modeling." *ASAIO J* Vol. 391 (1993), pp. M573-M577.

33. Saha LK, Van Stone JC. "Differences between Kt/v measuring during dialysis and Kt/V predicted from manufacturer clearance data." *Int J Artif Organs* Vol. 15 (1992), pp. 447-504.

34. Besarab A, Ross R, Frinak S, Zasuwa G. "Increased urea kinetic modeling, possible mechanisms and its signficance." *ASAIO J* Vol. 43 (1997) pp.303-310

35. Daugirda, J.T, Greene, T, Depner,T, Gotch, F.,Star, R.A., and the Hemodialysis Study Group (HEMO). Relationship between apparent (Single-pool) and true (double-pool) urea distribution volume. *Kindey International* Vol. 56 (1999) pp.1928-1933

36. Dinnar, Uri. Cardiovascular Fluid Dynamics. CRC Press, Inc. Boca Raton, Florida, 1981.

37. Taggart, Starr and Cecie Starr. Biology: The Unity and Diversity of Life. California: Wadsworth, 1989: 398.

38. "Blood." World Book Encyclopedia. Chicago: World Book, 1998: pp. 407.

39. "Blood." World Book Rush-Presbyterian-St. Lukes Medical Center Medical Encyclopedia 7th edition. Chicago: World Book, 1995: pp. 120-121.

40. "Blood." Encyclopedia Britannica. Chicago: Encyclopedia Britannica, 1973.

41. "Volume of Blood."New Book of Popular Science. Connecticut: Grolier, 1996: 197.

42. Cameron, John R.; James G. Skofronick & Roderick M. Grant. Physics of the Body. Second Edition. Madison, WI: Medical Physics Publishing, 1999: 182.

43. Schneditz D, Rainer F, Kenner T. "Viscoelastic properties of whole blood; influence of fast sedimenting red blood cell aggregates." *Biorheology* Vol. 24 (1987), pp. 13-22

44. Schneditz, Daniel, Nissenson, Allen R, Fine, Richard N. "Technological Aspects of Hemodialysis and Peritoneal Dialysis." Clinical Dialysis, 4th ed. McGraw-Hill Companies, Inc. 2005

45. Fournier, Ronald L. Basic Transport Phenomena in Biomedical Engineering. Taylor and Franci, Lillington, NC, 1998.

46. Cooney O, David. Biomedical Engineering Principles: An Introduction to Fluid, Heat, and Mass Transport Processes. Marcel Dekker, Inc, New York, NY, 1976.

47. Kallenbach, Judith Z.,Gutch, C.F.,Stoner, Martha H., Corea, Anna L. Review of Hemodialysis for Nurses and Dialysis Personnel. Elsevier, Inc. St. Louis, MS, 2005.

48. "Kidney: blood circulation." Photo. Encylopedia Britannica.com 19 Aug. 2009 <http://www.britannica.com/EBchecked/topic-art/409282/99765/There-are-approximately-one-million-nephrons-in-each-kidney-that>.

49. Coresh J, Selvin E, Stevens LA. "Prevalence of chronic kidney disease in the United States." *Journal of the American Medical Association* Vol. 298(17) (2007), pp. 2038–2047.

50. "Cost of Kidney Disease." World Kidney Day.org. 19 Aug. 2009 <http://www.worldkidneyday.org/pages/cost.php>.

51. United States Renal Data System. USRDS 2007 Annual Data Report. Bethesda, MD: National Institute of Diabetes and Digestive and Kidney Diseases, National Institutes of Health, U.S. Department of Health and Human Services; 2007.

52. "Chronic Kidney Disease Up 30% Over Past Decade. MedNews.com. 19 Aug. 2009 <http://www.mednews.com/usrds-kidney-report>.

53. "Kidney and Urologic Diseases Statistics for the United States." National Kidney and Urologic Diseases Information Clearinghouse (NKUDIC). 19 Aug. 2009 <http://kidney.niddk.nih.gov/kudiseases/pubs/kustats/>.

54. "Hemodialysis Machine." Photo. Isiconline.org. 19 Aug. 2009 <http://isiconline.org/departments/dialysis.htm>.

55. Clark, William R.,Hamburger, Richard J.,Lysaght, Michael J. "Effect of membrane composition and structure on solute removal and biocompatibility in Hemodialysis." *Kidney International* Vol. 56 (1999) pp. 2005–2015.

56. A Innes, A M Farrell, R P Burden, A G Morgan, R J Powell. "Complement Activation by Cellulosic Dialysis Membranes." *J Clin Pathol* Vol. 47 (1994)155-158.

57. L.B. Leverett, J.D. Hellums, C.P. Alfrey and E.C. Lynch, "Red Blood Cell Damage by Shear Stress." *Biophysical Journal* Vol. 12, Issue 3 (1972) pp.257-273)

58. Ronco C, Clark W. "Hollow-Fiber Dialyzers:Technical and Clinical Considerations." in Clinical Dialysis. 4th Edition. Ed. by Nissenson, Allen R, Fine, Richard N. McGraw-Hill Companies, Inc. 2005.

59. Lysaght MJ. "Evolution of Hemodialysis Membranes." *Contrib Nephrol* Vol. 61 (1988), pp.1-17.

60. Hoenich N, Woffindin C, Cox P, "Clinical characterization of a new cellulose membrane for haemodialysis." *Clin Nephrol* Vol. 48 (1997), pp.253-259.

61. Ronco, C. Ballestri, M., Cappelli, G. "Dialysis membranes in convective treatments." *Nephrol Dial Transplant* Vol. 15(Suppl 2) (200), pp.31-36.

62. Mulder, Marcel. Basic Principles of Membrane Technology. 2nd Edition. Kluwer Academic Publishers, Norwell, MA 2003.

63. Bird, R.B., Stewart, W.E. and Lightfoot, E.N. Transport Phenomena. 1st Ed. John Wiley & Sons, 1960.

64. Wingert, KJ, Weiner, MW. "Acetate transfer across membranes of artificial kidneys in vitro." *Kidney International* Vol. 15 (1979), pp.593-600.

65. Barzin, J, Feng, C, Khulbe, KC, Matsuura, T, Madaeni, SS, Mirzadeh, H. "Characterization of polyethersulfone hemodialysis membrane by ultrafiltration and atomic force microscopy." *Journal of Membrane Science* Vol. 237, Issues 1-2, (July 2004) pp.77-85.

66. Langsdorf, LJ, Zydney, AL. "Diffusive and convective solute transport through hemodialysis membranes: A hydrodynamic analysis." *Journal of Biomedical Materials Research.* Vol 28, Issue 5, pp.573-582.

67. Renkin, E.M. "Multiple pathways of capillary permeability." *Circulation Res.* Vol. 41 (1977) pp.745-743.

68. Ken-ichiro Yamamoto, Masayo Hayama, Masato Matsuda, Taiji Yakushiji, Makoto Fukunda, Takehiro Miyasaka, Kiyotaka Sakai. "Evaluation of asymmetrical structure dialysis membrane by tortuous capillary pore diffusion model." *Journal of Membrane Science* Vol. 287 (2007) pp.88-93.

69.Ken-ichi Kokubo, Kiyotaka Sakai. "Evaluation of Dialysis Membranes Using a Tortuous Pore Model." *AiChe Journal.* Vol. 44, (Dec 1998) no. 12, pp.2607-2619.

70.Schneditz D, Kaufman AM, Polaschegg H, Levin NW, Daugirdas JT: "Cardiopulmonary recirculation during hemodialysis." *Kidney Int* Vol. 42 (1992), pp.1450-1456.

71. Clark, WR , Macias, WL, Molitoris, BA, and Wang, L. "Plasma protein adsorption to highly permeable hemodialysis membranes." *Kidney Int* Vol. 48 (1995), pp.481-488.

72. Clark WR , Macias WL, Molitoris BA, and Wang L. "Membrane adsoroption of □2-microglobulin:Equilibrium and kinetic characterization." *Kidney Int* Vol. 46 (1994), pp.1140-1146.

73. Pascual M, Schifferli J, "Adsorption of complement factor D by poylyacrylonitrile dialysis membranes." *Kidney Int* Vol. 43 (1993), pg. 903-911.

74. Goldman M, Lagmiche M, Dhaene M, Amraoui Z, Thayse C, Vanherweghem JL. "Adsorption of beta 2-microglobulin on dialysis membranes: comparison of different dialyzers and effects of reuse procedures." *Int J Artif Organs* Vol. 12 (1989), pp.373-378.

75. Pascual M, Tolkoff-Rubin N, and Schifferli J. Is adsorption an important characteristic of dialysis membranes? Kindey Int Vol. 49 (1996), pp.309-31.